5-1-1990

Sensor Array Signal Processing via Eigenanalysis of Matrix Pencils Composed of Data Derived from Translationally Invariant Subarrays

Demosthenis Stavrinides
Purdue University

Michael D. Zoltowski
Purdue University

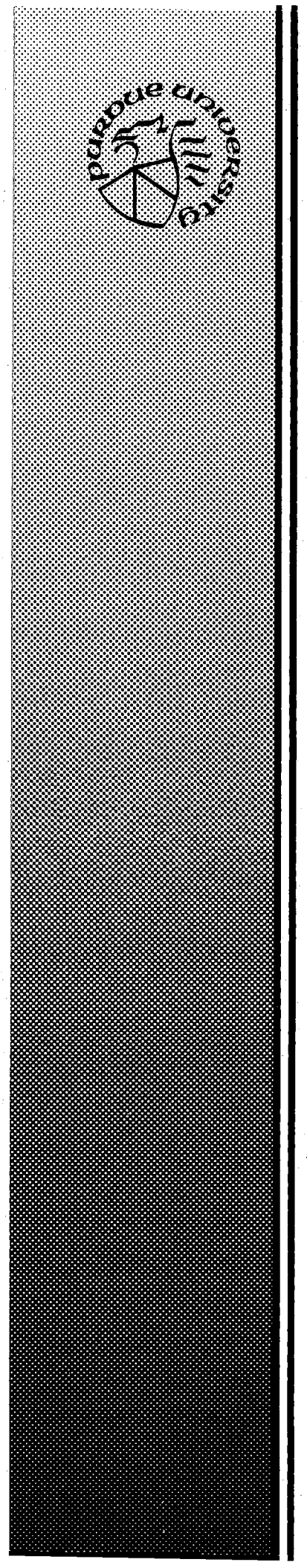

Sensor Array Signal Processing via Eigenanalysis of Matrix Pencils Composed of Data Derived from Translationally Invariant Subarrays

Demosthenis Stavrinides
Michael D. Zoltowski

TR-EE 90-31
May 1990

School of Electrical Engineering
Purdue University
West Lafayette, Indiana 47907

prepared for the National Science Foundation under contract number ECS-8707681

SENSOR ARRAY SIGNAL PROCESSING VIA EIGENANALYSIS OF MATRIX PENCILS COMPOSED OF DATA DERIVED FROM TRANSLATIONALLY INVARIANT SUBARRAYS

prepared for the National Science Foundation

under contract number ECS-8707681

Demosthenis Stavrinides

and

Michael D. Zoltowski

School of Electrical Engineering

Purdue University

West Lafayette, IN 47907

TR-EE-90-31

May 1990

TABLE OF CONTENTS

Page

LIST OF TABLES iv

LIST OF FIGURES v

ABSTRACT viii

CHAPTER 1 - INTRODUCTION 1

1.1 Motivation for the New Algorithm 1

CHAPTER 2 - THE **ESPRIT** STRUCTURE AND ARRAY GEOMETRY 12

2.1 Introduction to **ESPRIT** 12

CHAPTER 3 - EIGENANALYSIS OF THE **ESPRIT** DATA PENCIL 18

3.1 The **ESPRIT** Data Pencil With Noiseless Data 18
3.2 Reduction to DxD Pencil Via Simultaneous Subspace Rotations 19
3.3 The Significance of the Left and Right GEVEC's 23
3.4 Estimation of the Core Rotations Pencil with Noisy Data 29
3.5 On the Asymptotic Unbiasedness of **PRO–ESPRIT** 30
3.6 Invocation of Solution to Procrustes Problem: **PRO–ESPRIT** 31
3.7 Total Least Squares Interpretation of **PRO–ESPRIT** 32

CHAPTER 4 - **PRO–ESPRIT** AND THE UNIFORM LINEAR ARRAY 38

4.1 The Linear Array Geometry and the F-B Data Pencils 38
4.2 Construction and Analysis of the F-B Data Pencils 39
4.3 **PRO–ESPRIT** Eigenanalysis of the F-B Data Pencils 43
4.4 Simulations and Discussion 45

Page

CHAPTER 5 - **PRO–ESPRIT** AND PSEUDO F-B AVERAGING.....61

5.1 Pseudo-Forward-Backward Averaging (PFBAVG).....61
5.2 Procrustes Processing and Its Effects.....65
5.3 Incorporation of Array Manifold Modification.....69
5.4 Estimation of Number of Sources Via Invariance Exploitation.....74
5.5 Methods for Angle Pairing.....78
5.6 Computer Simulations.....81

CHAPTER 6 - APPLICATION OF **PRO–ESPRIT** IN BEAMSPACE.....98

6.1 Introduction.....98
6.2 Choice and Construction of the Beamforming Matrix.....99
6.3 Large Arrays and Ill-Conditioning Problems.....104
6.4 **PRO–ESPRIT** With F-B Averaging and White Noise.....106
6.5 Simulations and Discussion.....111

CHAPTER 7 - CONCLUSION.....116

LIST OF REFERENCES.....118

APPENDICES

Appendix A.....124
Appendix B.....125

LIST OF TABLES

Table Page

4.1 Performance of **PRO–ESPRIT** with real data. There are two sources located at at 3° and 5°. The estimates are listed as a function of the subarray length and the number of snapshots. F-B averaging was used.....59

4.2 The number of sources is now three, at 3°, 5° and −10°. The estimates are listed as a function of the subarray length and the number of snapshots. Only Forward averaging was used. 60

LIST OF FIGURES

Figure Page

1.1 The Corrugated Box Array. Figures 5.2(b), 5.2(c) and 5.2(d) show three out of the four possible ways we can construct the X and Y arrays. 3

1.2 A linear array of aperiodically spaced doublets and a planar array of randomly spaced doublets....10

2.1 The generalized **ESPRIT** structure....13

3.1 Schematic representation of the eigen-links between the data level and the core rotations level. 28

3.2 A summary of **PRO–ESPRIT**....33

4.1 The performance of **PRO–ESPRIT** when applied in a uniform linear array scenario consisting of 15 sensors, three sources at θ_1=6.5°, θ_2=10.3° and θ_3=–9°. The dashed curve represents the unit circle. The results of 100 independent trials are shown. 50

4.2 Comparison of **PRO–ESPRIT** performance for Procrustes processing "switched on" versus Procrustes processing "switched off". The scenario consisted of a uniform linear array of 15 sensors and three sources at θ_1=–9°, θ_2=6°, θ_3=12.3°. The results of 100 independent trials are plotted....54

4.3 A comparison of the sample variance of estimates obtained via **PRO–ESPRIT** and the Cramer Rao Lower Bound. In 4.3(a) the number of snapshots is allowed to vary, and in 4.3(b) the SNR varies....56

4.4 The number of sensors is held fixed and the subarray size is changed. Minimum variance is obtained when the subarray size is 2/3 of the total array size (L=10). 58

Figure Page

5.1 Comparison of the estimation of the u and v parameters via the original version of **PRO–ESPRIT** and the new one based on pseudo F-B Averaging. 5.3(a) and 5.3(b) compare the u estimates, while Figures 5.3(c) and 5.3(d) compare the v estimates. 88

5.2 Average eigenvalue distribution before and after array manifold modification. The eigenvalues are averaged over 200 independent trials. The sources are located at (θ_1,ϕ_1)=(45°,5°), (θ_2,ϕ_2)=(225°,5°) and (θ_3,ϕ_3)=(32°,20°). The SNR of the first two sources is 13.4 dB and are 95% correlated. The third source is uncorrelated with the first two and has an SNR of 15.8 dB. 25 snapshots were used. 92

5.3 Empirical probability of detecting the correct number of sources with the weighted Procrustes difference scheme. The array and source parameters are described in Figure 5.3. For each set of parameters, the corresponding probability was computed from the results of 200 independent runs....93

5.4 A comparison of the performance of pseudo F-B **PRO–ESPRIT** when it is applied to a linear array of 28 sensors. The estimated quantities are u_1 and u_2 for θ_1=–2° and θ_2=2°. In both cases the sensors in a doublet are separated by $\lambda/2$. In 5.6(a) the inter-doublet separation is $\lambda/2$ and in 5.6(b) it is $3\lambda/2$. 94

5.5 The probability of correct pairing of the u and v estimates obtained from **PRO–ESPRIT**. In 5.7(a) the SNR is held fixed and the number of snapshots changes. In 5.7(b) the number of snapshots is fixed and the SNR varies. 96

6.1 The performance of beamspace **PRO–ESPRIT** with a 64 element array and bands of 13 beams. The beams cover the range θ=–11° to θ=11°, or u=-.1875 to u=.1875. The source at θ=0° is at the peak of the beam centered at u=0....113

6.2 Effect caused by reducing the number of beams from 13 to 7. There is no significant change in the estimates....114

Figure Page

6.3 With 13 beams, the result of assigning one source a direction outside the visible interval $\theta=-11°$ to $\theta=11°$. The sources at $\theta=-5°$ and $\theta=6°$ are estimated almost perfectly. The source at $\theta=12.8$ appears as coming right from boreside. 115

ABSTRACT

An algorithm is developed for estimating characteristic parameters associated with a "scene" of radiating sources given the data derived from a pair of translationally invariant arrays, the X and Y arrays, which are displaced relative to one another. The algorithm is referred to as **PRO–ESPRIT** and is predicated on invoking two recent mathematical developments: (1) the SVD based solution to the Procrustes problem of optimally approximating an invariant subspace rotation and (2) the Total Least Squares method for perturbing each of the two estimates of a common subspace in a "minimal" fashion until the two perturbed spaces are the same. For uniform linear array scenarios, the use of forward-backward averaging (FBAVG) in conjunction with **PRO–ESPRIT** is shown to effect a substantial reduction in the computational burden, a significant improvement in performance, a simple scheme for estimating the number of sources and source decorrelation. These gains may be attributed to FBAVG's judicious exploitation of the diagonal invariance operator relating the Direction of Arrival matrix of the Y array to that associated with the X array. Similar gains may be achieved in the case where the X and Y arrays are either not linear or not uniformly spaced through the use of pseudo-forward-backward averaging (PFBAVG). However, the use of PFBAVG does not effect source decorrelation and reduces the maximum number of resolvable sources by a factor of two. Simulation studies and the results of applying **PRO–ESPRIT** to real data demonstrate the excellent performance of the method.

CHAPTER 1
INTRODUCTION

1.1 Motivation for the New Algorithm

In recent years, a number of model-based, high resolution schemes have been proposed for estimating the directions of radiating sources given the signals received at an array of antennas. A great deal of attention has focused on linear arrays which only allow for estimation of the angle of a source relative to the line on which the antennas are placed, i.e., they only allow one to determine the radial direction of a source relative to a cone of ambiguity whose axis of symmetry is the line of the array. Algorithms such as **MUSIC** [SCH86], Minimum Variance [CAP69,KAY88], etc., involve the construction of a 1-D "spatial spectrum" which when plotted ostensibly exhibits peaks at those angles from which the signals are arriving. The extension of high resolution techniques to planar arrays typically gives rise to a 2-D "spatial spectrum" which ideally exhibits peaks at those azimuth and elevation angles corresponding to the actual source directions. The price paid for the ability to determine without ambiguity the radial direction of a source is the tremendous computational burden of plotting and searching a multi-modal, 2-D surface.

A new array signal processing algorithm, **ESPRIT** [ROY86], has been developed which when utilized in conjunction with a special class of planar array geometries avoids the 2-D plot and search entirely. **ESPRIT** [ROY86] is a novel algorithm for estimating direction-of-arrival information and other characteristic parameters for classifying a "scene" of radiating sources. Contrary to previous schemes, the applicability of **ESPRIT** in a particular array scenario is dependent on the ability to decompose the overall array structure into at least one pair of translationally invariant subarrays, the X subarray and the Y subarray. As a consequence of the translational invariance, the respective Direction-of-Arrival (DOA) matrices associated with the X and Y subarrays are related through a diagonal unitary matrix referred to as the invariance operator [ROY89a]. The i-th element of the invariance operator accounts for the phase delay between corresponding sensors of the two arrays associated with the i-th source. These subarrays may or may not have sensor elements in common. For a given pair of

translationally invariant subarrays, so-called Single Invariance **ESPRIT** (SI **ESPRIT**) [ROY88a] may be applied to estimate the angle of each source relative to the displacement axis between the two respective subarrays. Due to judicious exploitation of the identical nature of the two arrays, SI **ESPRIT** is able to provide these source angle estimates without resorting to a search over the array manifold as required by **MUSIC**, for example. Recently, extensions of **ESPRIT**, referred to as Multiple Invariance **ESPRIT** (MI **ESPRIT**) [ROY88b], have been proposed for optimally exploiting the multiple translational invariances present in such structures as the uniformly linear array (ULA) [ROY88b,ROY89b] and its two-dimensional counterpart, the rectangular grid array. A detailed description of this special array system here referred to as the "**ESPRIT** array system" is found in Chapter 2.

As an example of an **ESPRIT** array system, consider the SI **ESPRIT** configuration depicted in Figure 1.1(a) referred to as the Corrugated Box Array. The Corrugated Box Array is composed of 28 sensors having identical phase and gain characteristics. Consider the pairwise groupings indicated in Figure 1.1(b) where the black dots indicate the position of the sensors in the x-y plane. Since any two sensors along the perimeter are identical, this particular grouping represents an array of 14 matched sensor pairs or doublets, to which **ESPRIT** or **PRO–ESPRIT** may be applied to estimate the radial direction of a source relative to the y-axis. The X and Y arrays are depicted in the center of Figure 1.1(b). At the same time, the pairwise groupings indicated in Figure 1.1(c) represent an array of 14 doublets to which **PRO–ESPRIT** may be employed to estimate the radial direction of a source relative to the x-axis. The X and Y arrays for this case are depicted in the center of Figure 1.1(c). Of course, if there is more than one radiating source, it is essential to determine which angle estimate obtained from the y-axis processing goes with a particular angle estimate obtained from the x-axis processing. Schemes that accomplish this are presented in Section 5.6. However, the beauty of this procedure is that it avoids the 2-D plot and search typically required in such a case by each of the algorithms mentioned at the beginning.

Since its inception, **ESPRIT** has attracted a great deal of attention. The attraction stems mainly from the fact that, in contrast to **MUSIC** [SCH86], **ESPRIT** does not require a search in order to estimate the arrival angles of the various plane waves impinging upon the array. These are simply determined by solving for the generalized eigenvalues (GEV's) of a matrix pencil constructed solely with the data extracted from the X and Y arrays. The array manifold need not be measured or stored. Of course, the formulation of **ESPRIT** was based on the identical nature of the X and Y arrays comprising the **ESPRIT** array system

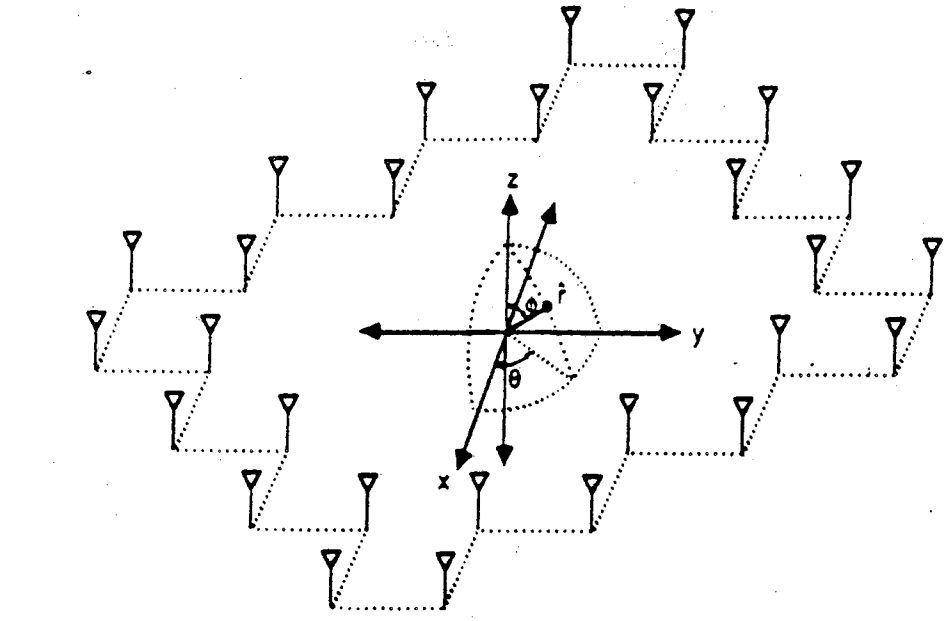

(a)

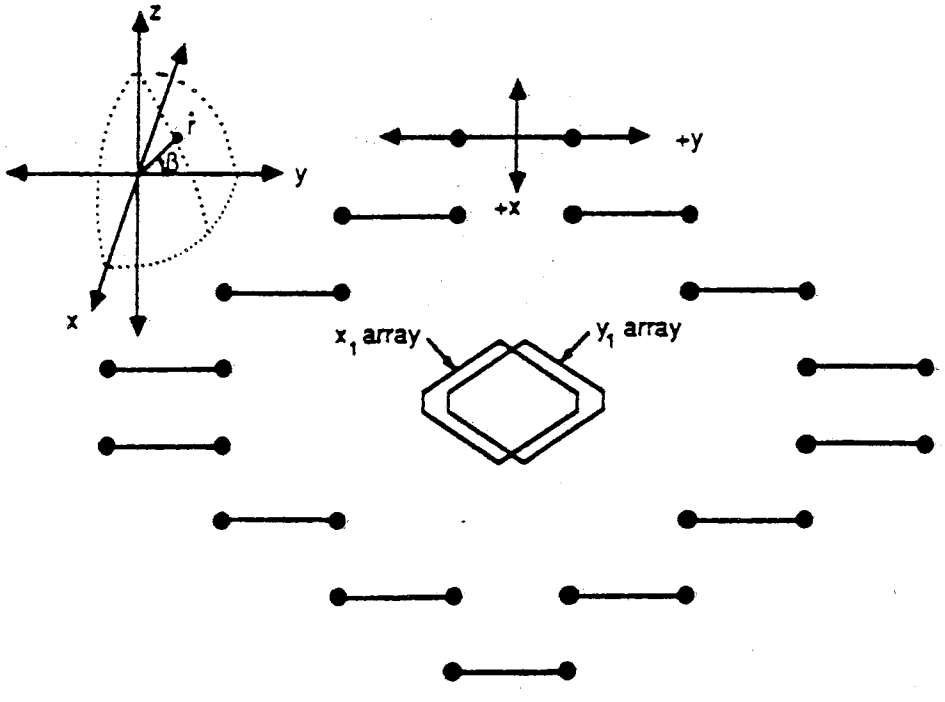

(b)

Figure 1.1 (a) 28 element Corrugated Box Array. Any two adjacent sensors are separated by a half wavelength. Sensor pairings for estimating source angles relative to (b) y-axis, (c) x-axis and (d) line y=x.

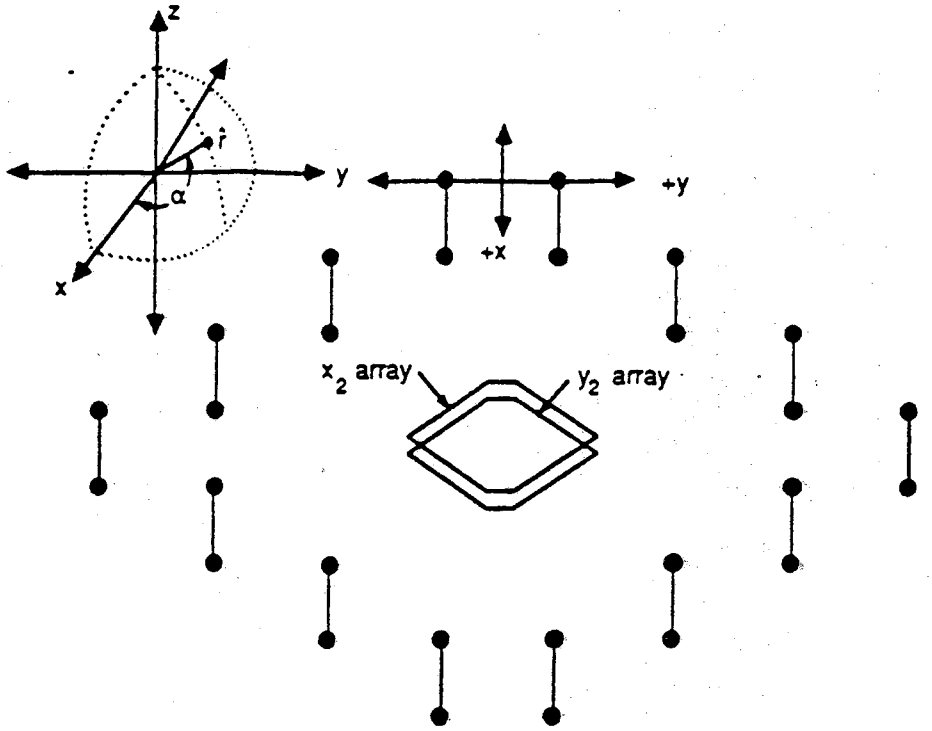

(c)

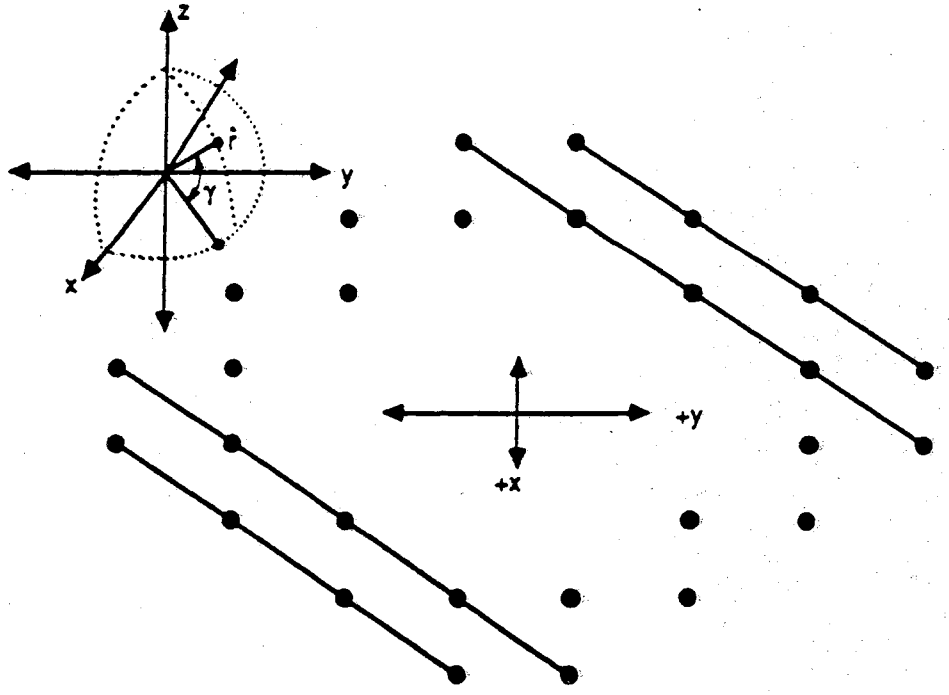

(d)

Figure 1.1 (continued)

such that **ESPRIT** is not as generally applicable as is **MUSIC**. As a consequence of this attribute of **ESPRIT**, a certain amount of skepticism has also surrounded the algorithm, with the primary concern being the sensitivity of the algorithm to deviations from this ideal array system. However, simulations conducted by the original inventors of **ESPRIT** have indicated that **ESPRIT** is, in fact, more robust to imperfections in the array model/data than **MUSIC** [ROY87a] *when applied to an array scenario exhibiting the* **ESPRIT** *structure.* We submit that this is due to a primary aspect of the **ESPRIT** array system which may be easily overlooked: *since the two arrays are identical there is an inherent redundancy built into* the **ESPRIT** array system. Furthermore, **ESPRIT** is specifically designed to exploit this redundancy. This redundancy manifests itself in terms of reducing the number of sources resolvable by **ESPRIT** to nearly half that possible with **MUSIC**. Specifically, with no sensors in common between the X and Y arrays such that there is 2M sensors total and no coherent sources, **MUSIC** can be used to estimate the directions of 2M-1 sources. In contrast, under the same conditions, **ESPRIT** can only resolve M-1 sources. However, the original manner in which **ESPRIT** exploits the redundancy built into the **ESPRIT** array system is sub-optimal in the sense that it does not exploit this redundancy in the fullest manner possible.

This dissertation develops a modification of **ESPRIT**, referred to as Procrustes ROtations based **ESPRIT**, or **PRO–ESPRIT** which is, in fact, **premised** on exploiting the redundancy built into the **ESPRIT** array system. We expand on the particular merits of **PRO–ESPRIT** while summarizing the thesis contents.

As explained in Section 3.1, **PRO–ESPRIT** is predicated on exploiting two fundamental properties of the noiseless X and Y data matrices comprising the **ESPRIT** data pencil: (1) they have the same row space, the signal subspace, and (2) they have the same column space, the source subspace. Exploitation of these two properties allow us to reduce the **ESPRIT** data pencil to an "equivalent" square matrix pencil having the same nonzero generalized eigenvalues (GEV's) but of a dimension equal to the number of sources, D. This is developed in Section 3.2 for the noiseless case. We find that the composition of the equivalent square DxD pencil, here referred to as the core information matrix (CIM), includes two unitary matrices: one which performs an invariant rotation on the signal subspace and one which performs an invariant rotation on the source subspace. Although we are able to formulate asymptotically unbiased estimators of these two unitary matrices in Section 3.4 for the case of noisy data, the estimates will, of course, never be unitary in practice. Our exploitation of the redundancy built into the **ESPRIT** array system allows us to make novel use of

a "tool" for compensating, in part at least, for deviations from the ideal array and source model. We argue in Section 3.6 that if either of the two core rotation matrices is not unitary, as it should be, it should be replaced by the respective "closest" unitary matrix. The respective "closest" unitary matrix in either case is easily found via an SVD-based, closed form solution which has its foundations in the solution to the classical subspace rotation problem posed by Procrustes. [GOLU83a], ergo the name **PRO–ESPRIT**. In Section 3.7, we present an alternative interpretation of **PRO–ESPRIT** based on the principle of Total Least Squares (TLS) [GOLU83b,GOLU80,ZOLT87c]. We emphasize that the application of the TLS concept as a way of interpreting **PRO–ESPRIT** is **fundamentally different** from the way it is applied in the **TLS–ESPRIT** algorithm [ROY87b,ROY88a] discussed shortly. The motivation for using TLS is the following. The X array data and the Y array data provide us with two different estimates of the signal subspace, and two different estimates of the source subspace as well. Total Least Squares is utilized as a means for perturbing each of the two estimates of the signal subspace, say, in some "minimal" fashion until they are equal. The common subspace after perturbation is then taken as a "better" estimate of the signal subspace. A "better" estimate of the source subspace is obtained in the same fashion. The core informations pencil is then obtained by optimally rotating, via the method of Procrustes, into these optimal subspaces. This interpretation of **PRO–ESPRIT** will further substantiate our claim that **PRO–ESPRIT** is predicated on exploiting the redundancies inherent in the **ESPRIT** array system.

Section 3.5 includes a discussion on the asymptotic unbiasedness of **PRO–ESPRIT**. It should be pointed out that the stand-alone algorithm developed in Section 3.4, without the added feature of Procrustes processing first introduced in Section 3.6, provides asymptotically unbiased estimates of the signal directions, the array manifold vectors, the optimal "signal copy" vectors, and the source covariance matrix. Thus, we stress that these refinements are introduced as a means for compensating for such troublesome array processing "nuisances" as

- imperfect array data contaminated by sensor dependent phase errors
- estimated noise correlation matrix not equal to true one
- deviations from ideal array model:
  - members of a given sensor pair not perfectly matched
  - variations in the displacement vector among the sensor pairs

Again, the ability to introduce these refinements is made possible due to the redundancy built into the **ESPRIT** array system. With regard to the second item listed above, we remark that one can incorporate into **PRO–ESPRIT** a highly successful technique developed by LeCadre [LEC89] for estimating the noise correlation matrix, to within a scalar multiple, from the overall signal-plus-noise correlation matrix which requires **no a-priori information about the noise.**

PRO–ESPRIT is not the only algorithm that attempts to exploit the redundancies built into the **ESPRIT** array system. The original inventors have proposed a novel modification of **ESPRIT** which is based in part on the method of Total Least Squares [GOLU83b]. We will here refer to the new algorithm as **TLS–ESPRIT** [ROY87b,ROY88a], for short. Actually, the foundation of **TLS–ESPRIT** is rather different than that for **ESPRIT**. The original version of **ESPRIT** was based on the structure of a matrix pencil composed of the correlation matrix formed from the X array data and the cross-correlation matrix formed from data extracted from both the X and Y arrays. Ideally, the nonzero generalized eigenvalues of the "cleaned" version of this pencil are on the unit circle and their respective arguments are simply related on a one-to-one basis with the signal directions relative to the displacement axis. On the other hand, **TLS–ESPRIT** is based on a fundamental relationship exhibited by the signal eigenvectors of the overall Z correlation matrix formed from the outer product of snapshot vectors produced by stacking the X array data on top of the Y array data. By approaching the problem in this alternative fashion, Roy and Kailath find that they may make use of TLS for dealing with deviations from the ideal array model which they were not able to invoke in the original version of **ESPRIT**. However, in terms of computational load and algorithm execution time, we find that in the case of arbitrary, 2-D **ESPRIT** arrays, **PRO–ESPRIT** offers significant advantages. These advantages of **PRO–ESPRIT** over **TLS–ESPRIT** are a direct result of the fact that **PRO–ESPRIT** works with the individual X and Y correlation matrices, as opposed to working with them jointly as components of the larger Z correlation matrix, i.e., the matrix formed by stacking the X array data on top of the Y array data. As a consequence, we find that for every eigenvalue decomposition (EVD) required by **TLS–ESPRIT**, **PRO–ESPRIT** requires two EVD's of half the dimension of that required by **TLS–ESPRIT**. Now, as M grows large the EVD of a 2Mx2M matrix becomes increasingly more computationally burdensome than the EVD of two MxM matrices. Over and above this is the fact that the two MxM EVD's required by **PRO–ESPRIT** can be performed independently, and hence, simultaneously, such that the computation time need only be that required to perform a single

MxM EVD, assuming the appropriate dedicated processing hardware is available. The concept of parallel processing is emphasized in the summary of **PRO–ESPRIT** delineated in Section 3.6.

In Chapter 4, we present some simplifications to **PRO–ESPRIT** applicable in a uniform linear array (ULA) scenario. This scenario is particularly intriguing for the application of **PRO–ESPRIT**, or for any derivative of **ESPRIT** for that matter, in light of the observation that every two adjacent sensors in the array is a matched sensor pair, assuming the sensors to be identical. An issue which arises in the estimation of the components of the invariance operator via SI **ESPRIT** is the merits of imposing a unit modulus constraint on them. Swindlehurst et. al. [ROY88b,ROY89b,OTT89,SWI89] have argued and demonstrated through simulation that the imposition of such substantially increases the computationally complexity of SI **ESPRIT** while only providing a modest improvement in performance. In the formulation of **PRO–ESPRIT** presented in Chapter 4, the unit modulus constraint on the estimate of the invariance operator is also omitted for the sake of computational expediency. It is argued with the help of simulations that, in general, the Procrustes processing in **PRO–ESPRIT** represents a sub-optimal means of incorporating this constraint. However, in the version of **PRO–ESPRIT** we develop for the ULA in Section 4.2, the unitary nature of the invariance operator is explicitly exploited by employing backward averaging in addition to forward averaging. The backward averaging effectively serves as an additional means of accounting for the unit modulus constraint without actually imposing it. Surprisingly, the incorporation of backward averaging in **PRO–ESPRIT** for ULA's also facilitates computational simplicity. That is, the version of **PRO–ESPRIT** which employs both forward and backward averaging is substantially less computationally burdensome than the version which employs forward averaging only. Our claims and observations are substantiated with simulations involving real data presented in Section 4.4.

Unfortunately, the manner in which backward averaging is employed in **PRO–ESPRIT** for ULA's is not possible in the single invariance case when the replicated array structure is arbitrarily shaped. In some applications it may not be either possible or desirable to employ uniform structures such as the ULA or the rectangular grid array. For example, in order to achieve a certain resolution capability with a limited number of elements, one may wish to employ a pair of identical aperiodic arrays. In the case of linear array processing, the doublets comprising the two identical subarrays may be spaced aperiodically over a large aperture as depicted in Figure 1.2(a) in order to achieve a higher resolution capability. Irrespective of the ability of **ESPRIT** to accurately locate sources separated by less than a beamwidth, its resolution capability is nevertheless

proportional to the aperture length. This is true for any high resolution algorithm. Similar comments hold with regard to two-dimensional array processing. Again, for the purpose of achieving a higher resolution capability with a limited number of elements, one may place the doublets in an aperiodic fashion over a large planar aperture as depicted in Figure 1.2(b). Alternatively, one may be forced to work with a doublet configuration as in Figure 1.2(b) due to physical constraints [ROY89a,ROY89b].

For SI **ESPRIT** applications in which the individual arrays are non-uniform and/or nonlinear, in Chapter 5 we introduce a variant of forward-backward averaging (FBAVG) referred to as pseudo-forward-backward averaging (PFBAVG). Similar to the role of backward averaging in the case of ULA's, PFBAVG serves as a generally applicable means of accounting for the aforementioned unit modulus constraint without actually imposing it. The incorporation of PFBAVG into **PRO–ESPRIT** also yields benefits similar to those achieved with backward averaging in the case of a ULA. Specifically, the use of PFBAVG in conjunction with **PRO–ESPRIT** effects a substantial reduction in the computational burden and, at the same time, a significant improvement in performance. However, in contrast to the situation with backward averaging in the case of the ULA, there is a penalty paid for these benefits. The price paid is a reduction in the maximum number of sources the algorithm is able to handle by a factor of two.

Another issue which arises with regard to **ESPRIT** has to deal with optimal estimation of the number of sources. Consider the single invariance case in which the two identical subarrays have no elements in common and the replicated array structure is arbitrarily shaped. In this case, neither **TLS–ESPRIT** or **PRO–ESPRIT** exploits the underlying invariance in the estimation of the number of sources. Let M be the number of elements comprising each of the two translationally invariant subarrays. In the covariance matrix formulation, **TLS–ESPRIT** initially works with the overall array of 2M sensors, examining the largest eigenvalues of the corresponding 2Mx2M covariance matrix in accordance with the Akaike Information Criteria (AIC) or the Minimum Description Length (MDL). **PRO–ESPRIT** initially works with the two subarrays individually, performing independent eigenanalyses of each of the two respective MxM covariance matrices. The eigenvalues of both matrices are examined but it is unclear how to optimally combine this information in the determination of the number of sources. In Section 5.5 we propose an ad-hoc scheme for estimating the number of sources which explicitly exploits the underlying invariance. The scheme is shown to provide accurate estimates of the number of sources.

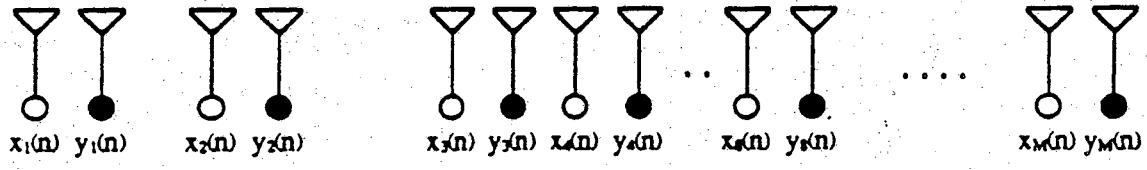

(a)

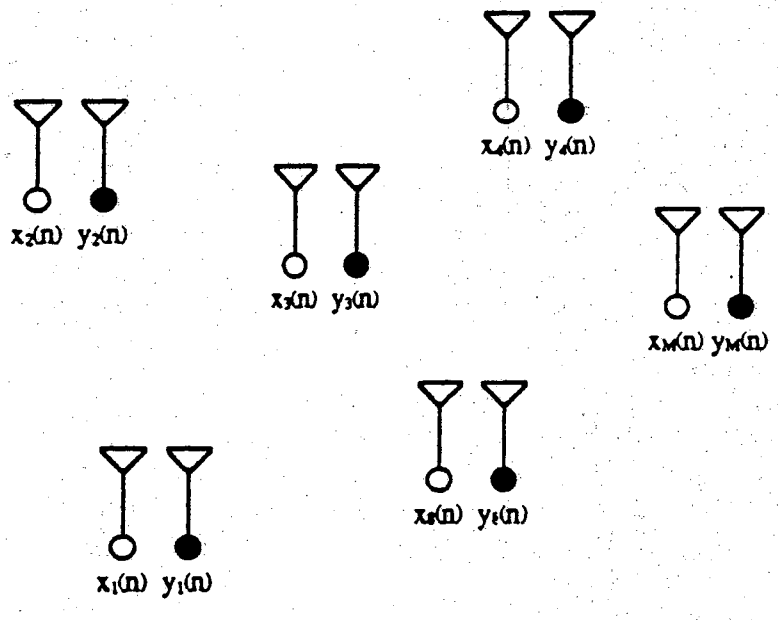

(b)

Figure 1.2 A linear array of aperiodically spaced doublets and a planar array of randomly spaced doublets.

Of course, the incorporation of PFBAVG in **PRO–ESPRIT** was not accomplished without complication. In Section 5.4 we show that there are specific scenarios under which PFBAVG can lead to severe ill-conditioning problems and, therefore, to a pejorative effect on the performance of **PRO–ESPRIT**. Fortunately, these conditions can be averted with negligible computational effort. Simple schemes that can accomplish this are also presented in this section.

Finally, in Chapter 6 we investigate dividing the angular region of interest into partially overlapping sectors, and then processing the data obtained for each sector independently and in parallel. Although the scheme is developed for the case of the ULA, it may be easily extended to cover the case of the rectangular grid array. In either case, the goal is to reduce the computational burden incurred with such arrays comprising of hundreds, even thousands of sensors. Contrary to the previous outline of **PRO–ESPRIT** where the input to the algorithm is taken to be the "raw" X array data and Y array data, in the new scheme the "raw" data are first acted upon by a beamformer matrix. In doing so, the dimensionality of the input data is lowered, making the use of **PRO–ESPRIT** under such a scenario more practical. For our purposes, we here consider one special beamformer matrix that allows the use of fast Discrete Fourier Transform methods to achieve the reduction in the dimensionality of the input data.

Before we proceed with the development of **PRO–ESPRIT**, we would like to comment on a misconception commonly associated with **ESPRIT**. By applying **ESPRIT** to an array structure composed of two identical sensor arrays displaced relative to one another, it is not claimed that the calibration problem is somehow avoided. On the contrary, the calibration involved in matching corresponding sensors in the X and Y arrays is certainly not a trivial task. However, the point is that if, in fact, we go to the trouble of constructing and calibrating such an array, there are many benefits to be reaped as discussed above and as first described by the original inventors, Roy and Kailath, in [PAUL85,ROY86,ROY87a]. Furthermore, the inherent redundancy built into the ideal **ESPRIT** array structure can be exploited to compensate for imperfect calibration such that corresponding sensors in the X and Y arrays need only be "approximately" identical. During the course of our work we came more and more to regard the **ESPRIT** concept, the initial **ESPRIT** algorithm and corresponding array design, as a breakthrough in the field of sensor array signal processing much to the credit of the original inventors, Roy and Kailath. Our purpose here, therefore, was to advance the robustness and practical application of the **ESPRIT** concept.

CHAPTER 2
THE ESPRIT STRUCTURE AND ARRAY GEOMETRY

2.1 Introduction to ESPRIT

In this section we examine the basic principles and assumptions on which **ESPRIT** is based. For this, we must first present: (1) the "**ESPRIT** array system" and (2) the underlying signal model. The "**ESPRIT** array system" has already been briefly introduced in Chapter 1. Here, however, we explain in a more rigorous mathematical fashion why, as a result of the translational invariance between the X and Y subarrays comprising the "**ESPRIT** array system", the DOA matrices associated with these two subarrays are related through an invariance operator. Of course, the analysis depends heavily on the assumed signal model. For this reason, we devote a large portion of this chapter to the development of the underlying signal model and its complex representation. We begin with a discussion of the "**ESPRIT** array system".

Consider the array geometry illustrated in Figure 2.1. It is composed of M sensor pairs, called doublets, positioned in the plane z=0. For convenience, we shall assume that the k-th doublet is composed of sensors x_k , y_k k=1 . . M. Let us fix a rectangular reference frame whose basis vectors are the unit vectors along the x and y-axis respectively. In this coordinate frame, the position vectors of the x_k and y_k will be given by vectors $\hat{r}_k^x$ and $\hat{r}_k^y$ respectively. The spherical coordinate system is more appropriate for indicating source locations. The range of a source can be arbitrary, so the radial direction of a source is uniquely defined by its azimuth angle, θ, and its elevation angle, ϕ. Both parameters are specified in Figure 2.1.

Sensors within a doublet must satisfy two requirements. The first requirement is that the two sensors comprising a doublet must possess identical gain and phase characteristics. However, these characteristics may differ from doublet to doublet. The second requirement is that the displacement vector, $\hat{r}^d$ joining the x and y sensors of a doublet must identical for all doublets. With these assumptions in mind, let us consider a source located at any point on the straight line from the origin passing through the point specified by the triple

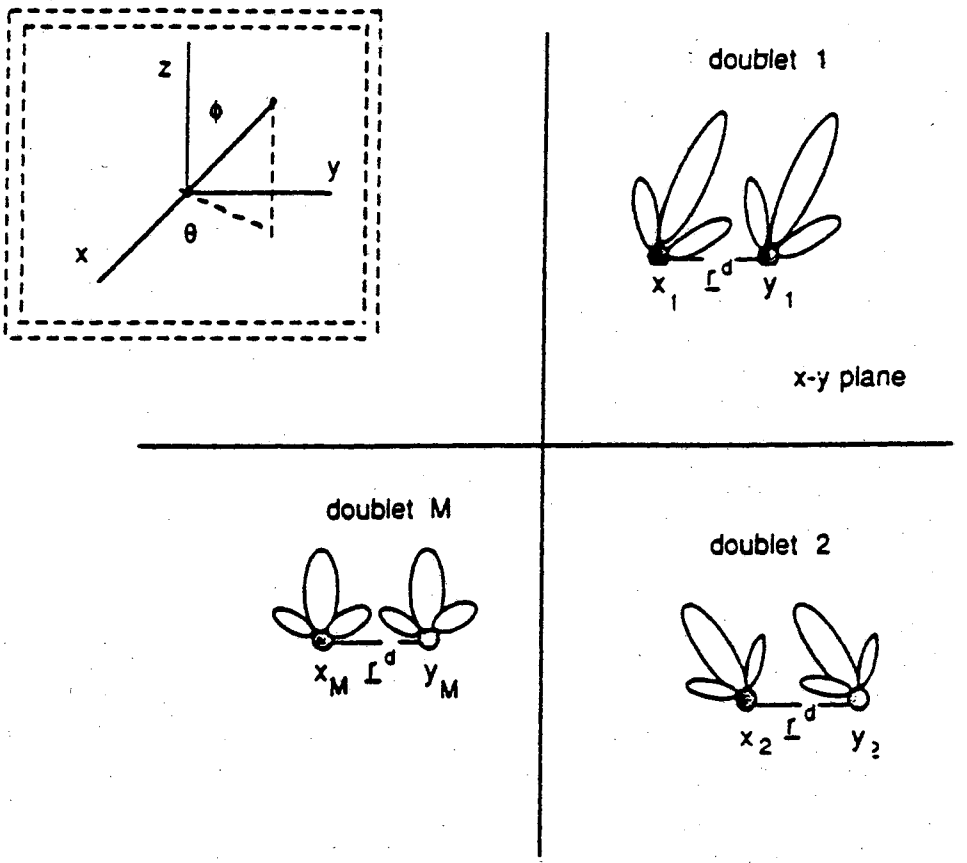

Figure 2.1 The generalized **ESPRIT** structure

$(\theta_p , \phi_p , \rho=1)$. If we take a unit vector along this direction, then the projection of this vector on the x-y plane is given by the vector

$$\hat{c}_p = u_p \hat{i} + v_p \hat{j} \quad \text{and} \tag{2.1}$$

$$u_p=\sin(\phi_p)\cos(\theta_p) \ , \ v_p=\sin(\phi_p)\sin(\theta_p)$$

$\hat{i}$ and $\hat{j}$ are the unit vectors along the x and y axis respectively. In literature, u_p and v_p are often referred to as the "direction cosines" of the source with respect to the x-axis and y-axis respectively. Let us, arbitrarily, take the origin as our reference point. Clearly, because of spatial separation, there will be a a temporal delay in the signal arriving at this point relative to the signal arriving at any other point on the array. If we concentrate on the k-th doublet, the delays τ_k^x and τ_k^y at sensors x_k and y_k respectively, corresponding to the p-th source are given by

$$\tau_k^x = \frac{\hat{c}_i \cdot \hat{r}_k^x}{c} \tag{2.2a}$$

$$\tau_k^y = \frac{\hat{c}_i \cdot \hat{r}_k^y}{c} = \tau_k^x + \frac{\hat{c}_i \cdot \hat{r}^d}{c} \tag{2.2b}$$

The speed of propagation of the wave in the given medium is denoted by the variable c. Referenced to the origin, the representation of a narrowband signal, u(t), received at a point on the array, is in general given by

$$u(t)=\sigma(t+\tau)\cos(2\pi f_o(t+\tau))$$

For simplicity, we assumed that the phase of u(t) is zero. If it is non-zero, but still of low frequency content compared to f_o, the final result will be the same. Let

$$\Psi(t)=u(t) + j\hat{u}(t) \tag{2.3}$$

where $\hat{u}(t)$ is the Hilbert transform of u(t). Then $\Psi(t)$ is the complex analytic representation of u(t). Under the assumption that $\sigma(t)$ is a low-pass signal,

$$\hat{u}(t)=\sigma(t+\tau)\sin(2\pi f_o(t+\tau))$$

and

$$\Psi(t)=\sigma(t+\tau)e^{j2\pi f_o\tau}e^{j2\pi f_o t} = s(t)e^{j2\pi f_o t} \tag{2.4a}$$

where

$$s(t) = \sigma(t+\tau)e^{j2\pi f_o\tau} \tag{2.4b}$$

The function s(t) is, by definition, the complex envelope of $\Psi(t)$. It is a trivial

task to show that the real and imaginary parts of s(t) can be obtained by frequency translation and low-pass filtering operations on u(t). For this reason, s(t) is, from now on, assumed to be the received signal.

If the p^{th} source generates a signal $s(t)=\sigma(t)$ at the origin, the signals generated at sensors x_k and y_k are delayed replicas of s(t), i.e.,

$$s_k^x(t)=\sigma(t)e^{j2\frac{\pi}{\lambda}\hat{c}_i \cdot \hat{r}_k^x} \tag{2.5}$$

$$s_k^y(t)=\sigma(t)e^{j2\frac{\pi}{\lambda}\hat{c}_i \cdot \hat{r}_k^x} e^{j2\frac{\pi}{\lambda}\hat{c}_i \cdot \hat{r}^d} \tag{2.6}$$

The low frequency content of $\sigma(t)$ has also allowed the approximation $\sigma(t+\tau) \simeq \sigma(t)$ to be used in (2.5) and (2.6). From these two equations follows that for each source there is a constant phase difference $2\frac{\pi}{\lambda}\hat{c}_p \cdot \hat{r}^d$ among the sensors comprising a doublet. **ESPRIT** exploits this fact to estimate the radial directions of the radiating sources. With D sources, $s_k^x(t)$ and $s_k^y(t)$ can be expressed as

$$s_k^x(t)=\sum_{l=1}^{D}\sigma_l(t)\alpha(l,k) + n_k^x(t) \tag{2.7}$$

$$s_k^y(t)=\sum_{l=1}^{D}\sigma_l(t)\phi(l)\alpha(l,k) + n_k^y(t) \tag{2.8}$$

where $\alpha(l,k)=\exp\{j2\frac{\pi}{\lambda}\hat{c}_l \cdot \hat{r}_k^x\}$, $\phi(l)=\exp\{j2\frac{\pi}{\lambda}\hat{c}_l \cdot \hat{r}^d\}$ and $n_k^x(t)$, $n_k^y(t)$ are, for the time being, assumed to be arbitrary random processes. In expressing $\alpha(l,k)$ as above we have assumed that the individual gain pattern of each antenna element is "broad", that is it is uniform for in the spatial interval we are interested in. For each sampling instant (snapshot), the data collected from $x_1\ x_2 \ldots x_M$ and $y_1\ y_2 \ldots y_M$ are grouped together in the Mx1 snapshot vectors

$$\mathbf{x}(n)=\left[x_1(n)\ x_2(n) \ldots\ldots x_M(n)\right]^T$$

$$\mathbf{y}(n)=\left[y_1(n)\ y_2(n) \ldots\ldots y_M(n)\right]^T$$

With N snapshots, the 2N snapshot vectors are appended next to each other to form the MxN matrices **X** and **Y**, where

$$\mathbf{X}=\left[\mathbf{x}(1)\ \mathbf{x}(2) \ldots\ldots \mathbf{x}(N)\right]$$

$$\mathbf{Y}=\left[\mathbf{y}(1)\ \mathbf{y}(2)\ .\ .\ .\ .\ .\ \mathbf{y}(N)\right]$$

X and Y can be easily decomposed into

$$\mathbf{X}=\mathbf{AS}+\mathbf{N_x}\ =\ \sum_{i=1}^{D}\mathbf{a}_i\mathbf{s}_i^T+\mathbf{N_x} \tag{2.9a}$$

$$\mathbf{Y}=\mathbf{A}\Phi\mathbf{S}+\mathbf{N_y}\ =\ \sum_{i=1}^{D}\Phi_{ii}\mathbf{a}_i\mathbf{s}_i^T+\mathbf{N_y} \tag{2.9b}$$

where :

$$\Phi=\mathrm{diag}\left[\Phi_{11},\Phi_{22}\ .\ .,\Phi_{DD}\right]\ ,\quad \Phi_{ii}=e^{j2\frac{\pi}{\lambda}\cos(\gamma_i)}\ ,\quad \cos(\gamma_i)=\hat{\mathbf{c}}_i.\hat{\mathbf{r}}^d \tag{2.10a}$$

$$\mathbf{S}=\left[\mathbf{s}_1\ \mathbf{s}_2\ .\ .\ .\ .\ .\ \mathbf{s}_D\right] \tag{2.10b}$$

$$\mathbf{s}_i^T=\left[\sigma_i(1)\ \sigma_i(2)\ \sigma_i(3)\ .\ .\ .\ .\ .\ \sigma_i(N)\right]$$

$$\mathbf{A}=\left[\mathbf{a}_1\ \mathbf{a}_2\ .\ .\ .\ .\ .\ \mathbf{a}_D\right] \tag{2.10c}$$

$$\mathbf{a}_i=\left[e^{j2\frac{\pi}{\lambda}\hat{\mathbf{c}}_i\,.\,\hat{\mathbf{r}}_1^x}\quad e^{j2\frac{\pi}{\lambda}\hat{\mathbf{c}}_i\,.\,\hat{\mathbf{r}}_2^x}\quad .\ .\ .\ .\ .\quad e^{j2\frac{\pi}{\lambda}\hat{\mathbf{c}}_i\,.\,\hat{\mathbf{r}}_M^x}\right]^T$$

The delineation assumptions underlying this model are in order. First, the D<M DOA vectors $\mathbf{a}_i$, comprising the columns of A, are linearly independent. This requires that no two sources have the same γ, the direction cosines with respect to the displacement axis. Finally, the D Nx1 vectors $\mathbf{s}_i$ must be linearly independent as well, i.e., no two signals can be fully correlated (coherent). A matrix pencil which possesses the structure exhibited in (2.9) is referred to as an **ESPRIT** data pencil. It can be constructed from any arbitrary array geometry which satisfies the previously mentioned conditions. A special case is the uniform linear array, which is discussed in Chapter 4. We point out that we are primarily interested in estimation of Φ_{ii} i=1,...,D, because the argument in the exponent of each Φ_{ii} contains the information relating to the bearing of the corresponding i^{th} source. The motivation behind **PRO–ESPRIT** is illustrated by the following observation.

$$\mathbf{Y}-\lambda\mathbf{X}=\sum_{j=1}^{D}(\Phi_{jj}-\lambda)\mathbf{a}_j\mathbf{s}_j^T \tag{2.11}$$

Under noise free conditions we observe that when $\lambda=\lambda_i=\Phi_{ii}$ the rank of the pencil

$\mathbf{Y}-\lambda\mathbf{X}$ drops by one. The set Φ_{11} , . , Φ_{DD} are thus generalized eigenvalues of the rectangular matrix pencil $\{\mathbf{Y}$, $\mathbf{X}\}$ under noise free conditions. This provides a means for isolating from the composite incident wave, that contribution due to a single source.

CHAPTER 3
EIGENANALYSIS OF THE ESPRIT DATA PENCIL

3.1 The ESPRIT Data Pencil With Noiseless Data

In this section, an analysis of the MxN **ESPRIT** data matrix pencil $\{\mathbf{Y},\mathbf{X}\}$ under idealized, noiseless conditions is made. The eigenstructure of the singular, rectangular matrix pencil obtained in this case is the foundation of the **PRO–ESPRIT** algorithm. That is, a treatment of the noiseless case is necessary for an understanding of the algorithms to be presented later in this section for dealing with the practical case of noise corrupted sensor data. Noise will be introduced and accounted for noise in the next section. In the no noise case, the data matrices, as defined by (2.9) with $\mathbf{N_x}=\mathbf{O}$ and $\mathbf{N_y}=\mathbf{O}$, are each of rank D, assuming $D<M$. We will emphasize this condition by a subscript D in the following manner

$$\mathbf{X_D} = \mathbf{AS} = \sum_{i=1}^{D} \mathbf{a}_i \mathbf{s}_i^T \tag{3.1a}$$

$$\mathbf{Y_D} = \mathbf{A\Phi S} = \sum_{i=1}^{D} \Phi_{ii} \mathbf{a}_i \mathbf{s}_i^T \tag{3.1b}$$

Examination of (3.1) reveals that the noiseless data matrices are quite similar in structure. Specifically, it is noted that they have the same D-dimensional column space, range$\{\mathbf{A}\}$, which is typically referred to in the literature as the "signal subspace", a term first coined by Schmidt [SCH86]. In addition to this, however, each matrix has the same row space, range$\{\mathbf{S}^T\}$, a D-dimensional subspace of N-dimensional space. This space, spanned by the D (complex) time series vectors, $\mathbf{s}_i$, $i=1,...,D$, associated with each of the D signal sources, is not so celebrated in the literature as is the signal subspace. Since this much neglected space has not heretofore been given a name, it will here referred to it as the "source subspace".

Exploiting these observations, a technique will be developed for reducing the MxN singular data matrix pencil $\{\mathbf{Y_D},\mathbf{X_D}\}$ to an "equivalent" square DxD matrix pencil having the same nonzero generalized eigenvalues (GEV's) as the original MxN pencil. The method hinges upon the use of the SVD to isolate the column

and row spaces of each of the data matrices, providing, in fact, orthonormal bases for each of these spaces. A brief expansion on this assertion using intuitive notions is in order; the mathematical derivation will follow shortly. The D "largest" left singular vectors of the "clean" Y data matrix, i. e., those associated with the D nonzero singular values, form an orthonormal basis for the signal subspace. The same is true of the D "largest" left singular vectors of the "clean" X data matrix. It follows, therefore, that a DxD unitary (invariant) transformation exists for rotating the one orthonormal basis into the other. Similar statements can be made regarding the right singular vectors. The D "largest" *right* singular vectors of the "clean" Y data matrix form an orthonormal basis for the *source* subspace, as do the the D "largest" right singular vectors of the "clean" X data matrix. Likewise, a DxD unitary transformation exists for rotating one of these into the other. These two unitary matrices, along with the two diagonal matrices containing the singular values of each of the two data matrices, are the sole components of the "equivalent" DxD (square) pencil. An eigenanalysis of this pencil will be referred to as processing at the *core rotations level.*

3.2 Reduction to DxD Pencil Via Simultaneous Subspace Rotations

Consider the singular value decompositions (SVD's) of the data matrices **X** and **Y** obtained with noiseless observations, i. e., with $\mathbf{N_x}=\mathbf{O}$ and $\mathbf{N_y}=\mathbf{O}$ in (2.9), and with each snapshot weighted by $\frac{1}{\sqrt{N}}$.

$$\frac{1}{\sqrt{N}}\mathbf{X}_D = \sum_{i=1}^{D} \sigma_{x_i} \mathbf{u}_{x_i} \mathbf{v}_{x_i}^H = \mathbf{U}_x^D \Sigma_x^D \mathbf{V}_x^{DH} \tag{3.2a}$$

$$\frac{1}{\sqrt{N}}\mathbf{Y}_D = \sum_{i=1}^{D} \sigma_{y_i} \mathbf{u}_{y_i} \mathbf{v}_{y_i}^H = \mathbf{U}_y^D \Sigma_y^D \mathbf{V}_y^{DH} \tag{3.2b}$$

A few comments are in order regarding the notation in (3.2). First the conventional SVD notation is adopted which presumes that the singular values are indexed in descending order. Second, the subscript D indicates that in the noiseless case, the data matrices are each of rank D as indicated previously. Third, the SVD description of the data matrices in (3.2) is such that only those right and left singular vectors associated with *nonzero* singular values are included. Consequently, $\mathbf{U}_x^D$, $\mathbf{V}_x^D$, and Σ_x^D are defined as follows

$$\mathbf{U}_x^D=[\mathbf{u}_{x_1}, \ldots, \mathbf{u}_{x_D}] \;\; ; \;\; \mathbf{V}_x^D=[\mathbf{v}_{x_1}, \ldots, \mathbf{v}_{x_D}] \tag{3.3}$$

$$\Sigma_x^D = \text{diag}\{\sigma_{x_1}, \ldots, \sigma_{x_D}\}$$

with similar definitions for $\mathbf{U}_y^D$, $\mathbf{V}_y^D$, and Σ_y^D. Finally, the weighting factor $\frac{1}{\sqrt{N}}$ is introduced so that the outer product of $\frac{1}{\sqrt{N}}\mathbf{X}$ with itself is the "standard" sample covariance matrix or, more specifically, the Maximum Likelihood (ML) estimate of the true covariance matrix when the data is corrupted by Gaussian noise. The weighting $\frac{1}{\sqrt{N}}$ may be also interpreted as a variance stabilizing factor. There is, of course, an intimate relationship between the SVD of $\frac{1}{\sqrt{N}}\mathbf{X}$ and the spectral decomposition (eigen-decomposition) of the sample covariance matrix. This relationship will be used shortly.

As a first step towards reducing the MxN **ESPRIT** data matrix pencil to a DxD pencil, note that in the noiseless case

$$\text{Range}\{\mathbf{U}_x^D\} = \text{Range}\{\mathbf{U}_y^D\} = \text{Range}\{\mathbf{A}\}$$

as described previously. This implies that the columns of $\mathbf{U}_x^D$ are an orthonormal basis for the signal subspace as are the columns of $\mathbf{U}_y^D$. As a consequence, the projection operator $\mathbf{U}_x^D\mathbf{U}_x^{DH}$ is identically equal to to the projection operator $\mathbf{U}_y^D\mathbf{U}_y^{DH}$, the unique projection operator onto the signal subspace. From this it follows that $\mathbf{Q}_u = \mathbf{U}_x^{DH}\mathbf{U}_y^D$ is unitary which can be seen from the following argument.

$$\mathbf{Q}_u^H\mathbf{Q}_u = \mathbf{U}_y^{DH}\mathbf{U}_x^D\mathbf{U}_x^{DH}\mathbf{U}_y^D = \mathbf{U}_y^{DH}\mathbf{U}_y^D\mathbf{U}_y^{DH}\mathbf{U}_y^D = \mathbf{I}_D$$

with a similar argument to show $\mathbf{Q}_u\mathbf{Q}_u^H = \mathbf{I}_D$. From these observations, it also follows that

$$\mathbf{U}_y^D = \mathbf{U}_x^D\mathbf{Q}_u \qquad \text{where: } \mathbf{Q}_u = \mathbf{U}_x^{DH}\mathbf{U}_y^D \tag{3.4}$$

which represents an invariant subspace rotation.

A similar development concerning the right singular vectors follows from the observation that in the noiseless case

$$\text{Range}\{\mathbf{V}_x^D\} = \text{Range}\{\mathbf{V}_y^D\} = \text{Range}\{\mathbf{S}^H\}$$

This implies that the columns of $\mathbf{V}_x^D$ are an orthonormal basis for the **source** subspace as are the columns of $\mathbf{V}_y^D$. Proceeding along lines similar to the above, it is easily shown that $\mathbf{Q}_v = \mathbf{V}_x^{DH}\mathbf{V}_y^D$ is the DxD unitary matrix which performs the following invariant subspace rotation.

$$\mathbf{V}_y^D = \mathbf{V}_x^D\mathbf{Q}_v \qquad \text{where: } \mathbf{Q}_v = \mathbf{V}_x^{DH}\mathbf{V}_y^D \tag{3.5}$$

The utility of the above observations, (3.4) and (3.5) specifically, becomes apparent after substituting and factoring out as follows

$$\frac{1}{\sqrt{N}}\mathbf{Y}_D - \lambda\frac{1}{\sqrt{N}}\mathbf{X}_D = \mathbf{U}_y^D\Sigma_y^D\mathbf{V}_y^{DH} - \lambda\mathbf{U}_x^D\Sigma_x^D\mathbf{V}_x^{DH} \tag{3.6}$$

$$= \mathbf{U}_x^D\mathbf{Q}_u\Sigma_y^D\mathbf{Q}_v^H\mathbf{V}_x^{DH} - \lambda\mathbf{U}_x^D\Sigma_x^D\mathbf{V}_x^{DH}$$

$$= \mathbf{U}_x^D\left\{\mathbf{Q}_u\Sigma_y^D\mathbf{Q}_v^H - \lambda\Sigma_x^D\right\}\mathbf{V}_x^{DH}$$

It is now immediately apparent that the GEV's of the DxD matrix pencil $\{\mathbf{Q}_u\Sigma_y^D\mathbf{Q}_v^H\ ,\ \Sigma_x^D\}$, referred to here as the *core information pencil (CIM)* for reasons that will become increasingly apparent later on, are the D nonzero (stable) GEV's of the MxN singular pencil $\{\frac{1}{\sqrt{N}}\mathbf{Y}_D,\ \frac{1}{\sqrt{N}}\mathbf{X}_D\}$. The algorithm based on this result is coined the Procrustes ROtations based **ESPRIT** algorithm, or **PRO–ESPRIT**. The reason for the reference to Procrustes will become apparent when noisy data are considered. **PRO–ESPRIT** states that the set $\{\Phi_{11},\Phi_{22},...,\Phi_{DD}\}$, defined in (2.10a), are the D generalized eigenvalues (GEV's) of the DxD CIM $\{\mathbf{Q}_u\Sigma_y^D\mathbf{Q}_v^H\ ,\ \Sigma_x^D\}$, or, equivalently, the eigenvalues (EV's) of the DxD matrix $\Sigma_x^{D-1}\mathbf{Q}_u\Sigma_y^D\mathbf{Q}_v^H$. Ultimately methods for estimating $\mathbf{Q}_u$ and $\mathbf{Q}_v$ in practice will be presented , based on the solution to the Procrustes problem. Before proceeding we must make some remarks regarding the computation of the SVD's of the two data matrices. These observations will have implications later with regard to the computation and bias of our estimators of the two unitary matrices, $\mathbf{Q}_u$ and $\mathbf{Q}_v$.

It is stressed that all the information needed to construct the SVD of $\frac{1}{\sqrt{N}}\mathbf{X}_D$, as described by (3.2a), can be extracted from an eigen-decomposition of the MxM noiseless ("clean") covariance matrix associated with the X array data, denoted $\mathbf{C}_{xx}$, defined by

$$\mathbf{C}_{xx} = \frac{1}{N}\mathbf{X}_D\mathbf{X}_D^H = \mathbf{A}(\frac{1}{N}\mathbf{S}\mathbf{S}^H)\mathbf{A}^H = \mathbf{A}\hat{\mathbf{R}}_{ss}\mathbf{A}^H \tag{3.7}$$

where $\hat{\mathbf{R}}_{ss} = \frac{1}{N}\mathbf{S}\mathbf{S}^H$ is the sample source covariance matrix. This is due to the observation that $\{\sigma_{x_i}^2\ ,\ \mathbf{u}_{x_i}\}$, i=1,...,D, are the D nonzero EV's and corresponding EVEC's, respectively, of $\mathbf{C}_{xx}$ and the fact that

$$\mathbf{v}_{x_i} = \frac{1}{\sigma_{x_i}}\frac{1}{\sqrt{N}}\mathbf{X}_D^H\mathbf{u}_{x_i} \qquad i=1,...,D \tag{3.8}$$

which follows from the classical relationship between the left and right singular vectors of a matrix. Given the quantities defined in (3.3), the D right singular

vectors described by (3.8) can be expressed in the following collective fashion

$$\mathbf{V}_x^D = \frac{1}{\sqrt{N}}\mathbf{X}^H\mathbf{U}_x^D\Sigma_x^{D-1} \tag{3.9}$$

Parallel statements can be made regarding the singular values and left and right singular vectors of $\frac{1}{\sqrt{N}}\mathbf{Y}_D$. Specifically, $\{\sigma_{y_i}^2, \mathbf{u}_{y_i}\}$ i=1,...,D, are the D nonzero EV's and corresponding EVEC's, respectively, of the "clean" Y covariance matrix, $\mathbf{C}_{yy}$, as indicated by

$$\mathbf{C}_{yy} = \frac{1}{N}\mathbf{Y}_D\mathbf{Y}_D^H = \mathbf{U}_y^{DH}\Sigma_y^{D\,2}\mathbf{U}_y^{DH} \tag{3.10}$$

Also, the D right singular vectors associated with the D nonzero singular values can be computed collectively according to

$$\mathbf{V}_y^D = \frac{1}{\sqrt{N}}\mathbf{Y}^H\mathbf{U}_y^D\Sigma_y^{D-1} \tag{3.11}$$

It should be noted, though, that the condition number of the correlation matrix is the square of the respective data matrix such that determination of the components of the SVD in this manner is typically not preferred due to numerical considerations [ZOLT87b]. Nonetheless, these relationships do lead to alternative formulations of **PRO–ESPRIT** which do not require computation of the SVD of two MxN data matrices, a task which may be quite cumbersome if N is large. This statement is clarified with the following observation. Note that by forming the product $\mathbf{V}_x^{DH}\mathbf{V}_y^D$ formed with the expressions for $\mathbf{V}_x^D$ and $\mathbf{V}_y^D$ in (3.9) and (3.11), respectively, and denoting $\mathbf{C}_{xy} = \frac{1}{N}\mathbf{X}_D\mathbf{Y}_D^H$ as the "clean" cross-correlation matrix between the X and Y arrays, one can obtain

$$\mathbf{Q}_v = \mathbf{V}_x^{DH}\mathbf{V}_y^D = \Sigma_x^{D-1}\mathbf{U}_x^{DH}\mathbf{C}_{xy}\mathbf{U}_y^D\Sigma_y^{D-1} \tag{3.12}$$

This indicates that the unitary transformation which rotates the **right** singular vectors of the X data matrix into that of the Y data matrix can be expressed in terms of the **left** singular vectors of both matrices, along with the corresponding nonzero singular values, and the MxM "clean" cross-correlation matrix, $\mathbf{C}_{xy}$. The utility of this result has to do with the fact that, in contrast to the situation with the left singular vectors and the singular values, it is not possible to extract asymptotically unbiased estimates of the right singular vectors from the data matrices. Although this issue will be addressed more fully later on, it is pointed out here that one can only do a perfect cleaning out of the **effect** of noise at the statistical level, the covariance level, for example, and this can only be done in the asymptotic case and requires some a-priori knowledge of the inter-sensor noise correlations. In contrast, there can not be a perfect cleaning out of the noise at the data level even in the asymptotic case. The virtue of (3.12) is that despite the fact that the development of **PRO–ESPRIT** was based on observations made at

the data level, it is possible nonetheless to express $\mathbf{Q}_v$ in terms of quantities for which there asymptotically unbiased estimators: Σ_x^D, $\mathbf{U}_x^{DH}$, $\mathbf{C}_{xy}$, $\mathbf{U}_y^D$, and Σ_y^D. In addition, this observation enables one to avoid working in N-dimensional space, which has implications in terms of both computational load and memory space if N is large as indicated above. It is worth mentioning again, however, that with regard to numerical stability, working with the data matrices directly, as opposed to working with the correlation matrices as sufficient statistics, may be preferred due to the issue of condition number mentioned previously [ZOLT87b]. The problem of "conditioning" has implications in scenarios where the sources are highly correlated or when the SNR is low.

3.3 The Significance of the Left and Right GEVEC's

In this section we examine the importance of the right and left generalized eigenvectors (GEVEC's) of the singular data pencil $\{\frac{1}{\sqrt{N}}\mathbf{Y}_D, \frac{1}{\sqrt{N}}\mathbf{X}_D\}$ and their relation to the corresponding GEVEC's of the CIM. These will be those left and right GEVEC's associated with the non-zero GEV's Φ_{ii}, i=1,..,D. The columns of $\mathbf{U}_x^D$ and $\mathbf{V}_x^D$ will used as an orthonormal basis for the signal and source subspace, respectively. Define a right GEVEC of the data matrix pencil, $\mathbf{r}_i$, in the following manner.

$$\left\{\mathbf{Y}_D-\lambda_i\mathbf{X}_D\right\}\mathbf{r}_i=\mathbf{0} \quad \mathbf{r}_i\in \text{Range}\{\mathbf{V}_x^D\} \quad i=1,..,D \tag{3.13}$$

In order to comply with the given constraint, let $\mathbf{r}_i=\mathbf{V}_x^D\beta_i$ where β_i is a Dx1 vector, and substitute

$$\left\{\mathbf{Y}_D-\lambda_i\mathbf{X}_D\right\}\mathbf{V}_x^D\beta_i=\mathbf{U}_x^D\left\{\mathbf{Q}_u\Sigma_y^D\mathbf{Q}_v^H-\lambda_i\Sigma_x^D\right\}\mathbf{V}_x^{DH}\mathbf{V}_x^D\beta_i=\mathbf{0} \tag{3.14}$$

But the columns of $\mathbf{V}_x^D$ are orthonormal and $\mathbf{U}_x^D$ has full rank, therefore β_i is a right eigenvector associated with the DxD matrix $\Sigma_x^{D-1}\mathbf{Q}_u\Sigma_y^D\mathbf{Q}_v^H$. For future purposes, define

$$\mathbf{B}=[\beta_1,\beta_2,....,\beta_D] \tag{3.15}$$

It will become apparent as we proceed that a lot of the quantifying information for classifying and extracting the various signal source components can be extracted from **B**. This is the motivation for the descriptor "core".

The significance of the right GEVEC's is determined by recalling that the noiseless form of the matrix in (3.2) to express the problem prescribed in (3.13) in the following manner.

$$\left\{\sum_{j=1}^{D}(\Phi_{ii}-\lambda_j)\mathbf{a}_j\mathbf{s}_j^T\right\}\mathbf{r}_i=\mathbf{0} \quad \mathbf{r}_i\in \text{span}\{\mathbf{s}_1^*,..,\mathbf{s}_D^*\} \tag{3.16}$$

When $\lambda_i=\Phi_{ii}$, the i-th term of the sum drops out. Assuming that the $\mathbf{s}_j^T$, $j=1,..,D$ are linearly independent, i.e, no two sources are 100% correlated, it follows that $\mathbf{r}_i$ is orthogonal to the conjugate of each of the signal vectors $\mathbf{s}_j$ except the i-th one. This relationship can be represented by

$$\mathbf{s}_j^T\mathbf{r}_i\propto\delta_{ij} \quad i,j=1,..,D \tag{3.17}$$

where δ_{ij} is the Kronecker delta. From this property the following relationship also holds.

$$\frac{1}{\sqrt{N}}\mathbf{X}_D\mathbf{r}_i=\mathbf{U}_x^D\Sigma_x^D\beta_i=\xi_i\mathbf{a}_i \tag{3.18}$$

That is, the vector $\mathbf{X}_D\mathbf{r}_i$ which can be obtained by telescoping from the core rotations level GEVEC β_i to the data level via the eigen-link transformation $\mathbf{U}_x^D\Sigma_x^D$ is a scalar multiple of the DOA vector of the i-th source. The presence of the unknown multiplicative constant ξ_i reflects a fundamental ambiguity that cannot be resolved and which arises in all **ESPRIT** like algorithms. Thus, we can only determine the relative gains and phases among the array elements in the direction of the D arriving waveforms. If the gain and phase characteristics of just one of the sensors is known, we can determine the DOA vectors for the D arrival directions as discussed by ROY [ROY88b].

We next consider the significance of the left GEVEC's of the data pencil $\{\frac{1}{\sqrt{N}}\mathbf{Y}_D, \frac{1}{\sqrt{N}}\mathbf{X}_D\}$. These vectors are defined in a manner analogous to (3.13).

$$\mathbf{l}_i^H\left\{\mathbf{Y}_D-\lambda_i\mathbf{X}_D\right\}=\mathbf{0} \quad \mathbf{l}_i\in\text{Range}\{\mathbf{U}_x^D\} \quad i=1,..,D \tag{3.19}$$

In order to comply with the constraint, let $\mathbf{l}_i=\mathbf{U}_x^D\alpha_i$ where α_i is a Dx1 vector, and substitute in (3.19).

$$\alpha_i^H\mathbf{U}_x^{DH}\left\{\mathbf{Y}_D-\lambda_i\mathbf{X}_D\right\}=\alpha_i^H\mathbf{U}_x^{DH}\mathbf{U}_x^D\left\{\mathbf{Q}_u\Sigma_y^D\mathbf{Q}_v^H-\lambda_i\Sigma_x^D\right\}\mathbf{V}_x^{DH}=\mathbf{0} \tag{3.20}$$

Since the columns of $\mathbf{U}_x^D$ are orthonormal and $\mathbf{V}_x^D$ is of full rank, it follows that α_i is a left GEVEC associated with the matrix pencil $\mathbf{Q}_u\Sigma_y^D\mathbf{Q}_v^H$, Σ_x^D. Note that if $\mathbf{B}$ is the matrix whose columns are the D right GEVEC's β_i $i=1,..,D$ of the core informations matrix as defined before, it can be easily shown that the columns of $(\mathbf{B}^H\Sigma_x^D)^{-1}$ are the α_i that we seek. That is

$$(\mathbf{B}^{H}\Sigma_{\mathbf{x}}^{D})^{-1} = [\alpha_1, \alpha_2, \ldots, \alpha_D] \tag{3.21}$$

The point is that only the right GEVEC's need to be computed since the left ones can be derived from the above relationship.

The significance of λ_i i=1,..,D is determined by recalling the noiseless form of the matrix pencil in (2.19) to rewrite the problem in (3.19) in the following manner:

$$\mathbf{l}_i^{H}\left\{\sum_{j=1}^{D}(\Phi_{ii}-\lambda_j)\mathbf{a}_j\mathbf{s}_j^{T}\right\}=\mathbf{0} \quad \mathbf{l}_i \in \text{ span}\{\mathbf{a}_1,..,\mathbf{a}_D\} \tag{3.22}$$

Again, if $\lambda_i=\Phi_{ii}$, the i-th term of the sum drops out. Take for example $\mathbf{l}_1$. It follows therefore that $\mathbf{l}_1 \propto \alpha_1 = \mathbf{P}_1^{\perp}\alpha_1$, where $\mathbf{P}_1^{\perp}$ is the projection operator onto the span of $\{\mathbf{a}_1,..,\mathbf{a}_D\}$. In other words, $\mathbf{l}_1$ produces an array pattern exhibiting a null in each of the directions $\vec{u}_2$ through $\vec{u}_D$ and has no projection on to the noise subspace. This is the so called "optimal signal copy vector"
that is a weight vector steered in the direction of $\vec{u}_1$ which minimizes the contribution due to the noise while constraint to have a null in each of the other source directions. This may be useful in cases when the remaining sources are some undesirable interference. Collectively, the left GEVEC's satisfy the following relationship.

$$\mathbf{l}_i^{H}\alpha_j \propto \delta_{ij} \quad i,i=1,..,D \tag{3.23}$$

Let $\mathbf{L}=[\mathbf{l}_1,..,\mathbf{l}_D] = \mathbf{U}_{\mathbf{x}}^{D}\Sigma_{\mathbf{x}}^{D-1}\mathbf{B}^{-H}$. Pre-multiplication of $\mathbf{X}_D$ by $\mathbf{L}^{H}$ produces the signal source matrix $\mathbf{S}$ to within a diagonal matrix as mathematically described below.

$$\mathbf{L}^{H}\mathbf{X}_D=\mathbf{B}^{-1}\Sigma_{\mathbf{x}}^{D-1}\mathbf{U}_{\mathbf{x}}^{DH}\mathbf{A}\mathbf{S}=\Lambda_{\mathbf{A}}\mathbf{S} \tag{3.24}$$

or individually,

$$\mathbf{l}_i^{H}\mathbf{x}_D=\alpha_i^{H}\mathbf{U}_{\mathbf{x}}^{DH}\mathbf{X}_D=\alpha_i^{H}\Sigma_{\mathbf{x}}^{D}\mathbf{V}_{\mathbf{x}}^{DH}=\zeta_i\mathbf{s}_i^{T} \tag{3.25}$$

where $\Lambda_{\mathbf{A}}$ is a DxD diagonal matrix. So we have that $\mathbf{l}_i^{H}\mathbf{X}_D$ is a scalar multiple of $\mathbf{s}_i^{T}$, the Nx1 vector containing the N samples of the narrowband signal associated with the i-th wavefront. Once again, the presence of the unknown factor ζ_i reflects a fundamental ambiguity that cannot be resolved.

It should be noted that the left and right GEVEC's of the rectangular data pencil as defined before are normalized according to the same convention a the left and right GEVEC's of a square matrix. For example, the left and right GEVEC's of the core informations matrix, α_i and β_i i=1,..,D respectively, are normalized as follows.

$$\alpha_i^H \mathbf{Q}_u \Sigma_y^D \mathbf{Q}_v^H \beta_i = \Phi_{ii} \qquad \alpha_i^H \Sigma_x^D \beta_i = 1 \quad i=1,..,D \tag{3.26}$$

The eigen-links between the left and right GEVEC's of $\{\frac{1}{\sqrt{N}}\mathbf{Y}_D\ ,\ \frac{1}{\sqrt{N}}\mathbf{X}_D\}$ and those of the DxD core informations pencil is given by $\mathbf{l}_i = \mathbf{U}_x^D \alpha_i$ and $\mathbf{r}_i = \mathbf{V}_x^D \beta_i$ respectively. In the noiseless case, it is not hard to see that the following expressions must hold

$$\mathbf{l}_i^H \frac{1}{\sqrt{N}} \mathbf{Y}_D \mathbf{r}_i = \Phi_{ii} \qquad \mathbf{l}_i^H \frac{1}{\sqrt{N}} \mathbf{X}_D \mathbf{r}_i = 1 \tag{3.27}$$

which follow from the relationship between α_i and β_i above.

From before,

$$\mathbf{l}_i = \eta_i \{\alpha_i - \mathbf{P}_i^{\downarrow} \alpha_i\} \quad , \quad \frac{1}{\sqrt{N}} \mathbf{X}_D \mathbf{r}_i = \xi_i \alpha_i, i=1,..,D \tag{3.28}$$

where η_i and ξ_i are unknown multiplicative constants. Let $\gamma_i = \mathbf{a}_i^H [\mathbf{I} - \mathbf{P}_i^{\downarrow}] \mathbf{a}_i$ such that (3.24) can be written as

$$\mathbf{l}_i^H \mathbf{X}_D = \zeta_i \mathbf{s}_i^T = \eta_i^* \gamma_i \mathbf{s}_i^T \quad i=1,..,D \tag{3.29}$$

This indicates that $\zeta_i = \eta_i^* \gamma_i \mathbf{s}_i^T$. Invoking the normalization criteria described before, it follows that

$$\mathbf{l}_i^H \frac{1}{\sqrt{N}} \mathbf{X}_D \mathbf{r}_i = \zeta_i \xi_i = 1 \quad i=1,..,D \tag{3.30}$$

That is, although without any prior information we cannot determine the unknown multiplicative constants, we know that their product is unity. This information combined with previous results lead us to a means for decomposing the incident wavefield based on the following result.

$$\frac{1}{\sqrt{N}} \mathbf{X}_D \mathbf{r}_i \mathbf{l}_i^H \mathbf{X}_D = \xi_i \mathbf{a}_i \zeta_i \mathbf{s}_i^T = \mathbf{a}_i \mathbf{s}_i^T \quad i=1,..,D \tag{3.31}$$

This result indicates that we are able to isolate from the composite wavefield that contribution due to a single source without ambiguity. An alternative expression for decomposing the incident wavefield in terms of eigen-information derived from the core rotations level.

$$\mathbf{U}_x^D \Sigma_x^D \{\beta_i \alpha_i^H\} \mathbf{U}_x^{DH} \mathbf{X}_D = \mathbf{a}_i \mathbf{s}_i^T \quad i=1,..,D \tag{3.32}$$

This exemplifies the process of telescoping from the core rotations level to the data level via eigen-link transformations derived at the covariance level.

These results can further be used to extract elements of the sample covariance matrix $\hat{\mathbf{R}}_{ss}$ from the **ESPRIT** data pencil. The elements of $\hat{\mathbf{R}}_{ss}$ will give estimates of the source powers and their correlation. From the properties of the left GEVEC's, of the data pencil, it follows that

$$\frac{1}{N}\mathbf{L}^{H}\mathbf{X}_{D}\mathbf{X}_{D}^{H}\mathbf{L}=\mathbf{L}^{H}\mathbf{C}_{xx}\mathbf{L}=\Lambda_{A}\frac{1}{N}\mathbf{S}\mathbf{S}^{H}\Lambda_{A}^{*}=\Lambda\hat{\mathbf{R}}_{ss}\Lambda_{A}^{*} \tag{3.33}$$

where Λ_A is an unknown DxD core rotations matrix defined before. Telescoping to the core rotations level via the relationships $\mathbf{L}=\mathbf{U}_{x}^{D}\Sigma_{x}^{D-1}\mathbf{B}^{-H}$ and $\mathbf{C}_{xx}=\mathbf{U}_{x}^{D}\Sigma_{x}^{D2}\mathbf{U}_{x}^{DH}$ gives

$$\frac{1}{N}\mathbf{L}^{H}\mathbf{X}_{D}\mathbf{X}_{D}^{H}\mathbf{L}=\frac{1}{N}\mathbf{B}^{-1}\mathbf{B}^{-H}=\frac{1}{N}(\mathbf{B}^{H}\mathbf{B})^{-1} \tag{3.34}$$

We can use these results to get rid of the ambiguity due to the presence of Λ_A in (3.33). For this, consider the following result.

$$\frac{1}{\sqrt{N}}\mathbf{r}_{i}^{H}\mathbf{X}_{D}^{H}\{\frac{1}{\sqrt{N}}\mathbf{X}_{D}\mathbf{r}_{i}\mathbf{l}_{i}^{H}\mathbf{X}_{D}\}\mathbf{X}_{D}^{H}\mathbf{l}_{i}=\|\mathbf{a}_{i}\|^{2}\mathbf{s}_{i}^{T}\mathbf{s}_{i}^{*} \tag{3.35}$$

where $\|\|$ os the standard 2-norm. We again telescope to the core rotations level via the appropriate eigen-links to express the above result in the following form.

$$(\alpha_{i}^{H}\Sigma_{x}^{D2}\alpha_{i})(\beta_{i}^{H}\Sigma_{x}^{D2}\beta_{i})=\|\mathbf{a}_{i}\|^{2}\mathbf{s}_{i}^{T}\mathbf{s}_{i}^{*} \qquad i=1,..,D \tag{3.36}$$

Assume for a moment that the magnitude of the DOA vectors is known and consider dividing both sides of (3.36) by $\|\mathbf{a}_i\|^2$ and N, to obtain

$$\mathbf{R}_{ss_{ii}}=\frac{1}{N}\mathbf{s}_{i}^{T}\mathbf{s}_{i}^{*}=\frac{1}{N}(\alpha_{i}^{H}\Sigma_{x}^{D2}\alpha_{i})\left\{\frac{(\beta_{i}^{H}\Sigma_{x}^{D2}\beta_{i})}{\|\mathbf{a}_{i}\|^{2}}\right\} \qquad i=1,..,D \tag{3.37}$$

where $\hat{\mathbf{R}}_{ss}$ is the sample covariance matrix. It is easily verified invoking the relations between right and left GEVEC's that $(\alpha_{i}^{H}\Sigma_{x}^{D2}\alpha_{i})$, i=1,..,D are the diagonal elements of $(\mathbf{B}^{H}\mathbf{B})^{-1}$. Hence, define

$$\Lambda_{P_{ii}}=\left\{\frac{(\beta_{i}^{H}\Sigma_{x}^{D2}\beta_{i})}{\|\mathbf{a}_{i}\|^{2}}\right\}^{1/2} \qquad i=1,..,D \tag{3.38}$$

such that the diagonal elements of

$$|\hat{\mathbf{R}}_{ss}|=\Lambda_{P}\frac{1}{N}(\mathbf{B}^{H}\mathbf{B})^{-1}\Lambda_{p} \tag{3.39}$$

agree exactly with those of $\hat{\mathbf{R}}_{ss}$. The off diagonal elements of the two matrices differ by some scalar of unity magnitude. So this is one method for estimating the source powers and cross correlations to within some unknown phase. The only drawback of this method is that it requires prior knowledge of the DOA vectors. A schematic representation of the eigen-links between the data level and core rotations level is shown in Figure 3.1.

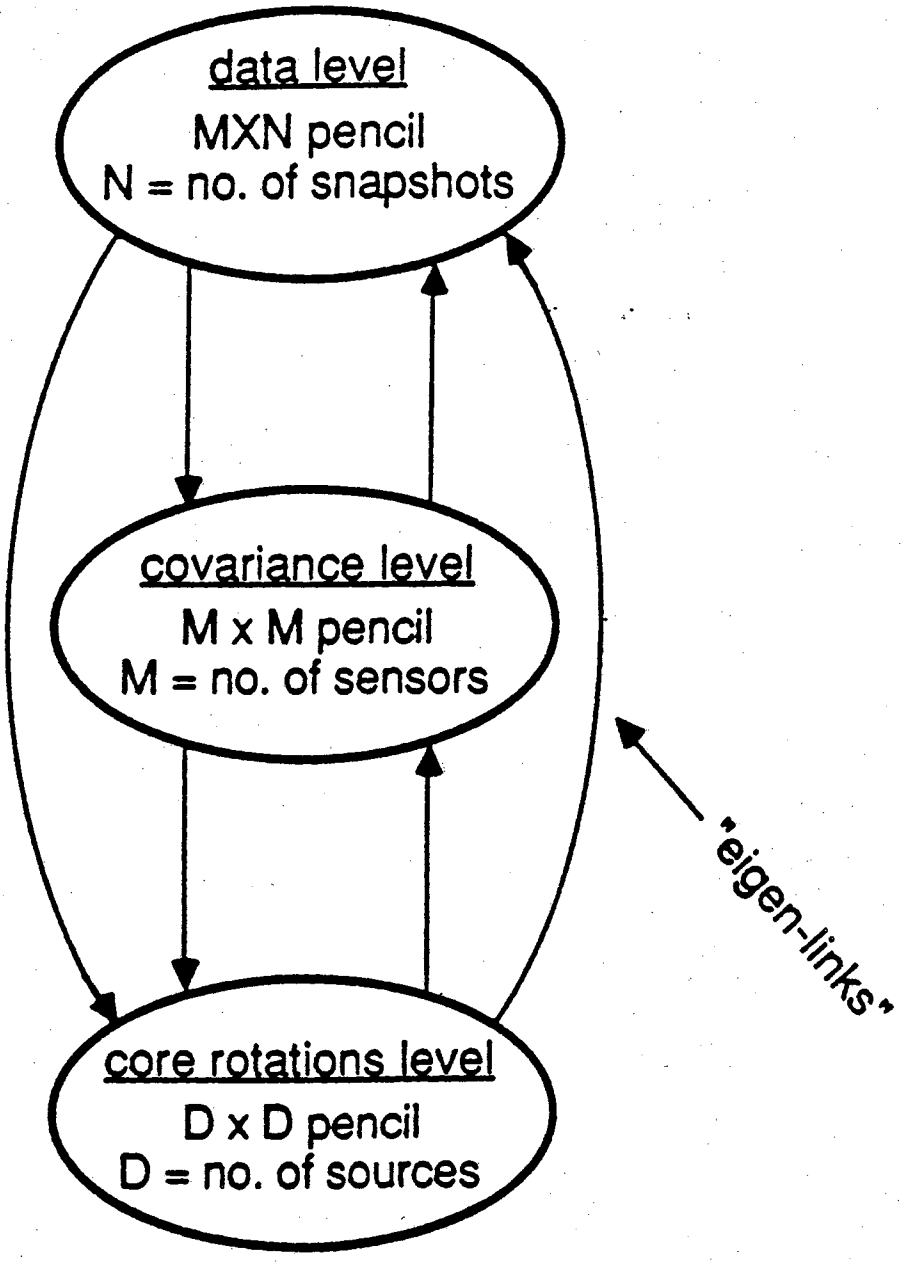

Figure 3.1 Schematic representation of the eigen-links between the data level and the core rotations level.

3.4 Estimation of the Core Rotations Pencil with Noisy Data

The discussion in this subsection centers around the topic of noise corrupting the sampled data and the measures that can be taken to counteract its effect. Although **PRO–ESPRIT** was based on the properties governing the column and row spaces of the **X** and bold **Y** matrix pencils , it was finally concluded that having clean estimates of the auto and cross-correlation matrices of **X** and **Y** was sufficient to construct the core rotations matrix pencil $\{\mathbf{Q}_U\Sigma_Y^D\mathbf{Q}_V^H , \Sigma_X^D\}$. As the first step of the "cleaning" procedure , define **Z** and its associated correlation matrix $\mathbf{R}_{ZZ}$ in the following manner ,

$$\mathbf{Z} = \begin{bmatrix}\mathbf{X}\\ \mathbf{Y}\end{bmatrix} \quad , \quad \hat{\mathbf{R}}_{ZZ}=\frac{1}{N}\mathbf{Z}\mathbf{Z}^H \tag{3.40}$$

The noise is additive , therefore asymptotically $\hat{\mathbf{R}}_{ZZ}$ can be expressed as

$$\hat{\mathbf{R}}_{ZZ} = \mathbf{C}_{ZZ} + \lambda_{min}^{ZZ}\mathbf{R}_{nn}^{ZZ} \tag{3.41}$$

where $\mathbf{C}_{ZZ}$ can be partitioned into

$$\mathbf{C}_{ZZ} = \begin{bmatrix}\mathbf{C}_{XX} & \mathbf{C}_{XY}\\ \mathbf{C}_{YX} & \mathbf{C}_{YY}\end{bmatrix} \tag{3.42}$$

$\mathbf{C}_{XX}$, $\mathbf{C}_{YY}$ and $\mathbf{C}_{XY}$ are the "clean" quantities that are required to derive the core information matrix pencil. Depending on the a-priori information about the noise correlation matrix $\mathbf{R}_{nn}^{ZZ}$, a different cleaning procedure must be followed accordingly. In the first case , suppose that $\mathbf{R}_{nn}^{ZZ}$ is a predetermined matrix but λ_{min}^{ZZ} is unknown. Asymptotically , $\mathbf{C}_{ZZ}$ should be of rank 2M-D so in considering its eigenvalue decomposition , the eigenvalue λ=0 should have a multiplicity also 2M-D. Let $\mathbf{e}_i$ be an eigenvector of $\mathbf{C}_{ZZ}$ corresponding to λ=0. Thus $\mathbf{C}_{ZZ}\mathbf{e}_i = 0$. By simple manipulations , it can be shown that

$$\mathbf{R}_{ZZ}\mathbf{e}_i = \lambda_{min}^{ZZ}\mathbf{R}_{nn}^{ZZ}\mathbf{e}_i \tag{3.43}$$

In words , (3.43) says that if a generalized eigenvalue decomposition (GEV) of the matrix pencil $\{\mathbf{R}_{ZZ} , \mathbf{R}_{nn}^{ZZ}\}$ is performed , then the smallest 2M-D eigenvalues should be equal to λ_{min}^{ZZ}. Of course this is an asymptotic result. With a finite number of snapshots , the arithmetic mean of the smallest 2M-D eigenvalues of the above pencil provides a reasonably good estimate of $\hat{\lambda}_{min}^{ZZ}$. Knowing $\mathbf{R}_{nn}^{ZZ}$ and $\hat{\lambda}_{min}^{ZZ}$, $\mathbf{C}_{ZZ}$ is obtained from (3.41).

Frequently however , there is no knowledge concerning the structure of $\mathbf{R}_{nn}^{ZZ}$. A technique to estimate it was recently presented by LeCadre [LEC89]. The method is based on ARMA model of the sensor noises in the spatial domain , as

opposed to the temporal domain. Once an estimate of $\mathbf{R}_{nn}^{zz}$ is obtained , the procedure described for the first case can be utilized to predict $\hat{\lambda}_{min}^{zz}$ and ultimately $\mathbf{C}_{zz}$

3.5 On the Asymptotic Unbiasedness of PRO-ESPRIT

From the discussion so far , it follows that **PRO–ESPRIT** can provide asymptotically unbiased estimates (a.u.e's) for the following components of the core rotations and **ESPRIT** data pencil.

- a. u. e. of "clean" X-Y cross-correlation matrix $\mathbf{C}_{xy}$
- a. u. e.'s of "clean" eigendata: $\mathbf{U}_x^D$, Σ_x^D, $\mathbf{U}_y^D$, and Σ_y^D
- a. u. e.'s of unitary matrices $\mathbf{Q}_u$ and $\mathbf{Q}_v$
- a. u. e.'s of core information pencil eigendata: Φ_{ii}, α_i, and β_i, i=1,...,D.
- a. u. e.'s of array manifold vectors $\mathbf{a}_i$, i=1,...,D, each to within a scalar multiple.
- a. u. e.'s of optimum signal copy vectors: $\mathbf{l}_i$, i=1,...,D.
- a. u. e. of source covariance matrix, $\mathbf{R}_{ss}$, to within a diagonal unitary matrix

The $\mathbf{l}_i$'s are defined as the left generalized eigenvectors of the MxN pencil $\{\frac{1}{\sqrt{N}}\mathbf{Y}_D , \frac{1}{\sqrt{N}}\mathbf{X}_D\}$ and $\mathbf{R}_{ss}$ is the source covariance matrix. A detailed discussion on these quantities and a procedure on how they can be derived from the corresponding quantities of the core information pencil can be found in [ZOLT89a]. The major items missing from the above list are the source time series vectors, $\mathbf{s}_i^T$, i=1,...,D, i. e., the message signals associated with each source, and the right singular vectors of the noiseless X and Y data matrices, $\hat{\mathbf{v}}_{x_i}$ and $\hat{\mathbf{v}}_{y_i}$, respectively, i=1,...,D. Of course, their omission from the above list is due to a fundamental limitation: noise at the data level cannot be "cleaned out" entirely even in the asymptotic case. Perfect "cleaning" is only theoretically possible at the statistical level, as is the case with the X and Y correlation matrices, for example, and only in the case of an infinite number of snapshots at that. Thus, the estimates of the message signals obtained via **PRO–ESPRIT** are, in fact, biased even in the case of an infinite number of snapshots. All that can be said is that, for each source, the asymptotic error in the **PRO–ESPRIT** estimate of the associated message signal is orthogonal to the message signal.

3.6 Invocation of Solution to Procrustes Problem: PRO–ESPRIT

The procedures outlined previously allow one to obtain asymptotically unbiased estimates (a.u.e.'s) of $\mathbf{U}_x^D$ and $\mathbf{U}_y^D$ such that $\hat{\mathbf{Q}}_u = \hat{\mathbf{U}}_x^{DH} \hat{\mathbf{U}}_y^D$ is asymptotically equal to the unitary matrix obtained under noiseless conditions which performs an invariant subspace rotation on the signal subspace. In practice, however, $\hat{\mathbf{U}}_x^{DH} \hat{\mathbf{U}}_y^D$ will not be unitary due to a finite number of snapshots, imperfections in the array data, etc. The logical alternative is to consider the "best" unitary matrix which approximates $\hat{\mathbf{U}}_x^{DH} \hat{\mathbf{U}}_y^D$. Actually, for use in **PRO–ESPRIT**, one desires the "best" unitary matrix which rotates $\hat{\mathbf{U}}_x^D$ into $\hat{\mathbf{U}}_y^D$. This criterion is referred to in the literature as the Procrustes problem [GOLU83a,BARN80]. Hence, the algorithm which incorporates the Procrustes processing option is referred to as the Procrustes ROtations based **ESPRIT** algorithm or **PRO–ESPRIT**. Not surprisingly, the "best" $\mathbf{Q}_u$ satisfies both criteria which are described below.

$$\text{(i)}\ \ \text{Min}\ \|\hat{\mathbf{U}}_x^{DH} \hat{\mathbf{U}}_y^D - \mathbf{Q}_u\|_F \qquad \text{(ii)}\ \ \text{Min}\ \|\hat{\mathbf{U}}_y^D - \hat{\mathbf{U}}_x^D \mathbf{Q}_u\|_F \qquad (3.44)$$

$$\text{subject to } \mathbf{Q}_u^H \mathbf{Q}_u = \mathbf{I}.$$

The minimizing $\mathbf{Q}_u$ in both cases is obtained by taking the SVD of the DxD matrix $\hat{\mathbf{U}}_x^{DH} \hat{\mathbf{U}}_y^D$ and forcing all the singular values to be unity [GOLU83a,BARN80]. Mathematically, if $\hat{\mathbf{U}}_x^{DH} \hat{\mathbf{U}}_y^D = \mathbf{U}_l \Sigma_l \mathbf{V}_l^H$ is the SVD, then $\hat{\mathbf{Q}}_u = \mathbf{U}_l \mathbf{V}_l^H$ is the unitary matrix which satisfies both of the criterion in (3.17).

A similar procedure is followed with respect to the estimate of the unitary transformation, $\mathbf{Q}_v$, which rotates the **right** singular vectors of the X data matrix into that of the Y data matrix. It was found in Section III that this matrix can be expressed in terms of the **left** singular vectors of both matrices, along with the corresponding nonzero singular values, and the MxM "clean" X-Y cross-correlation matrix, $\mathbf{C}_{xy}$, quantities for which there are asymptotically unbiased estimators. However, $\hat{\mathbf{Q}}_v$ will never be unitary in practice. As in the case of $\hat{\mathbf{Q}}_u$, the "closest" unitary matrix approximating $\hat{\mathbf{Q}}_v$ is obtained by taking the respective SVD and forcing all the singular values to be unity. Mathematically, if $\hat{\mathbf{Q}}_v = \hat{\Sigma}_x^{D-1} \hat{\mathbf{U}}_x^{DH} \hat{\mathbf{C}}_{xy} \hat{\mathbf{U}}_y^D \hat{\Sigma}_y^{D-1} = \mathbf{U}_r \Sigma_r \mathbf{V}_r^H$ is the SVD, then $\mathbf{Q}_v = \mathbf{U}_r \mathbf{V}_r^H$ is the unitary matrix which satisfies criterion similar to (3.17). It should be noted that despite $\mathbf{Q}_u$ and $\mathbf{Q}_v$ being unitary , the matrix $\Sigma_x^{D-1} \mathbf{Q}_u \Sigma_y^D \mathbf{Q}_v^H$ is not unitary , therefore there is no guarantee that the roots will have unity magnitude. However , simulations have demonstrated that the Procrustes operation pushes the roots closer to the unit circle.

A flow chart summarizing the **PRO–ESPRIT** algorithm is shown in Figure 3.1. It is worth noting the parallel fashion in which we can perform the essential operations of the algorithm in order to reduce the execution time.

3.7 Total Least Squares Interpretation of PRO–ESPRIT

In this section we present an interesting interpretation of the **PRO–ESPRIT** algorithm, which is based on the concept of Total Least Squares (TLS) [GOLU80,ZOLT89e]. The idea behind this approach is simple. The X array data and the Y array data provide us with two different estimates of the signal subspace, and two different estimates of the source subspace as well. Total Least Squares is utilized as a means for perturbing each of the two estimates of the signal subspace, say, in some "minimal" fashion until they are equal. The common subspace after perturbation is then taken as a "better" estimate of the signal subspace. A "better" estimate of the source subspace is obtained in the same fashion. The CIM is then obtained by rotating into these optimal subspaces. Here, we only go as far as deriving the structure of the CIM and its components. The equivalency between this CIM matrix and the one developed in Section 3.2 was established by Hua in [HUA88b].

A natural concern which may have arisen during the development of **PRO–ESPRIT** in Section 3.2 has to deal with the fact that no justification was given for defining the left and right GEV's of the data matrix pencil $\{\frac{1}{\sqrt{N}}\hat{\mathbf{Y}}_D\ ,\ \frac{1}{\sqrt{N}}\hat{\mathbf{X}}_D\}$ in terms of the right and left singular vectors of $\frac{1}{\sqrt{N}}\mathbf{X}$, as signified by the dependence of the expressions in (3.18) and (3.21) on $\hat{\mathbf{U}}_x$ and $\hat{\mathbf{V}}_x$. We could have just as well worked with the left and right singular vectors of $\frac{1}{\sqrt{N}}\mathbf{Y}_D$. However, the question arises as to whether the singular vector information from either data matrix should be given preference. To remedy this dilemma we make use of the TLS technique as a means of determining the "best" set of D orthonormal vectors which approximate range$\{\mathbf{A}\}$, the signal subspace, and the best set of D orthonormal vectors which approximate range$\{\mathbf{S}^H\}$, the source subspace. These are placed as the columns of $\mathbf{U}_o^D$ and $\mathbf{V}_o^D$, respectively. We will argue shortly that the appropriate vectors comprising $\mathbf{U}_o^D$ are the D left singular vectors of $[\hat{\mathbf{U}}_x^D|\hat{\mathbf{U}}_y^D]$ associated with the D largest singular values. Similarly, the appropriate vectors comprising $\mathbf{V}_o^D$ are the D left singular vectors of $[\hat{\mathbf{V}}_x^D|\hat{\mathbf{V}}_y^D]$ associated with the D largest singular values. We will substantiate these claims below and address some computational issues as well. Before we proceed with this, let us consider the structure of the CIM dictated by this approach.

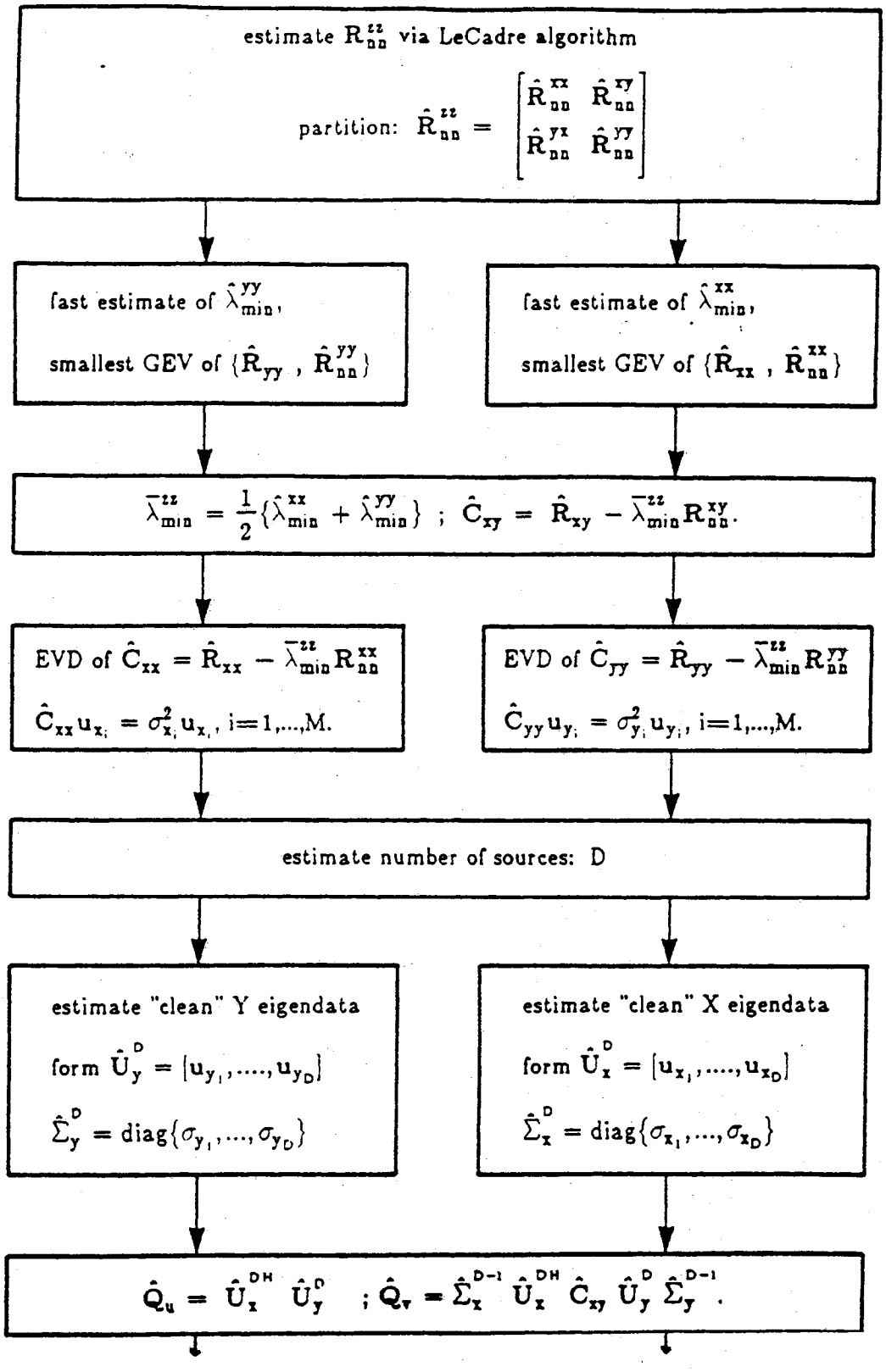

Figure 3.2 **A summary of PRO–ESPRIT**

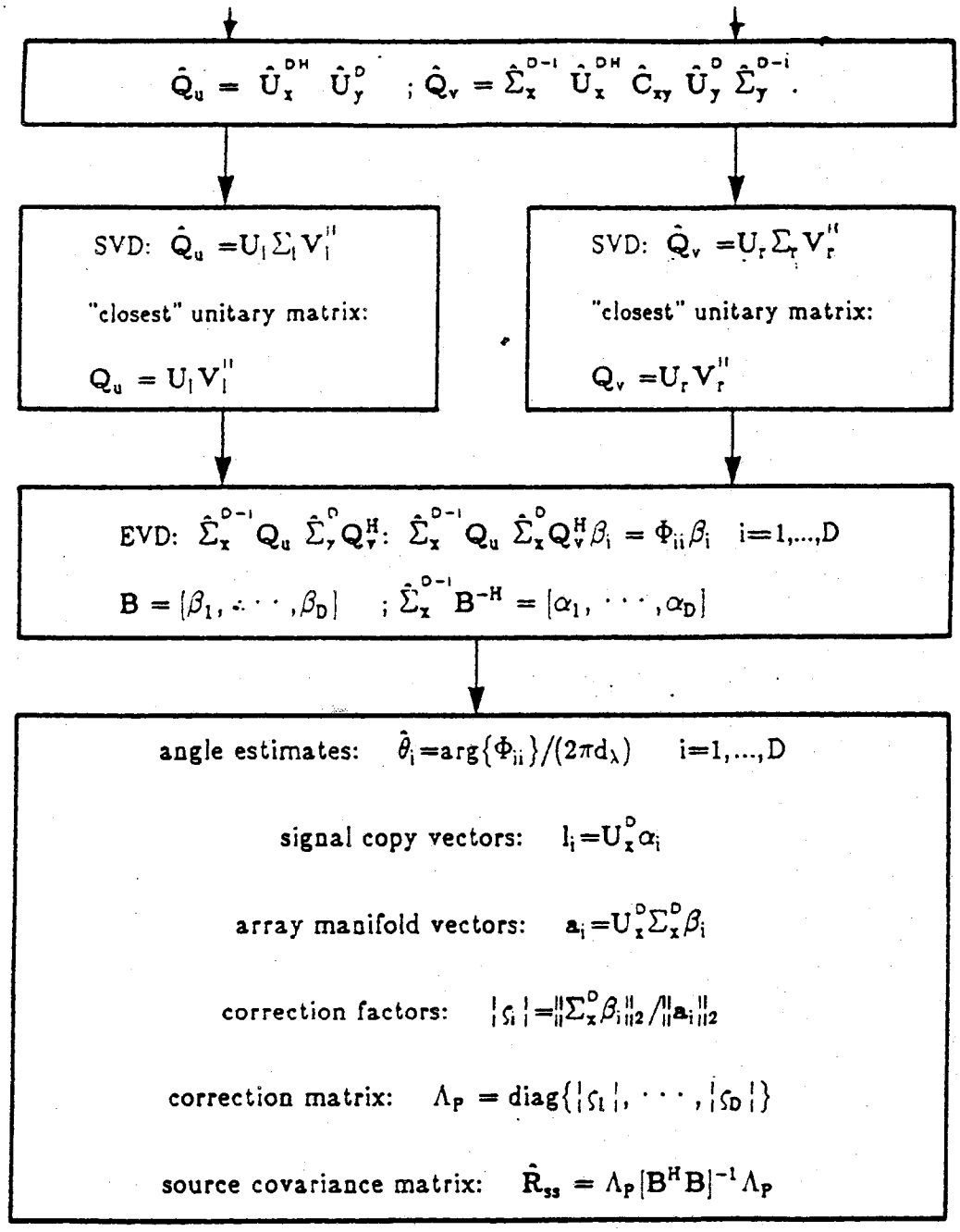

Figure 3.2 (continued)

Given $\mathbf{U}_o^D$ and $\mathbf{V}_o^D$ via TLS processing, we proceed similar to the original development to find the best set of DxD unitary matrices, $\mathbf{Q}_u^y, \mathbf{Q}_v^y$, $\mathbf{Q}_u^x, \mathbf{Q}_v^x$, invoking the solution to the Procrustes problem, such that

$$\mathbf{U}_y^D \approx \mathbf{U}_o^D \mathbf{Q}_u^y \qquad \mathbf{V}_y^D \approx \mathbf{V}_o^D \mathbf{Q}_v^y$$

$$\mathbf{U}_x^D \approx \mathbf{U}_o^D \mathbf{Q}_u^x \qquad \mathbf{V}_x^D \approx \mathbf{V}_o^D \mathbf{Q}_v^x$$

That is, we find the "best" unitary matrix approximating each of the following DxD matrices: $\mathbf{U}_o^{DH}\mathbf{U}_y^D$, $\mathbf{V}_o^{DH}\mathbf{V}_y^D$, $\mathbf{U}_o^{DH}\mathbf{U}_x^D$, and. $\mathbf{V}_o^{DH}\mathbf{V}_x^D$. The reduction to the core rotations level is then accomplished by substitution into the **ESPRIT** data pencil estimate in the following manner.

$$\frac{1}{\sqrt{N}}\left\{\hat{\mathbf{Y}}_D - \lambda\hat{\mathbf{X}}_D\right\} = \hat{\mathbf{U}}_y^D \Sigma_y^D \hat{\mathbf{V}}_y^{DH} - \lambda \mathbf{U}_x^D \Sigma_x^D \mathbf{V}_x^{DH} \tag{3.45}$$

$$\approx \mathbf{U}_o^D \left\{\mathbf{Q}_u^y \Sigma_y^D \mathbf{Q}_v^{yH} - \lambda \mathbf{Q}_u^x \Sigma_x^D \mathbf{Q}_v^{xH}\right\} \mathbf{V}_o^{DH}$$

The DxD pencil $\{\mathbf{Q}_u^y\ \Sigma_y^D \mathbf{Q}_v^{yH},\ \mathbf{Q}_u^x\ \Sigma_x^D \mathbf{Q}_v^{xH}\}$ is then the CIM pencil in the TLS interpretation of **PRO–ESPRIT**. The implication is that the estimates of Φ_{ii}, defined by (2.9), are then found as the GE's of this pencil. However, it has been shown by Hua [HUA88b] that the GE's of this pencil are practically identical to the GE's of the matrix pencil derived in (3.6). Besides establishing the fact that if **PRO–ESPRIT** is approached via the TLS principle it actually reduces to the algorithm developed in Section 3.2, this result by Hua also goes to substantiate our previous claim that **PRO–ESPRIT** exploits the inherent redundancies in the array system to the fullest.

We now present the process of estimating the signal and source subspaces via the TLS principle. We begin with the estimation of the signal subspace. For our purposes here, we make use of Total Least Squares (TLS) as a technique for solving the following type of problem:

$$\text{Minimize:} \quad \|[\Delta\mathbf{A} \mid \Delta\mathbf{B}]\|_F$$

$$\text{subject to:} \quad \text{range}\{\mathbf{B}+\Delta\mathbf{B}\} \subseteq \text{range}\{\mathbf{A}+\Delta\mathbf{A}\}$$

where $\mathbf{A}$ is mxn and $\mathbf{B}$ is mxk, with m>n. This problem is derived from the problem of solving the over-determined linear system of equations $\mathbf{AX}=\mathbf{B}$. Consider the situation with the left singular vectors. In the asymptotic case, the columns of $\hat{\mathbf{U}}_x^D$ form an orthonormal basis for the same subspace as that spanned by the orthonormal basis comprising the columns of $\hat{\mathbf{U}}_y^D$, the signal subspace. In the practical case, where the number of snapshots may not be that large, it seems

logical to **exploit this redundancy** to find the "best" estimate of the signal subspace. To this end, we pose the following problem which is similar in form to the above TLS problem.

$$\text{Minimize:} \quad \|[\Delta \mathbf{U}_x \mid \Delta \mathbf{U}_y]\|_F$$

$$\text{subject to:} \quad \text{range}\{\hat{\mathbf{U}}_x^D + \Delta \mathbf{U}_x\} = \text{range}\{\hat{\mathbf{U}}_y^D + \Delta \mathbf{U}_y\}$$

That is, we wish to find the perturbing matrices $\Delta \mathbf{U}_x$ and $\Delta \mathbf{U}_y$ of minimum Frobinius norm such that the range space of the perturbed matrix $\hat{\mathbf{U}}_x^D + \Delta \mathbf{U}_x$ is exactly equal to the range space of the perturbed matrix $\hat{\mathbf{U}}_y^D + \Delta \mathbf{U}_y$. The common D-dimensional range space of the two *perturbed* matrices should then be a better estimate of the signal subspace. In actuality, we do not need to compute the perturbing matrices $\Delta \mathbf{U}_x$ and $\Delta \mathbf{U}_y$, if we are, in fact, only interested in the common range space. Invoking the TLS solution developed by Golub and Van Loan [GOLU80], we find that the common range space is that spanned by the D left singular vectors of $[\hat{\mathbf{U}}_x^D | \hat{\mathbf{U}}_y^D]$ associated with the D largest singular values, as indicated previously. These can also be found as the D "largest" EVEC's of the MxM matrix $\hat{\mathbf{U}}_x^D \hat{\mathbf{U}}_x^{DH} + \hat{\mathbf{U}}_y^D \hat{\mathbf{U}}_y^{DH}$.

We proceed similarly to again exploit the inherent redundancy in the **ESPRIT** data pencil to obtain a better estimate of range$\{\mathbf{S}^H\}$, the source subspace. Following the exact same argument and sequence of steps as above, we find that the appropriate vectors comprising $\mathbf{V}_o^D$ are the D left singular vectors of $[\hat{\mathbf{V}}_x^D | \hat{\mathbf{V}}_y^D]$ associated with the D largest singular values. Alternatively, this may be achieved through the following sequence of steps. Compute the eigen-decomposition of the 2Dx2D matrix

$$[\hat{\mathbf{V}}_x^D | \hat{\mathbf{V}}_y^D]^H [\hat{\mathbf{V}}_x^D | \hat{\mathbf{V}}_y^D] = \mathbf{V} \Sigma^2 \mathbf{V}^H \tag{3.46}$$

Of course, it follows that the columns of $\mathbf{V}$ in (3.46) are the right singular vectors of $[\mathbf{V}_x^D | \mathbf{V}_y^D]$ and the elements of Σ (not squared) are the corresponding singular values. If we let Σ_D be a diagonal matrix comprised of the D largest singular values derived from the eigen-decomposition above and $\mathbf{V}_D$ be comprised of the corresponding right singular vectors, then the D associated left singular vectors may be computed from the relationship between the left and right singular vectors of a matrix in the following manner.

$$\mathbf{V}_o^D = [\hat{\mathbf{V}}_x^D | \hat{\mathbf{V}}_y^D] \mathbf{V}_D \Sigma_D^{-1} \tag{3.47}$$

We note that even with TLS processing, we do not obtain a.u.e.'s of the right singular vectors of the noiseless data matrices. This is in contrast to the case with the left singular vectors where a.u.e.'s are obtained even without the TLS

processing. In light of this, we develop the TLS-based procedure for estimating $\mathbf{V}_o^D$ a little further to insure ourselves that the estimates of $\mathbf{Q}_v^x$ and $\mathbf{Q}_v^y$ are nonetheless asymptotically unbiased. Invoking the orthonormality of $\hat{\mathbf{V}}_x^D$ and $\hat{\mathbf{V}}_y^D$ in the expansion of the left hand side of (3.46) gives

$$[\hat{\mathbf{V}}_x^D|\hat{\mathbf{V}}_y^D]^H[\hat{\mathbf{V}}_x^D|\hat{\mathbf{V}}_y^D] = \begin{bmatrix} \hat{\mathbf{V}}_x^{DH} \\ \hat{\mathbf{V}}_y^{DH} \end{bmatrix}[\hat{\mathbf{V}}_x^D|\hat{\mathbf{V}}_y^D] = \begin{bmatrix} \mathbf{I} & \hat{\mathbf{Q}}_v \\ \hat{\mathbf{Q}}_v^H & \mathbf{I} \end{bmatrix} \tag{3.48}$$

where $\hat{\mathbf{Q}}_v = \hat{\mathbf{V}}_x^{DH}\hat{\mathbf{V}}_y^D$. From previous analysis, we know that an asymptotically unbiased estimate of the unitary matrix $\mathbf{Q}_v = \mathbf{V}_x^{DH}\mathbf{V}_y^D$ obtained in the noiseless case is given by $\hat{\mathbf{Q}}_v = \hat{\Sigma}_x^{D-1}\hat{\mathbf{U}}_x^{DH}\hat{\mathbf{C}}_{xy}\hat{\mathbf{U}}_y^D\hat{\Sigma}_y^{D-1}$. Hence, Σ_D^2 and $\mathbf{V}_D$ used in (3.47) are constructed from the D largest eigenvalues and corresponding eigenvectors, respectively, of the 2Dx2D matrix on the right hand side of (3.48) with this expression substituted for $\mathbf{Q}_v$. Consider

$$\hat{\mathbf{Q}}_v^x = \hat{\mathbf{V}}_x^{DH}\mathbf{V}_o^D = \hat{\mathbf{V}}_x^{DH}[\hat{\mathbf{V}}_x^D|\hat{\mathbf{V}}_y^D]\mathbf{V}_D\Sigma_D^{-1} \approx [\mathbf{I}|\hat{\mathbf{Q}}_v]\mathbf{V}_D\Sigma_D^{-1} \tag{3.49}$$

where we again substitute $\hat{\mathbf{Q}}_v = \hat{\Sigma}_x^{D-1}\hat{\mathbf{U}}_x^{DH}\hat{\mathbf{C}}_{xy}\hat{\mathbf{U}}_y^D\hat{\Sigma}_y^{D-1}$. The appropriate $\mathbf{Q}_v^x$ to be substituted into the **PRO–ESPRIT–TLS** core rotations pencil is then the "best" unitary matrix, invoking the solution to the Procrustes problem, approximating the far right hand side of (3.49). Likewise, the appropriate $\mathbf{Q}_v^y$ to be substituted into the **PRO–ESPRIT–TLS** core rotations pencil is the "best" unitary matrix approximating $\hat{\mathbf{Q}}_v^y = [\hat{\mathbf{Q}}_v^H|\mathbf{I}]\,\mathbf{V}_D\Sigma_D^{-1}$.

CHAPTER 4
PRO-ESPRIT AND THE UNIFORM LINEAR ARRAY

4.1 The Linear Array Geometry and the F-B Data Pencils

Of all array geometries and designs, perhaps the one with the most redundancy built into it is the uniformly-spaced array composed of identical sensors. An array of this sort will be referred to as a **uniform linear array** where it is understood that the uniformity is in both spacing and element pattern. In fact, bothered by a perception of inefficiency with the uniform array, many have sought to design so-called non-redundant or minimum redundancy arrays [BEDR86,PILL86]. However, it would seem more judicious to use the uniform linear array structure to our advantage by exploiting the inherent redundancy to compensate as much as possible for any imperfections in the array data and any inadequacy in the array model, as elaborated upon in chapter 3, *and to reduce computation as well.* The uniformly-spaced array geometry is particularly intriguing for the application of **ESPRIT**, or any of its numerous derivatives such as **PRO–ESPRIT**, since it is inherently composed of a number of so-called doublets or matched sensor pairs, assuming the sensors to be identical. Specifically, every two adjacent sensors in the array is a doublet such that a uniform linear array of M sensors is composed of M-1 doublets. This is an observation which has recently captured the interest of a number of those pursuing applications of **ESPRIT** [PAUL85,ZOLT87c,SPEI87,VAN87]. Following the lead of Ouibrahim [QUIB86,QUIB87] and Hua [HUA88a] the data derived from a uniform linear array will be used to construct a matrix pencil having the structure required by **PRO–ESPRIT**. The impetus for constructing pencils in the manner described by these gentlemen has its foundations in the concept of forward-backward spatial smoothing [QUIB87,QUIB88,HUA88a]. Thus this pencil will be referred to , as the forward-backward data pencil , or the F-B data pencil, for short.

The reasons for working with the F-B data pencil in the uniform linear array case are many. The first and foremost is that it facilitates a significant reduction in the computation required by **PRO–ESPRIT**. This reduction in computation is due to the fact that the X data matrix and (the conjugate of the) Y data

matrix comprising the F-B data pencil are related through simple unitary transformations such that the SVD of one can be obtained from the other via simple, known transformations. These relationships, which will be derived shortly, can be exploited by **PRO–ESPRIT** since it works with the X and Y data matrices "individually". A good reason for considering the application of **PRO–ESPRIT** in the uniform linear array case has to deal with the fact that the GEV's of an **ESPRIT** data pencil are estimates of quantities which should lie on the unit circle, the Φ_{ii}, i=1,...,D, as defined by (2.8). In the development of **PRO–ESPRIT**, this constraint was not incorporated due to the fact that it did not lead to a closed-form solution. Instead, it was indicated that the Procrustes-based processing served as a sub-optimal, closed-form means for accommodating this constraint. In the case of a uniform linear array scenario, it is found that the process of forward-backward averaging serves as an additional means of accounting for this constraint. A brief argument will be provided for this shortly. In addition, there are the usual benefits associated with F-B averaging: it effectively increases the number of data vectors over which the average is obtained and it also serves to effectively decorrelate highly-correlated or coherent signals [QUIB87,QUIB88,HUA88a,SHAN85]. Now these points will be validated.

4.2 Construction and Analysis of the F-B Data Pencils

Denote $x_i(n)$ as the output signal from the i-th sensor of the uniform linear array, i=1,...,M, recorded at the n-th snapshot, n=1,...,N. The F-B data pencil is constructed in the manner prescribed by Ouibrahim [QUIB88] and Hua [HUA88a] by effectively breaking the array up into subarrays of L<M contiguous elements. There are M-L+1 such subarrays in the array defined such that two adjacent subarrays have L-1 sensors in common. The F-B data pencil is then constructed via the following the following three steps.

CONSTRUCTION OF F-B DATA PENCIL

(1) for each snapshot, form the following two Lx(M-L) matrices:

$$\mathbf{D}_1(n) = \begin{bmatrix} x_1(n) & x_2(n) & \cdots & x_{M-L}(n) \\ x_2(n) & x_3(n) & \cdots & x_{M-L+1}(n) \\ \cdot & \cdot & \cdot & \cdot \\ \cdot & \cdot & \cdot & \cdot \\ \cdot & \cdot & & \cdot \\ x_L(n) & x_{L+1}(n) & \cdots & x_{M-1}(n) \end{bmatrix}$$

$$\mathbf{D}_2(n) = \begin{bmatrix} x_2(n) & x_3(n) & \cdots & x_{M-L+1}(n) \\ x_3(n) & x_4(n) & \cdots & x_{M-L+2}(n) \\ \cdot & \cdot & \cdot & \cdot \\ \cdot & \cdot & \cdot & \cdot \\ \cdot & \cdot & & \cdot \\ x_{L+1}(n) & x_{L+2}(n) & \cdots & x_M(n) \end{bmatrix}$$

(2) concatenate the matrices constructed in (1) as follows to form the forward data pencil (F-pencil) of dimension Lx[N(M-L)].

$$\mathbf{X}_F = \left[\mathbf{D}_1(1), \mathbf{D}_1(2), \cdots, \mathbf{D}_1(N)\right] \quad ; \quad \mathbf{Y}_F = \left[\mathbf{D}_2(1), \mathbf{D}_2(2), \cdots, \mathbf{D}_2(N)\right]$$

(3) construct the Lx[2N(M-L)] F-B data pencil from the F-data pencil in (2) as follows

$$\mathbf{X}_{FB} = \left[\mathbf{X}_F \mid \tilde{\mathbf{I}}\mathbf{Y}_F^*\right] \quad ; \quad \mathbf{Y}_{FB} = \left[\mathbf{Y}_F \mid \tilde{\mathbf{I}}\mathbf{X}_F^*\right] \tag{4.1}$$

where $\tilde{\mathbf{I}}$ is the reverse permutation matrix of appropriate dimensions defined by

$$\tilde{\mathbf{I}} = \begin{bmatrix} 0 & 0 & & 1 \\ 0 & 0 & . & 0 \\ \cdot & \cdot & \cdot & \cdot \\ \cdot & \cdot & \cdot & \cdot \\ 0 & 1 & & 0 \\ 1 & 0 & & 0 \end{bmatrix} \tag{4.2}$$

Note that $\tilde{\mathbf{I}}$ satisfies $\tilde{\mathbf{I}}^T = \tilde{\mathbf{I}}$ and $\tilde{\mathbf{I}}\,\tilde{\mathbf{I}} = \mathbf{I}$ which indicates that it is is a unitary matrix equal to its own transpose. A comment on the bounds on the choice of L is made at a later point. Now, a detailed description of the elements of the F-B data pencil in the noiseless case, and hence a verification of its **ESPRIT**

structure, can be found in Ouibrahim's dissertation [QUIB87]. Before applying **PRO–ESPRIT** to the F-B data pencil , a brief analysis of this pencil will demonstrate why backward averaging, in fact, serves to "partially" account for the fact that the Φ_{ii} are on the unit circle.

It is easy to show that in the noiseless case the forward data pencil, or F data pencil, for short, constructed in step (2) above has the following structure.

$$\mathbf{X}_F = \mathbf{A}_L \mathbf{S}_F \quad ; \quad \mathbf{Y}_F = \mathbf{A}_L \Phi \mathbf{S}_F \tag{4.3}$$

where $\mathbf{A}_L$ is the array manifold associated with each identical subarray composed of L identical sensors

$$\mathbf{A}_L = \begin{bmatrix} 1 & 1 & & 1 \\ \Phi_{11} & \Phi_{22} & & \Phi_{DD} \\ \Phi_{11}^2 & \Phi_{22}^2 & \vdots & \Phi_{DD}^2 \\ \vdots & \vdots & & \vdots \\ \Phi_{11}^{L-1} & \Phi_{22}^{L-1} & & \Phi_{DD}^{L-1} \end{bmatrix} \tag{4.4}$$

and $\mathbf{S}_F = \left[\mathbf{S} \mid \Phi\mathbf{S} \mid \cdots \mid \Phi^{M-L-1}\mathbf{S}\right]$, a Dx[N(M-L)] matrix. Recall that the D rows of $\mathbf{S}$ are the complex envelopes associated with each of the D signals as defined previously. Therefore, $\mathbf{X}_{FB}$ as constructed in (4.1), or step (3), can be expressed as

$$\mathbf{X}_{FB} = \left[\mathbf{A}_L \mathbf{S}_F \mid \tilde{\mathbf{I}}\mathbf{A}_L^* \Phi^* \mathbf{S}_F^*\right] = \mathbf{A}_L \left[\mathbf{S}_F \mid \Phi^{L-2}\mathbf{S}_F^*\right] \tag{4.5}$$

where we have used the pseudo-centro-symmetric property [BRES86] $\mathbf{A}_L = \tilde{\mathbf{I}}\,\mathbf{A}_L^*\,\Phi^{L-1}$ which follows from the Vandermonde structure of $\mathbf{A}_L$ and the fact that the Φ_{ii} are on the unit circle such that $\Phi^{-1} = \Phi^*$. Likewise ,

$$\mathbf{Y}_{FB} = \left[\mathbf{A}_L \Phi \mathbf{S}_F \mid \mathbf{A}_L \Phi^{L-1} \mathbf{S}_F^*\right] = \mathbf{A}_L \Phi \left[\mathbf{S}_F \mid \Phi^{L-2}\mathbf{S}_F^*\right] \tag{4.6}$$

Comparing the far right-hand-side (RHS) of (4.6) with that of (4.5), it can be concluded that the F-B data pencil, $\{\mathbf{X}_{FB}\mathbf{Y}_{FB}\}$, obtained in the noiseless case, does indeed possess the **ESPRIT** structure. However, it is apparent that the whole argument hinged on the property $\mathbf{A}_L = \tilde{\mathbf{I}}\,\mathbf{A}_L^*\,\Phi^{L-1}$ which only holds if the Φ_{ii}, i=1,...,D, lay on the unit circle. If the Φ_{ii} do not lie on the unit circle, the F-B data pencil does not possess the desired **ESPRIT** structure. In contrast, the F-pencil exhibits the **ESPRIT** structure whether the Φ_{ii} lie on the unit circle or not. This development then serves as a "loose" argument for why the use of backward averaging in a uniform linear array scenario serves as a simple means for "sub-optimally" complying with the constraint that the Φ_{ii} lie on the unit

circle in the application of **PRO–ESPRIT** (or any "**ESPRIT**-like" algorithm for that matter). It is stressed, though that it does not guarantee us that the roots will lie on the unit circle.

Now , some observations pertaining to the similarity in structure of $\mathbf{X}_{FB}$ and $\mathbf{Y}_{FB}$ which will serve to reduce the computation associated with an eigenanalysis of the F-B data pencil via **PRO–ESPRIT**. To this end, observe that $\mathbf{X}_{FB}$ and $\mathbf{Y}_{FB}$, as constructed in (4.1), or step (3) above, contain exactly the same information; they are related through a simple permutation as follows:

$$\mathbf{Y}_{FB} = \tilde{\mathbf{I}}\, \mathbf{X}_{FB}^{*}\, \tilde{\mathbf{J}} \tag{4.7}$$

where $\tilde{\mathbf{J}}$ is a block reverse permutation matrix defined by

$$\tilde{\mathbf{J}} = \begin{bmatrix} \mathbf{O}_{N'} & \mathbf{I}_{N'} \\ \mathbf{I}_{N'} & \mathbf{O}_{N'} \end{bmatrix} \tag{4.8}$$

where $N'=N(M-L)$; the integer subscripts serve to indicate the dimension of the respective square matrix. It is easy to verify that similar to the case with the reverse permutation matrix $\tilde{\mathbf{I}}$, $\tilde{\mathbf{J}}$ is unitary and equal to its own transpose. As a consequence of the relationship in (4.7), it is not too surprising to find that the respective SVD's of $\mathbf{X}_{FB}$ and $\mathbf{Y}_{FB}$ are related through simple transformations. The appropriate transformations can be arrived at by a simple development. To this end, let $\mathbf{X}_{FB} = \mathbf{U}_x \Sigma_x \mathbf{V}_x^{H}$ denote the SVD of $\mathbf{X}_{FB}$ and substitute this into (4.7).

$$\mathbf{Y}_{FB} = \{\tilde{\mathbf{I}}\, \mathbf{U}_x^{*}\} \Sigma_x \{\mathbf{V}_x^{T}\, \tilde{\mathbf{J}}\} \tag{4.9}$$

where it is important to recognize the difference between hermitian transpose denoted by subscript H and regular transpose without conjugation denoted by subscript T. Since the product of two unitary matrices is unitary, it follows that $\tilde{\mathbf{I}}\, \mathbf{U}_x^{*}$ is a unitary matrix as is $\mathbf{V}_x^{T}\, \tilde{\mathbf{J}}$. Let $\mathbf{Y}_{FB} = \mathbf{U}_y \Sigma_y \mathbf{V}_y^{H}$ denote the SVD of $\mathbf{Y}_{FB}$. It follows from the property that an SVD is unique that the following relationships hold.

$$\mathbf{U}_y = \tilde{\mathbf{I}}\, \mathbf{U}_x^{*} \quad \Sigma_y = \Sigma_x \quad \mathbf{V}_y = \tilde{\mathbf{J}}\, \mathbf{V}_x^{*} \tag{4.10}$$

It is emphasized that these relationships hold whether noise is present or not and are not based on any type of asymptotic argument. However, they only hold for the F-B data pencil; they do not hold for the F data pencil, which is constructed based on forward averaging only. These relationships are now exploited as promised.

4.3 PRO-ESPRIT Eigenanalysis of the F-B Data Pencils

An eigenanalysis of the F-B data pencil via **PRO–ESPRIT**, according to the algorithm outlined in chapter 3, requires, initially at least, an estimate of the noiseless or "clean" F-B cross-correlation matrix $\mathbf{C}_{FB}^{xy} = \frac{1}{2N'}\mathbf{X}_{FB}\ \mathbf{Y}_{FB}^{H}$ and, ostensibly, EVD's (eigenvalue decompositions) of "cleaned" estimates of the F-B auto-correlation matrices $\mathbf{C}_{FB}^{xx} = \frac{1}{2N'}\mathbf{X}_{FB}\ \mathbf{X}_{FB}^{H}$ and $\mathbf{C}_{FB}^{yy} = \frac{1}{2N'}\mathbf{Y}_{FB}\ \mathbf{Y}_{FB}^{H}$ where $N'=N(M-L)$, as defined previously. However, it is obvious from the preceding development that an EVD of $\mathbf{C}_{FB}^{yy}$ is not necessary since its eigen-information is simply related to that of $\mathbf{C}_{FB}^{xx}$ in accordance with the respective relationships between the singular values and left singular vectors of $\mathbf{Y}_{FB}$ and $\mathbf{X}_{FB}$ in (4.10). This reduces the problem at hand to estimating $\mathbf{C}_{FB}^{xy}$ and the EVD of $\mathbf{C}_{FB}^{xx}$. To this end, let us assume the additive noise to be "spatially white" such that the expected power of the noise at each sensor, denoted σ_n^2, is equal. This assumption will be relaxed at a later point. As might be expected, the initial "cleaning" step required by **PRO–ESPRIT** is greatly simplified under this condition. Accordingly, the following observations are in order. It easily proved that the "spatial whiteness" of the noise is preserved by the process of forward-backward averaging [QUIB87,QUIB88,HUA88a], such that

$$\lim_{N\ \text{large}} \hat{\mathbf{R}}_{FB}^{xx} = \lim_{N\ \text{large}} \frac{1}{2N'}\hat{\mathbf{X}}_{FB}\hat{\mathbf{X}}_{FB}^{H} = \mathbf{C}_{FB}^{xx} + \sigma_n^2\mathbf{I} \tag{4.11}$$

Also, as observed by Roy et al [ROY86] and Ouibrahim [QUIB86,QUIB87], note that

$$\lim_{N\ \text{large}} \hat{\mathbf{R}}_{FB}^{xy} = \lim_{N\ \text{large}} \frac{1}{2N'}\hat{\mathbf{X}}_{FB}\hat{\mathbf{Y}}_{FB}^{H} = \mathbf{C}_{FB}^{xy} + \sigma_n^2\Gamma \tag{4.12}$$

where Γ is a matrix having all ones along the first sub-diagonal below the main diagonal and zeros everywhere else. (4.11) indicates, of course, that asymptotically the eigenvectors of $\hat{\mathbf{R}}_{FB}^{xx}$ are the same as those of $\mathbf{C}_{FB}^{xx}$, and that the respective eigenvalues differ only by the additive amount σ_n^2 which may be computed as the smallest eigenvalue of $\hat{\mathbf{R}}_{FB}^{xx}$, denoted $\bar{\lambda}_{min}^{xx}$, assuming $D<L$. Thus, an EVD of $\hat{\mathbf{R}}_{FB}^{xx}$ provides all the information necessary to construct the EVD of $\hat{\mathbf{C}}_{FB}^{xx}$ required by **PRO–ESPRIT**. In addition, (4.12) and the above observations lead us to the following simplistic scheme for estimating the "clean" cross-correlation matrix.

$$\hat{\mathbf{C}}_{FB}^{xy} = \frac{1}{2N'}\hat{\mathbf{X}}_{FB}\hat{\mathbf{Y}}_{FB}^{H} - \bar{\lambda}_{min}^{xx}\Gamma \tag{4.13}$$

After all this, an outline to the **PRO–ESPRIT** eigenanalysis of the F-B data

pencil can be presented. The steps are delineated below.

PRO-ESPRIT FOR UNIFORM ARRAY (WHITE NOISE)

(1.) form $\hat{\mathbf{X}}_{FB}$ and $\hat{\mathbf{Y}}_{FB}$.

(2.) form LxL $\hat{\mathbf{R}}_{FB}^{xx} = \frac{1}{2N'}\hat{\mathbf{X}}_{FB}\,\hat{\mathbf{X}}_{FB}^{H}$ and LxL $\hat{\mathbf{R}}_{FB}^{xy} = \frac{1}{2N'}\hat{\mathbf{X}}_{FB}\,\hat{\mathbf{Y}}_{FB}^{H}$.

(3.) EVD of $\hat{\mathbf{R}}_{FB}^{xx}$: $\hat{\mathbf{R}}_{FB}^{xx}\hat{\mathbf{u}}_{x_i} = \hat{\lambda}_{x_i}\,\hat{\mathbf{u}}_{x_i}$, i=1,...,L.

(4.) estimate number of sources, D.

(5.) with $\hat{\bar{\lambda}}_{min}^{xx} = \frac{1}{L-D}\sum_{i=D+1}^{L}\hat{\lambda}_{x_i}$, "clean" $\hat{\mathbf{R}}_{FB}^{xy}$: $\hat{\mathbf{C}}_{FB}^{xy} = \hat{\mathbf{R}}_{FB}^{xy} - \hat{\bar{\lambda}}_{min}^{xx}\Gamma$.

(6.) form: $\hat{\mathbf{U}}_x^D = [\mathbf{u}_{x_1}, \ldots, \mathbf{u}_{x_D}]$; $\hat{\Sigma}_x^D = \mathrm{diag}\{(\hat{\lambda}_{x_1} - \hat{\bar{\lambda}}_{min}^{xx})^{1/2}, \ldots, (\hat{\lambda}_{x_D} - \hat{\bar{\lambda}}_{min}^{xx})^{1/2}\}$

(7.) form DxD $\hat{\mathbf{Q}}_u = \hat{\mathbf{U}}_x^{DH}\,\tilde{\mathbf{I}}\,\hat{\mathbf{U}}_x^{D*}$ and DxD $\hat{\mathbf{Q}}_v = \hat{\Sigma}_x^{D\,-1}\,\hat{\mathbf{U}}_x^{DH}\,\hat{\mathbf{C}}_{FB}^{xy}\,\tilde{\mathbf{I}}\,\hat{\mathbf{U}}_x^{D*}\,\hat{\Sigma}_x^{D\,-1}$.

(8.) SVD of $\hat{\mathbf{Q}}_u$ and $\hat{\mathbf{Q}}_v$: $\hat{\mathbf{Q}}_u = \mathbf{U}_l\Sigma_l\mathbf{V}_l^H$ and $\hat{\mathbf{Q}}_v = \mathbf{U}_r\Sigma_r\mathbf{V}_r^H$

(9.) form $\mathbf{Q}_u = \mathbf{U}_l\mathbf{V}_l^H$ and $\mathbf{Q}_v = \mathbf{U}_r\mathbf{V}_r^H$.

(10.) DxD EVD: $\hat{\Sigma}_x^{D\,-1}\mathbf{Q}_u\,\hat{\Sigma}_x^{D}\mathbf{Q}_v^H = \mathbf{B}\Phi\mathbf{B}^{-1}$.

Sifting through this algorithm, the major computational tasks are found to be the LxL EVD in step (3), the two DxD SVD's in step (8), and the DxD EVD in step (10). Note that $L \leq M$ and is typically chosen to be $L = \frac{2}{3}M$. Comparing with a **PRO–ESPRIT** eigenanalysis of a general **ESPRIT** data pencil, the primary reduction in computation is due to the fact that an EVD of $\hat{\mathbf{R}}_{FB}^{yy}$ is not required. It is stressed that this reduction in computation is only valid when backward averaging is employed. To bring home the point, note that it is perfectly valid to set L equal to M-1 in the procedure for constructing the F-B data pencil, i. e., the relationships in (4.10) hold even in the case of L=M-1. Thus, it is required that $L \leq M-1$. It is also required that $L \geq D+1$; the additional one allows the estimation of σ_n^2. This implies that with M uniformly-spaced sensors, **PRO–ESPRIT** as outlined above can handle M-2 sources. Another reduction in computation realized in the uniform linear array scenario is the avoidance of the initial "cleaning" step required by **PRO–ESPRIT**. This simplification resulted due to the fact an EVD of $\hat{\mathbf{R}}_{FB}^{xx}$ is "as good" as an EVD of of $\hat{\mathbf{C}}_{FB}^{xx}$ and provides the necessary information to "clean out" the noise in $\hat{\mathbf{C}}_{FB}^{xy}$ as well.

4.4 Simulations and Discussion

The first simulation example is offered as testament to the power of **PRO–ESPRIT** as it involves a scenario whose characteristics are: sources separated by less than a beamwidth , low signal to noise ratios as well as small number of snapshots plus high correlation coefficient amongst the sources. The array that was used was a uniformly spaced linear array of 15 sensors (M=15) and the noise was spatially white. The number of sources was 3 (D=3) and they were located at the following angles with respect to the normal to the line of the array: θ_1=6.5° , θ_2=10.3° and θ_3=–9°. For an array of this size , the 3 dB beamwidth is approximately 8.7°. Therefore , the first and second sources separated by almost half a 3 dB. The third source is approximately 2 beamwidths away from the first source. The individual signal powers and the correlations amongst them are described by the 3x3 source covariance matrix , $\mathbf{R}_{ss}$. With the noise power normalized to unity , i.e. σ_n^2=1 , the true covariance matrix for the scenario under consideration was as follows.

$$\mathbf{R}_{ss} = \begin{bmatrix} 3 & 2 & 1 \\ 2 & 4 & 1 \\ 1 & 1 & 5 \end{bmatrix}$$

With these parameters , we tested the performance of the version of **PRO–ESPRIT** developed in this chapter as a function of the number of snapshots. Specifically , we let the number of snapshots (N) be equal to N=3, N=5, N=10 and N=15. The results of one hundred independent trials are plotted in Figures 4.1(a), 4.1(b), 4.1(c) and 4.1(d) respectively. In each independent run, the F-B data pencil was constructed according to the procedure outlined before , with the subarray length (L) equal to L=10 , i.e. 2/3 of the overall array. For each of the four cases , the sample mean and variance was computed and listed in the corresponding figure. Observe that even with 3 snapshots , that is the case when the number of snapshots was the minimum number that could be used , the algorithm performed quite well , and the two sources that were separated by less than half of a beamwidth were resolved. The sample mean of the angle estimate for each of the 3 sources was off by 0.1° for the first source and 0.3° for the second and third. The variance of the estimates decreases quite fast as the number of snapshots is increased from N=3 to N=15. Before going on to the next simulations we would like to comment on the following observation. If the plots presented thus far are examined more closely, it becomes apparent that there exists some dependency amongst the roots, that is more obvious for the ones whose magnitude is not identically equal to one. For example, in Figure 4.1(a), if one draws a straight line from the origin to any of

the roots, then this line must also intersect one other root. This is not a coincidence but has a mathematical justification. Analysis of this phenomenon is postponed until Chapter 5 because it re-appears there as well. We emphasize, however, that this is a result of simultaneous F-B averaging and Procrustes processing and it is not observed is either of these processes is avoided.

The effects of Procrustes processing , that is the replacement of each of the two estimated core rotations matrices by their respective unitary matrices is clearly illustrated by the results of our next simulation example which are displayed in Figure 4.2. The specific array and source scenario simulated in this case again consisted of 3 sources , a uniformly spaced linear array of 15 sensors and spatially white noise. The DOA's in this case where: θ_1=−9.0° , θ_2=6.0° and θ_3=12.3°. The number of snapshots was now N=8 , and since the simplified version of **PRO–ESPRIT** was used , the length of each subarray consisted of ten sensors. The noise power was again normalized to unity and the source covariance matrix was

$$\mathbf{R}_{ss} = \begin{bmatrix} 1.0 & 0.2 & 0.0 \\ 0.2 & 1.0 & 0.0 \\ 0.0 & 0.0 & 1.0 \end{bmatrix}$$

Thus , the signal to noise ratio was 0 dB for each of the three sources. Once more , the results of 100 independent runs are shown. Figure 4.2(a) shows the outcome of the estimator with out the Procrustes processing option , while 4.2(b) shows the outcome of the estimator with the Procrustes processing option. A comparison of these two plots illustrates the tendency of Procrustes processing to place the GEV's of the core rotations pencil on the unit circle. This simulation , therefore , serves to substantiate the earlier claim that Procrustes processing serves as a sub-optimal , closed form means for accommodating the constraint that the GEV's of the core informations pencil lie on the unit circle.

The purpose of the next simulations is to compare the variance of the estimated directions of arrival against the Crame-Rao lower bound (CRLB). Obtaining explicit expressions for the variance of the estimated eigendata via **PRO–ESPRIT** is an impossible task because of the series of eigenvalue and singular value decompositions that are involved. Some work has been done in this area that examines the asymptotic case of infinitely many snapshots. This has partially enabled the asymptotic analysis of MUSIC and **TLS–ESPRIT**. However the results cannot be applied to **PRO–ESPRIT** for the reason that **PRO–ESPRIT**, unlike the former methods, also works with the eigenvalues of the sample X and Y correlation matrices. Also of relevance here is the work done by Hua and Sarkar in [HUA88b] in which they consider first order perturbations

away from the clean data. The basic conclusion there is that, if the perturbations are small, then all five algorithms they investigated, including **PRO–ESPRIT** and **TLS–ESPRIT**, are equivalent, giving estimates of similar bias and variance. For these reasons we shall here compare the CRLB with the sample variance of the estimates. The scenario we were working with was the following. Three signals were arriving from directions θ_1=–2.2°, θ_2=7.1° and θ_3=15.6°. The array consisted of 15 sensors, uniformly spaced on a line and separated by half a wavelength. The F-B averaging version of **PRO–ESPRIT** was used, with each subarray containing 10 elements. In the first simulation, we compare the variance of the estimates of θ_1 versus the associated CRLB, as the number of snapshots changed. The signal to noise ratio of each source was held fixed at 4 dB and all three sources were uncorrelated from each other. The sample variance was obtained from 200 independent runs of our algorithm. The results are plotted in Figure 4.3(a). The most notable feature of this plot is the initial big rate of decrease of the sample variance as the number of snapshots increased. This is attributed to the fact that the noise subtraction process at the covariance level becomes more and more accurate as the number of snapshots increases. In other words, the sample noise correlation matrix approaches more closely the assumed true noise correlation matrix, which in this case was a multiple of the Identity. In the second simulation the results of which are presented in Figure 4.3(b) the parameter that was varied was the SNR ratio of each source. The power of all three sources was changed equally, while the number of snapshots was held fixed at nine. The variance indicated was that of the estimates of θ_1. The same pattern is observed here as well, with the sample variance initially falling at a fast rate, and, although not visible on the graph, after 25 dB it approaches the CRLB quite closely. Finally, we consider the sample variance of our estimates as a function of the subarray length but with a fixed number of elements. What was done was the following. The number of sensors was held fixed at 15. Then, the subarray length was varied, and for each length, the number of subarrays was adjusted so that both forward and backward matrices incorporated the maximum number of possible data. The same three DOA's were assumed as above, while the number of snapshots and SNR of each source was held fixed at 9 and 5.2 dB respectively. In Figure 4.4 we plot the results for the sample variance of θ_1. Observe that the curve obtains its minimum when the size of the subarray is 2/3 of the total array size. This ratio was also cited by Hua in [HUA88a] as the optimal ratio that minimizes the CRLB when the noise perturbation is assumed small.

So far we have been testing our algorithms against simulated data. In the following simulations we will be using real data that were kindly provided by Dr.

Kaveh at the University of Minnesota. Their source is a linear acoustic array of eight uniformly spaced ultra sound sensors. The frequency of the received sound wave is 40KHz. Assuming that the speed of propagation of the sound waves was 330 meters per second, this implies that the wavelength of the signals was about λ=0.825cm. Unlike the typical case when the sensor separation is $\lambda/2$, in this case the separation was 2.13λ. For this particular separation, sources in the region θ=−13.6° to 13.6° are resolved without any angular, but there is ambiguity for signals received from outside of this region. For example, to the array, a source at θ=13.6° and a source at θ=−13.6° appear the same. This ambiguity problem is discussed further in the simulations section of Chapter5. The 3dB beamwidth for this array is given by the inverse sine of 1/(8x2.13), i.e., 3.4°. It is assumed that the source of the sound waves was far from the receivers so that the plane wave equation was obeyed by each one of them. To compensate for array imperfections, the received raw data were calibrated before being processed. The calibration process involved the determination of the array response at 0.5° intervals, and the use of this information to compensate for the deviations away from the ideal array model.

The first case we consider involved two signals coming from θ_1=5° and θ_2=3°. Note that the source separation is less than the 3dB beamwidth. The total number of snapshots we were provided with was N=100. The two sources were uncorrelated, however, the noise was non-white, with unknown correlation matrix. Since the array is linear, to get the **ESPRIT** structure we must break the array into overlapping subarrays, hoping that calibration has ensured identical phase and gain responses by all eight sensors. Knowing that there are two sources, the subarray size must be no less than three. In this case we chose to use the F-B version of **PRO–ESPRIT**. Of interest is the fact both the AIC and the MDL criteria fail to estimate correctly the number of sources when applied to this as well as to the next set of data. First we consider the angle estimates as a function of the subarray length, with all 100 snapshots being used. The results are summarized in Table 4.1(a). It is seen that with a subarray of length 3, the estimates are well off their actual value, especially the one for θ_2. The estimates improve as the subarray length begins to increase, and as seen, the least total absolute error between the estimates and their actual values is achieved when the subarray length is six. This is in accordance with our earlier claim that the optimal subarray length is approximately 2/3 of the overall array length. In Table 4.2(b) we present tabulate the estimates and the absolute error as a for a fixed subarray of length five, and changing number of snapshots. The thing to note here is that the estimates show little, if no improvement as the number of snapshots goes from 10 to 100. This is in accordance with the results of the first

simulation claiming that as a function of the number of snapshots, **PRO–ESPRIT** achieves its top performance at a small such number, and the effect of other parameters such as SNR then predominates. The next scenario was slightly different. It involved three signals coming from $\theta_1=-10°$, $\theta_2=5°$ and $\theta_3=3°$. Tables 4.2(a) and 4.2(b) tabulate the estimates and the total absolute error as a function of the subarray length and as a function of the number of snapshots respectively. For this case we used **PRO–ESPRIT** without the F-B option. For some inexplicable reason, with the use of F-B averaging **PRO–ESPRIT** failed to resolve θ_2 and θ_3, so we chose not to use it at all. The AIC and MDL criteria fail again to estimate the true number of sources. All three sources were uncorrelated with unknown power, and the noise was was given as spatially and temporally white. The results here are less consistent compared to the previous ones. For example, subarrays of length four result into better estimates than subarrays of length five, while the opposite would be expected. A similar inconsistency is observed in the estimates with changing snapshot numbers and subarray length fixed at six.

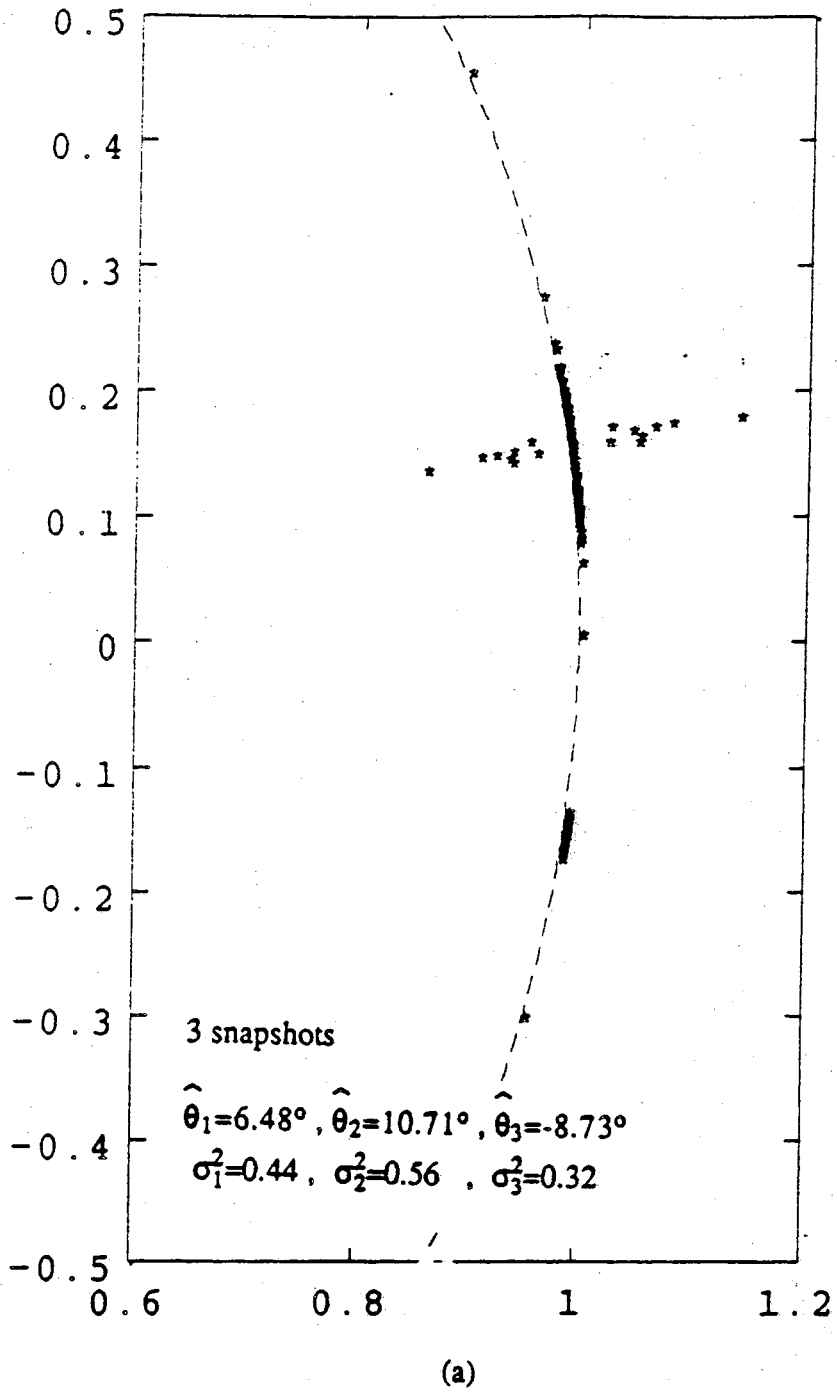

(a)

Figure 4.1 The performance of **PRO–ESPRIT** when applied in a uniform linear array scenario consisting of 15 sensors, three sources at θ_1=6.5°, θ_2=10.3° and θ_3=–9°. The dashed curve represents the unit circle. The results of 100 independent trials are shown.

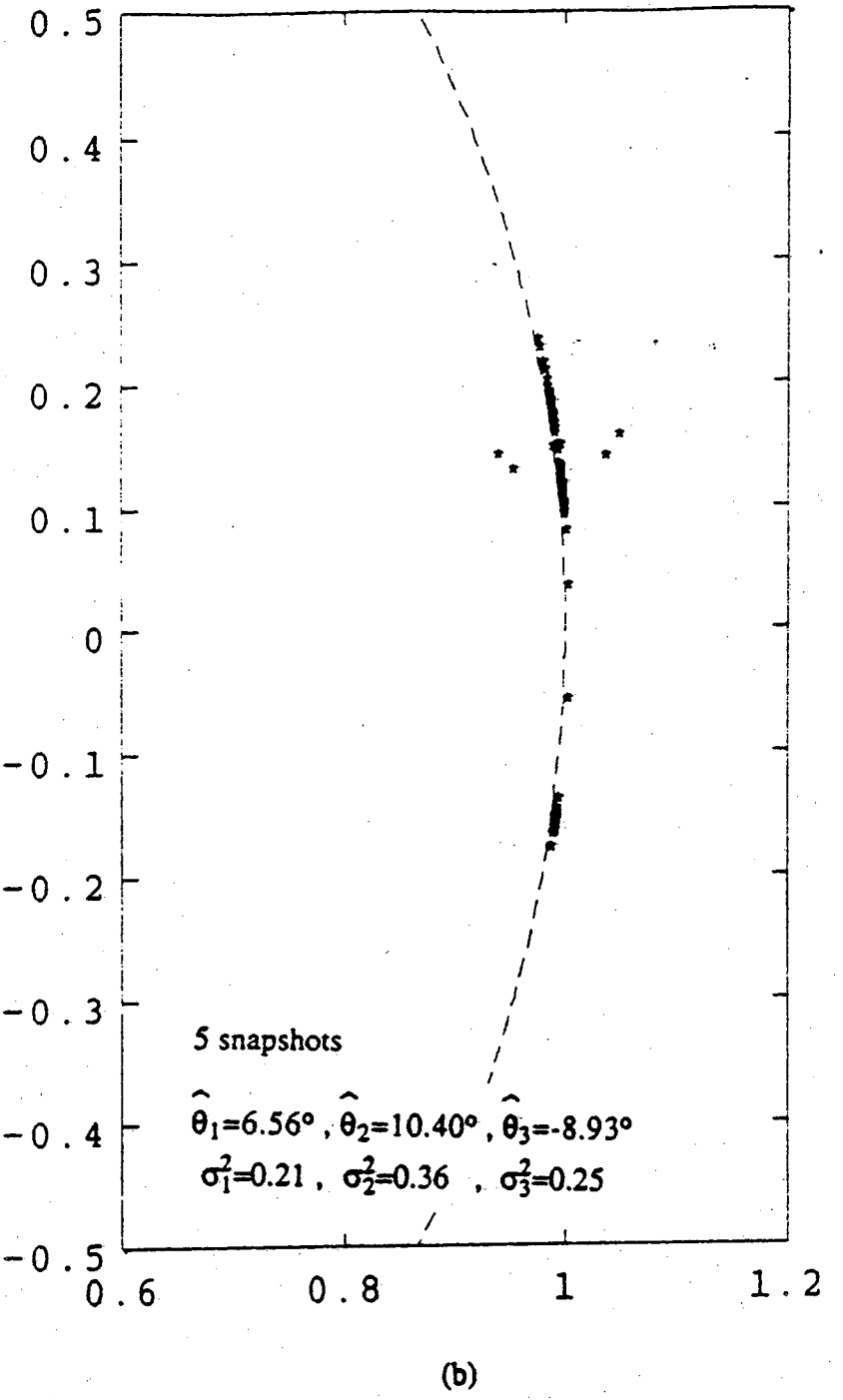

(b)

Figure 4.1 (continued)

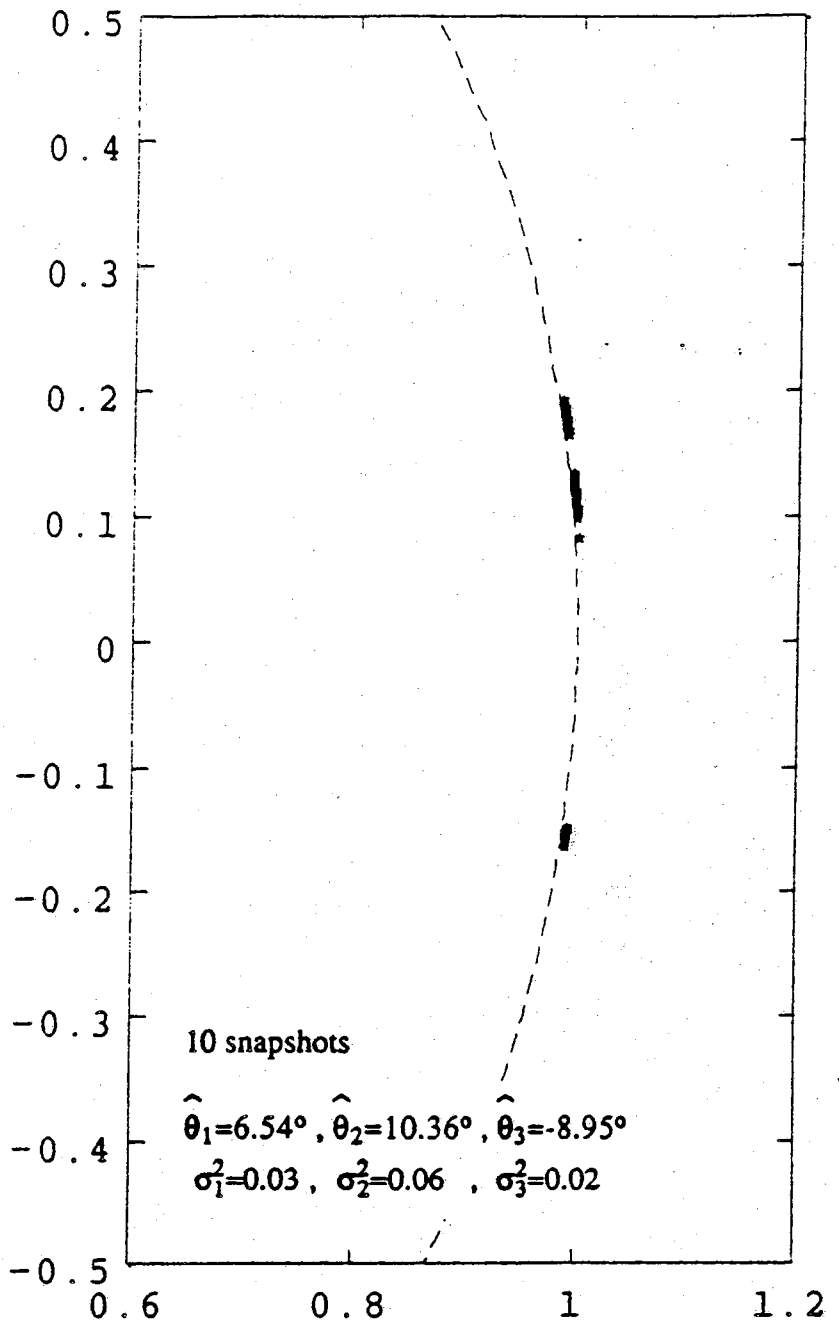

(c)

Figure 4.1 (continued)

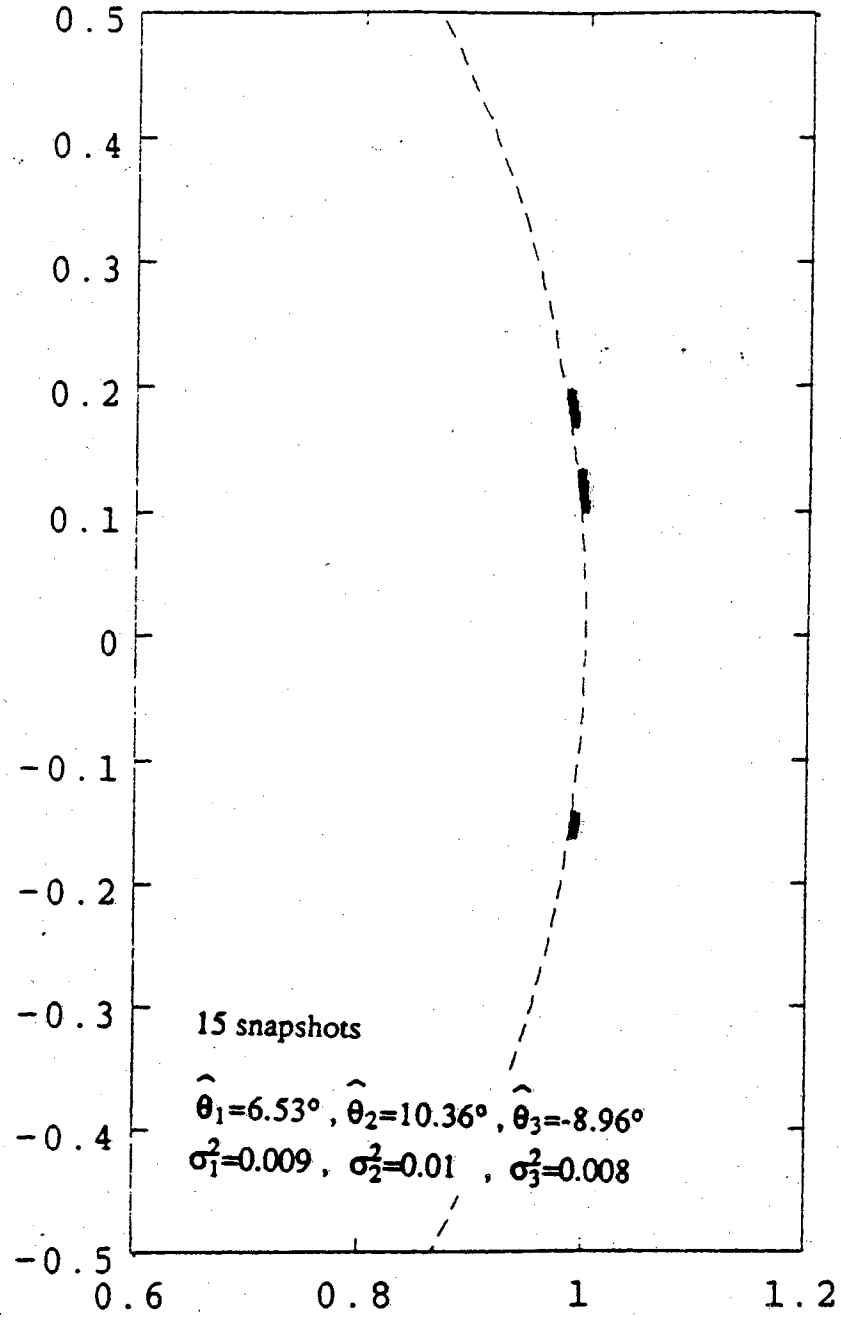

(d)

Figure 4.1 (continued)

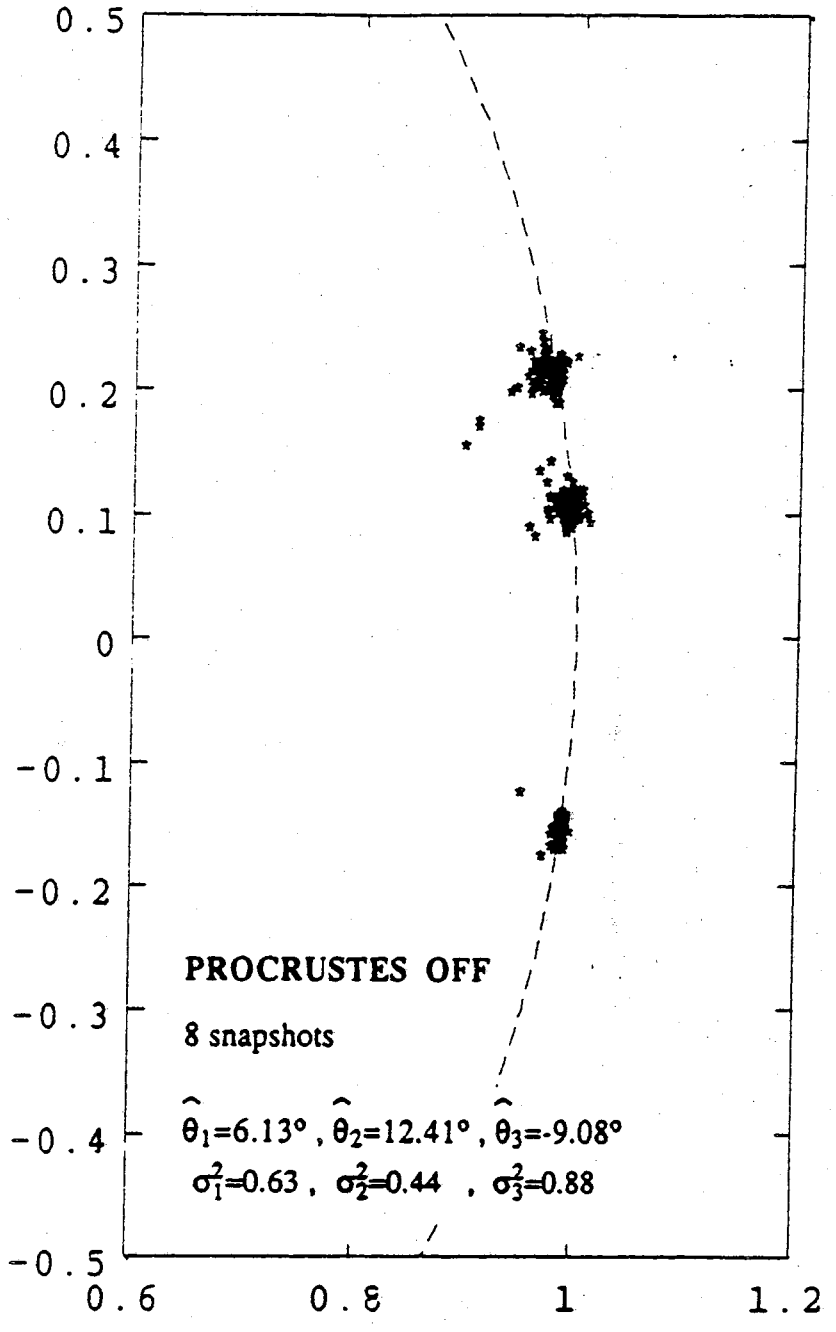

(a)

Figure 4.2 Comparison of **PRO–ESPRIT** performance for Procrustes processing "switched on" versus Procrustes processing "switched off". The scenario consisted of a uniform linear array of 15 sensors and three sources at θ_1=–9°, θ_2=6°, θ_3=12.3°. The results of 100 independent trials are plotted.

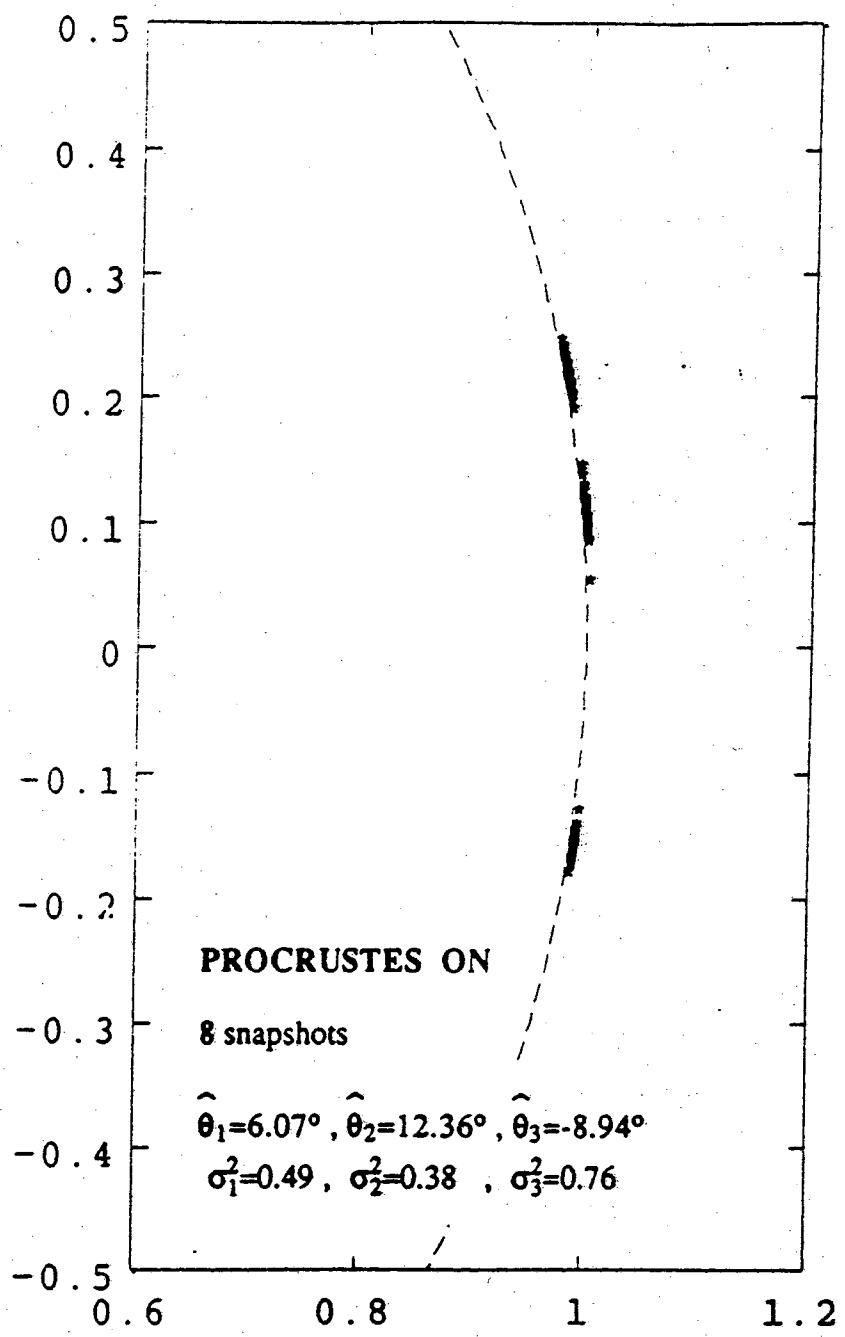

(b)

Figure 4.2 (continued)

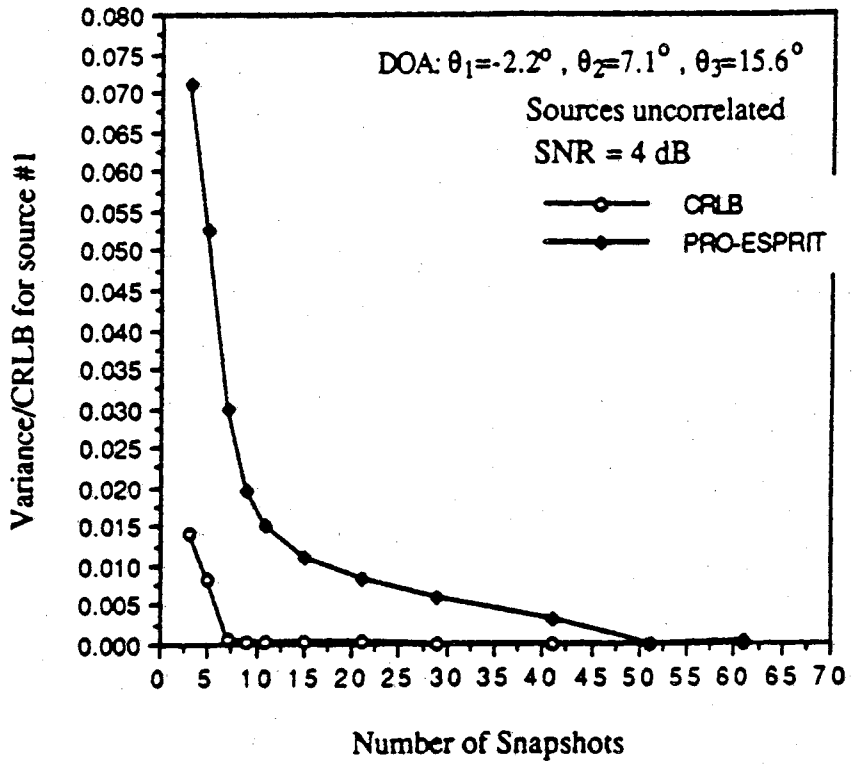

(a)

Figure 4.3 A comparison of the sample variance of estimates obtained via **PRO–ESPRIT** and the Cramer Rao Lower Bound. In 4.3(a) the number of snapshots is allowed to vary, and in 4.3(b) the SNR varies.

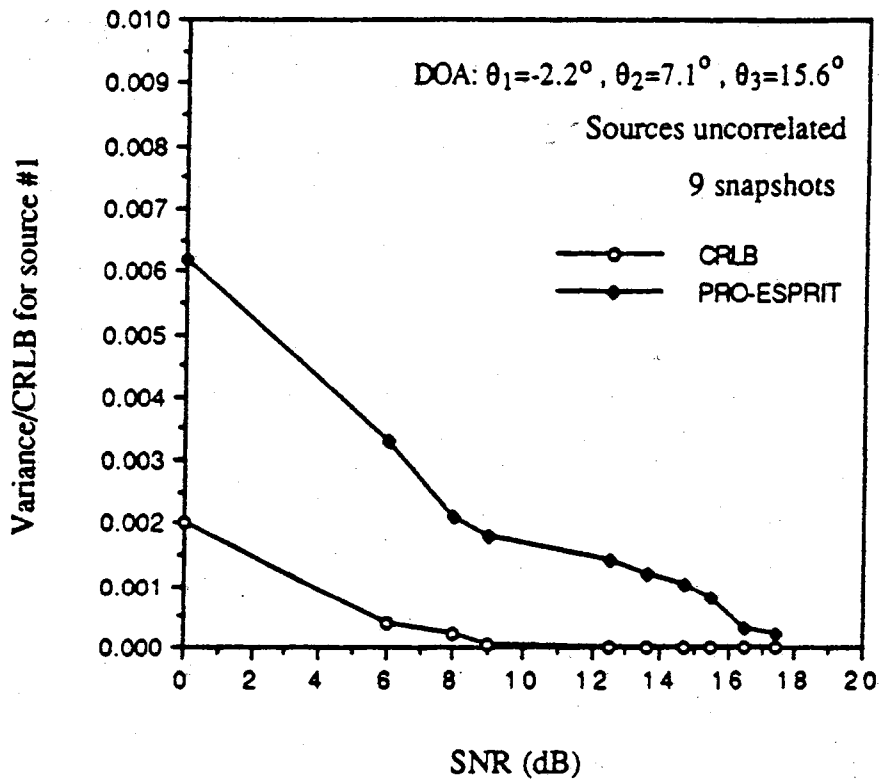

(b)

Figure 4.3 (continued)

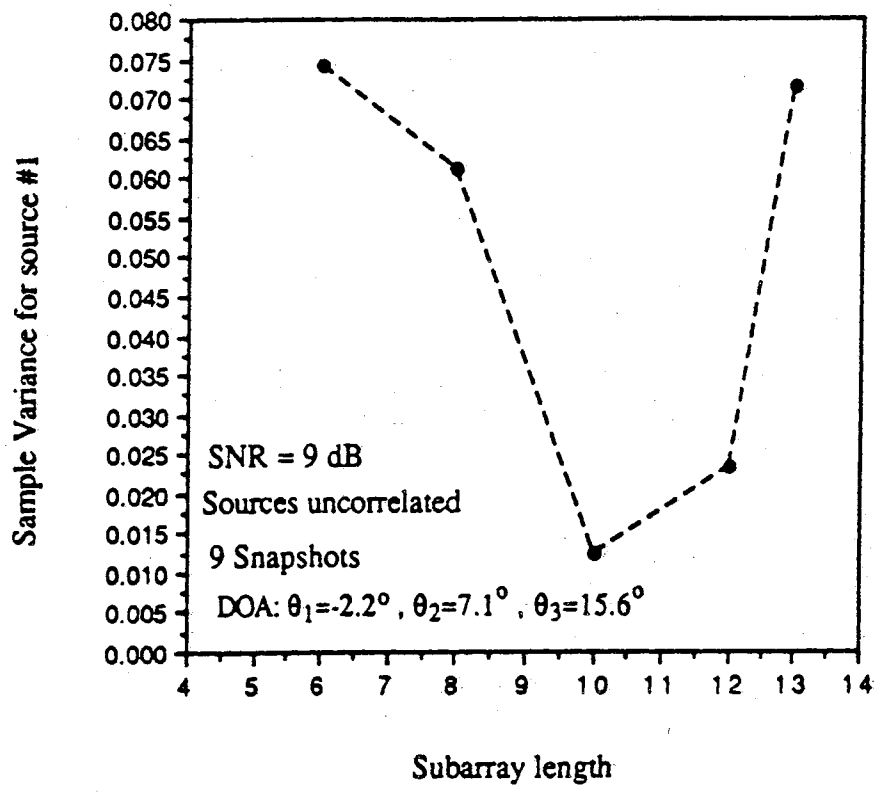

Figure 4.4 The number of sensors is held fixed and the subarray size is changed. Minimum variance is obtained when the subarray size is 2/3 of the total array size (L=10).

Table 4.1 Performance of **PRO–ESPRIT** with real data. There are two sources located at 3° and 5°. The estimates are listed as a function of the subarray length and the number of snapshots. F-B averaging was used.

Subarray length	$\hat{\theta}_1$	$\hat{\theta}_2$	Absolute error
3	4.25	-0.63	4.38
4	4.29	2.33	1.42
5	4.95	3.45	0.5
6	4.82	3.25	0.43
7	4.63	3.16	0.53

(a)

No. of snapshots	$\hat{\theta}_1$	$\hat{\theta}_2$	Absolute error
10	4.81	3.29	0.48
30	4.93	3.35	0.42
50	5.02	3.44	0.46
70	5.03	3.41	0.44
90	4.95	3.46	0.51
100	4.95	3.46	0.51

(b)

Table 4.2 The number of sources is now three, at 3°, 5° and −10°. The estimates are listed as a function of the subarray length and the number of snapshots. Only Forward averaging was used.

Subarray length	$\hat{\theta}_1$	$\hat{\theta}_2$	$\hat{\theta}_3$	Absolute Error
4	-10.11	4.32	2.01	1.78
5	-10.29	4.02	1.88	2.39
6	-10.51	4.12	3.07	1.46
7	-10.62	5.28	1.07	2.83

(a)

No. of snapshots	$\hat{\theta}_1$	$\hat{\theta}_2$	$\hat{\theta}_3$	Absolute error
10	-10.14	4.33	-5.13	8.94
30	-10.43	4.09	-1.54	5.88
50	-10.45	9.45	2.56	5.34
70	-10.64	4.10	1.09	3.45
90	-10.69	3.95	0.32	4.42
100	-10.51	4.12	3.07	1.46

(b)

CHAPTER 5
PRO-ESPRIT AND PSEUDO F-B AVERAGING

5.1 Pseudo-Forward-Backward Averaging (PFBAVG)

The motivation behind the development of PFBAVG here is the computation reduction and performance improvement achieved when conventional FBAVG [GOLU83a,WAX85] is employed in the case of **PRO–ESPRIT** applied in a uniform linear array (ULA) scenario [ZOLT89a]. Unfortunately, conventional FBAVG is not generally applicable for arbitrary array geometries. However, similar benefits may be reaped by exploiting the fact that the elements of the invariance operator Φ in (3.1) lie on the unit circle. To this end, we introduce an entity referred to as the FB data pencil, denoted $\{\mathbf{X}_{FB}\ ,\ \mathbf{Y}_{FB}\}$. The two components of this pencil, $\mathbf{X}_{FB}$ and $\mathbf{Y}_{FB}$, are constructed from the X and Y data matrices defined in Chapter 2 according to the following prescription:

$$\mathbf{X}_{FB} = \left[\mathbf{X} : \mathbf{Y}^*\right] \quad , \quad \mathbf{Y}_{FB} = \left[\mathbf{Y} : \mathbf{X}^*\right] \tag{5.1}$$

Two questions immediately arise. First, does the FB data pencil satisfy the requirements necessary for meaningful application of **PRO–ESPRIT**? Second, what is the advantage of working with the FB data pencil? These two questions are answered in succession below.

The applicability of **PRO–ESPRIT** in the case of the FB data pencil is demonstrated under noiseless conditions. With $\mathbf{N}_x = \mathbf{O}$ and $\mathbf{N}_y = \mathbf{O}$ in (2.9a) and (2.9b), respectively, $\mathbf{X} = \mathbf{AS}$ and $\mathbf{Y} = \mathbf{A\Phi S}$. Substituting these expressions for $\mathbf{X}$ and $\mathbf{Y}$ in (5.1) yields

$$\mathbf{X}_{FB}^{2D} = \left[\mathbf{AS} : \mathbf{A}^*\Phi^*\mathbf{S}^*\right] = \left[\mathbf{A} : \mathbf{A}^*\Phi^*\right]\begin{bmatrix}\mathbf{S} & \mathbf{O}\\ \mathbf{O} & \mathbf{S}^*\end{bmatrix} \tag{5.2a}$$

$$\mathbf{Y}_{FB}^{2D} = \left[\mathbf{A\Phi S} : \mathbf{A}^*\Phi^*\Phi\mathbf{S}^*\right] = \left[\mathbf{A} : \mathbf{A}^*\Phi^*\right]\begin{bmatrix}\Phi & \mathbf{O}\\ \mathbf{O} & \Phi\end{bmatrix}\begin{bmatrix}\mathbf{S} & \mathbf{O}\\ \mathbf{O} & \mathbf{S}^*\end{bmatrix} \tag{5.2b}$$

where in (5.2b) we have exploited the fact that $\Phi\Phi^* = \mathbf{I}$. The super-script 2D is

intended to indicate that these are the noiseless forms of the matrices in which case each is of rank 2D. Now, consider the pencil difference $\mathbf{Y}_{FB}^{2D} - \lambda\mathbf{X}_{FB}^{2D}$:

$$\mathbf{Y}_{FB}^{2D} - \lambda\mathbf{X}_{FB}^{2D} = \left[\mathbf{A} : \mathbf{A}^*\Phi^*\right]\begin{bmatrix}\Phi - \lambda\mathbf{I} & \mathbf{0} \\ \mathbf{0} & \Phi - \lambda\mathbf{I}\end{bmatrix}\begin{bmatrix}\mathbf{S} & \mathbf{0} \\ \mathbf{0} & \mathbf{S}^*\end{bmatrix} \tag{5.3}$$

For the moment, assume the Mx2D matrix $[\mathbf{A} : \mathbf{A}^*\Phi^*]$ to be of full rank equal to the number of columns equal to 2D. Cases where this is not true will be dealt with in Section 5.3. Observing (5.3), it is noted that when $\lambda = \Phi_{ii}$, an entry from each of the block matrices $\Phi - \lambda\mathbf{I}$ is nullified reducing the rank of $\mathbf{Y}_{FB}^{2D} - \lambda\mathbf{X}_{FB}^{2D}$ from 2D to 2D-2. Therefore, under noiseless conditions, each Φ_{kk}, k=1,...,D, is a GEV of the pencil $\{\mathbf{X}_{FB}^{2D}, \mathbf{Y}_{FB}^{2D}\}$ as desired. However, in contrast to the situation with the noiseless pencil $\{\mathbf{X}^D, \mathbf{Y}^D\}$, each Φ_{kk}, k=1,...,D, is a GEV of multiplicity two, as opposed to multiplicity one. The implications of this will be addressed shortly. A comparison of (5.2a) with (5.2b) also reveals that the respective column and row spaces of $\mathbf{X}_{FB}^{2D}$ and $\mathbf{Y}_{FB}^{2D}$ are identical, a 2D-dimensional subspace in each case. These observations certify the applicability of **PRO–ESPRIT**.

The advantage of working with the F-B data pencil arises from the fact that $\mathbf{X}_{FB}$ and $\mathbf{Y}_{FB}$ satisfy the following relationship:

$$\mathbf{Y}_{FB} = \mathbf{X}_{FB}^*\,\Gamma \tag{5.4}$$

where Γ is a 2Nx2N block reverse permutation matrix defined by

$$\Gamma = \begin{bmatrix}\mathbf{O}_{NxN} & \mathbf{I}_{NxN} \\ \mathbf{I}_{NxN} & \mathbf{O}_{NxN}\end{bmatrix} \tag{5.5}$$

The fact that one component of the FB data pencil may be constructed from the other is not surprising since each contains the same information. In light of the relationship in (5.4), it turns out that an SVD of $\mathbf{X}_{FB}$ is sufficient to construct the SVD of $\mathbf{Y}_{FB}$. To justify this assertion, consider the SVD of $\mathbf{X}_{FB}$: $\mathbf{X}_{FB} = \mathbf{U}_X\Sigma_X\mathbf{V}_X^H$. Substituting into (5.4) yields

$$\mathbf{Y}_{FB} = \{\mathbf{U}_X^*\}\,\Sigma_X\,\{\Gamma\mathbf{V}_X^*\}^H \tag{5.6}$$

Note that Γ in (5.5) is a symmetric, unitary matrix, i.e., it satisfies $\Gamma = \Gamma^T$ and $\Gamma^T\Gamma = \mathbf{I}$. Thus, the matrix product $\Gamma\mathbf{V}_X^*$ is unitary. If $\mathbf{Y}_{FB} = \mathbf{U}_Y\Sigma_Y\mathbf{V}_Y^H$ represents the SVD of $\mathbf{Y}_{FB}$, it is deduced from uniqueness considerations that the following relationships hold:

$$\mathbf{U}_Y = \mathbf{U}_X^* \quad , \quad \Sigma_Y = \Sigma_X \quad , \quad \mathbf{V}_Y = \Gamma\,\mathbf{V}_X^* \tag{5.7}$$

Note that these relationships hold regardless of whether noise is present or not. These relationships may be exploited to construct a 2Dx2D core information

matrix solely from the SVD of $\mathbf{X}_{FB}$. We elaborate on this point.

Consider the SVD of the noiseless matrix $\mathbf{X}_{FB}^{2D}$ in (5.2a):

$$\mathbf{X}_{FB}^{2D} = \mathbf{U}_X^{2D} \Sigma_X^{2D} \mathbf{V}_X^{2D\,H} \tag{5.8}$$

Note that this SVD representation only includes the 2D nonzero singular values of $\mathbf{X}_{FB}^{2D}$ such that Σ_X^{2D} is a 2Dx2D diagonal matrix. It follows from the argument above that the SVD of the noiseless $\mathbf{Y}_{FB}^{2D}$ in (5.2b) may be expressed as follows:

$$\mathbf{Y}_{FB}^{2D} = \{\mathbf{U}_X^{2D}\}^* \, \Sigma_X^{2D} \, \{\Gamma \mathbf{V}_X^{2D*}\}^H \tag{5.9}$$

Now, since the range space of $\mathbf{X}_{FB}^{2D}$ is the same as that of $\mathbf{Y}_{FB}^{2D}$, it follows that

$$\text{Range}\{\mathbf{U}_X^{2D}\} = \text{Range}\{\mathbf{U}_X^{2D*}\} = \text{Range}\left\{\left[\mathbf{A} : \mathbf{A}^* \Phi^*\right]\right\} \tag{5.10}$$

Hence, $\mathbf{U}_X^{2D}$ may be rotated into $\{\mathbf{U}_X^{2D}\}^*$ via a 2Dx2D unitary matrix as follows:

$$\{\mathbf{U}_X^{2D}\}^* = \mathbf{U}_X^{2D} \, \mathbf{Q}_U \quad \text{where: } \mathbf{Q}_U = \{\mathbf{U}_X^{2D}\}^H \{\mathbf{U}_X^{2D}\}^* \quad (2Dx2D) \tag{5.11}$$

In addition, since the range space of $\mathbf{X}_{FB}^{2D\,H}$ is the same as that of $\mathbf{Y}_{FB}^{2D\,H}$, it follows that

$$\text{Range}\{\mathbf{V}_X^{2D}\} = \text{Range}\{\Gamma \, \mathbf{V}_X^{2D*}\} = \text{Range}\left\{\begin{bmatrix} \mathbf{S}^H & \mathbf{O} \\ \mathbf{O} & \mathbf{S}^T \end{bmatrix}\right\} \tag{5.12}$$

Hence, $\mathbf{V}_X^{2D}$ may be rotated into $\Gamma \, \mathbf{V}_X^{2D*}$ via a 2Dx2D unitary matrix as follows:

$$\Gamma \, \mathbf{V}_X^{2D*} = \mathbf{V}_X^{2D} \, \mathbf{Q}_V \quad \text{where: } \mathbf{Q}_V = \{\mathbf{V}_X^{2D}\}^H \, \Gamma \, \{\mathbf{V}_X^{2D}\}^* \quad (2Dx2D) \tag{5.13}$$

The cumulative effect of these observations is that the pencil difference $\mathbf{Y}_{FB}^{2D} - \lambda \mathbf{X}_{FB}^{2D}$ may be expressed in the following form:

$$\begin{aligned} \mathbf{Y}_{FB}^{2D} - \lambda \mathbf{X}_{FB}^{2D} &= \{\mathbf{U}_X^{2D}\}^* \, \Sigma_X^{2D} \, \{\Gamma \mathbf{V}_X^{2D*}\}^H - \lambda \mathbf{U}_X^{2D} \Sigma_X^{2D} \mathbf{V}_X^{2D\,H} \\ &= \mathbf{U}_X^{2D} \{\mathbf{Q}_U \Sigma_X^{2D} \mathbf{Q}_V^H - \lambda \, \Sigma_X^{2D}\} \mathbf{V}_X^{2D\,H} \end{aligned} \tag{5.14}$$

where $\mathbf{Q}_U$ and $\mathbf{Q}_V$ are given by (5.11) and (5.13), respectively. From (5.14), it is deduced that each Φ_{kk} k=1,..D, is an EV of the 2Dx2D core information matrix (CIM)

$$\Psi_{2D} = \{\Sigma_X^{2D}\}^{-1} \mathbf{Q}_U \Sigma_X^{2D} \mathbf{Q}_V^H \tag{5.15}$$

of multiplicity 2. Note that all the information required to construct Ψ_{2D} may be obtained from an SVD of the Mx2N matrix $\mathbf{X}_{FB}^{2D}$. However, this does not save computation since the SVD of an Mx2N matrix requires more computation than

the SVD of two MxN matrices. Also, in the case of noisy data, it is not possible to obtain unbiased estimates of the right singular vectors of $\mathbf{X}_{FB}^{2D}$. Hence, we now present alternative means for extracting the information necessary to construct the 2Dx2D CIM Ψ_{2D} defined by (5.15).

We first note that the information necessary to construct $\mathbf{U}_X^{2D}$ and Σ_X^{2D} may be gleaned from an EVD of the MxM noiseless FB correlation matrix $\mathbf{C}_{FB}^{XX} = \frac{1}{2N}\mathbf{X}_{FB}^{2D}\mathbf{X}_{FB}^{2DH}$. This matrix may be expressed in terms of the MxM noiseless correlation matrices $\mathbf{C}_{XX}$ and $\mathbf{C}_{YY}$ as follows:

$$\mathbf{C}_{FB}^{XX} = \frac{1}{2N}\mathbf{X}_{FB}^{2D}\mathbf{X}_{FB}^{2DH} = \frac{1}{2N}\left[\mathbf{X}^{D} \vdots \mathbf{Y}^{D*}\right]\begin{bmatrix}\mathbf{X}^{DH} \\ \mathbf{Y}^{DT}\end{bmatrix} = \frac{1}{2}\{\mathbf{C}_{XX} + \mathbf{C}_{YY}^{*}\} \qquad (5.16)$$

The expression on the far RHS of (5.16) is referred to as a pseudo-forward-backward average. Second, computation of the right singular vectors of $\mathbf{X}_{FB}^{2D}$ may be avoided if the classical relationship between the left and right singular vectors of a matrix is invoked. Invoking such, we find that $\mathbf{V}_X^{2D} = \mathbf{X}_{FB}^{2DH}\mathbf{U}_X^{2D}\{\Sigma_X^{2D}\}^{-1}$ which leads to the following alternative expression for $\mathbf{Q}_V$ defined in (5.13):

$$\mathbf{Q}_V = \{\Sigma_X^{2D}\}^{-1}\{\mathbf{U}_X^{2D}\}^{H}\,\mathbf{C}_{FB}^{XY}\,\{\mathbf{U}_X^{2D}\}^{*}\{\Sigma_X^{2D}\}^{-1} \qquad (5.17)$$

Here $\mathbf{C}_{FB}^{XY} = \frac{1}{2N}\mathbf{X}_{FB}^{2D}\mathbf{Y}_{FB}^{2DH}$ and may be expressed in terms of the noiseless cross-correlation matrix $\mathbf{C}_{XY}$ as follows:

$$\mathbf{C}_{FB}^{XY} = \frac{1}{2N}\mathbf{X}_{FB}^{2D}\mathbf{Y}_{FB}^{2DH} = \frac{1}{2N}\left[\mathbf{X}^{D} \vdots \mathbf{Y}^{D*}\right]\begin{bmatrix}\mathbf{Y}^{DH} \\ \mathbf{X}^{DT}\end{bmatrix} = \frac{1}{2}\{\mathbf{C}_{XY} + \mathbf{C}_{XY}^{T}\} \qquad (5.18)$$

Note that $\mathbf{C}_{FB}^{XY}$ is a symmetric matrix, i. e., $\mathbf{C}_{FB}^{XYT} = \mathbf{C}_{FB}^{XY}$. This property will be invoked at a later point. Note, though, that $\mathbf{C}_{FB}^{XY}$ is not Hermitian in general.

Construction of an estimate of the 2Dx2D CIM Ψ_{2D}, therefore, requires an estimate of the following three quantities: $\mathbf{C}_{XX}$, $\mathbf{C}_{YY}$, and $\mathbf{C}_{XY}$. In the case of noisy data, these quantities may be estimated by a partitioning of the "cleaned" 2Mx2M Z correlation matrix formed in accordance with the following prescription

$$\hat{\mathbf{C}}_{ZZ} = \hat{\mathbf{R}}_{ZZ} - \lambda_{min}^{zz}\mathbf{R}_{nn}^{ZZ} = \begin{bmatrix}\hat{\mathbf{C}}_{XX} & \hat{\mathbf{C}}_{XY} \\ \hat{\mathbf{C}}_{YX} & \hat{\mathbf{C}}_{YY}\end{bmatrix} \qquad (5.19)$$

Here $\hat{\mathbf{R}}_{ZZ} = \frac{1}{N}\mathbf{Z}\mathbf{Z}^{H}$ where $\mathbf{Z} = \begin{bmatrix}\mathbf{X} \\ \mathbf{Y}\end{bmatrix}$. Also, $\mathbf{R}_{nn}^{ZZ}$ is an estimate of the normalized noise covariance matrix associated with the overall Z array. Finally, $\hat{\lambda}_{min}^{zz}$ is the smallest GEV of the pencil $\{\mathbf{R}_{ZZ}, \mathbf{R}_{nn}^{ZZ}\}$. Inverse iteration may be employed in order to obtain a "fast" estimate of λ_{min}^{zz}; only a "rough" estimate of λ_{min}^{zz} is

required. If an estimate of $\mathbf{R}_{nn}^{ZZ}$ is not available a-priori via experimental measurements or parametric modeling, it may be extracted from $\hat{\mathbf{R}}_{ZZ}$ via the method of LeCadre [LEC89].

With the estimates $\hat{\mathbf{C}}_{XX}$, $\hat{\mathbf{C}}_{YY}$ and $\hat{\mathbf{C}}_{XY}$ obtained in this fashion, the 2Dx2D CIM Ψ_{2D} is constructed from $\hat{\mathbf{C}}_{FB} = \frac{1}{2}\{\hat{\mathbf{C}}_{XY} + \hat{\mathbf{C}}_{XY}^{T}\}$ and the rank 2D truncated EVD of the MxM matrix $\hat{\mathbf{C}}_{FB}^{XX} = \frac{1}{2}\{\hat{\mathbf{C}}_{XX} + \hat{\mathbf{C}}_{YY}^{*}\}$. This procedure requires a single MxM EVD to construct the 2Dx2D CIM Ψ_{2D}, whereas **PRO–ESPRIT** without PFBAVG requires two MxM EVD's to construct the DxD CIM Ψ_{D}. Both procedures also require the initial coarse "cleaning" of the Z correlation matrix [ZOLT89a] described by (5.19). The price paid for the reduction in computation achieved via PFBAVG is an attendant reduction in the maximum number of sources the algorithm is able to handle. Specifically, as a consequence of the dual multiplicity of each of the GEV's, the maximum number of sources **PRO–ESPRIT** with PFBAVG can handle is M/2 -1. Recall that the total number of sensors is 2M. Without PFBAVG, **PRO–ESPRIT** is able to handle up to M-1 sources.

It would also appear that there is an additional trade-off due to the fact the CIM Ψ_{2D} constructed in the case of PFBAVG is 2Dx2D. With no PFBAVG, the CIM Ψ_{D} is DxD. If we are only interested in the directions of each source, it suffices to construct the characteristic equation of Ψ_{2D} and compute the associated roots. $|\Psi_{2D} - \lambda\mathbf{I}|$ is a polynomial of order 2D. Ideally, this polynomial has D double roots, with each root lying on the unit circle. This property may be exploited to reduce the problem to that of solving a polynomial of order D having exactly the same roots in the ideal case. We first refine the estimate of Ψ_{2D} to incorporate Procrustes processing.

5.2 Procrustes Processing and Its Effects

In the prescription for constructing Ψ_{2D} according to (5.15), $\mathbf{Q}_U$ and $\mathbf{Q}_V$ are constructed according to (5.11) and (5.17), respectively, which we repeat here:

$$\mathbf{Q}_U = \{\mathbf{U}_X^{2D}\}^H \{\mathbf{U}_X^{2D}\}^* \tag{5.20}$$

$$\mathbf{Q}_V = \{\Sigma_X^{2D}\}^{-1}\{\mathbf{U}_X^{2D}\}^H \frac{1}{2}\{\hat{\mathbf{C}}_{XY} + \hat{\mathbf{C}}_{XY}^{T}\} \{\mathbf{U}_X^{2D}\}^*\{\Sigma_X^{2D}\}^{-1} \tag{5.21}$$

where the columns of $\mathbf{U}_X^{2D}$ comprise the 2D "largest" EVEC's of $\hat{\mathbf{C}}_{FB}^{XX} = \frac{1}{2}\{\hat{\mathbf{C}}_{XX} + \hat{\mathbf{C}}_{YY}^{*}\}$. In the case of noisy data, these expressions provide asymptotically unbiased estimates of the unitary matrices obtained under

noiseless conditions. However, in the practical case of a finite number of snapshots, these matrices will not be unitary. In accordance with the original development of PRO-ESPRIT in [ZOLT89a], an improvement in performance can be achieved if we replace each of the two matrices $\mathbf{Q}_U$ and $\mathbf{Q}_V$ by the respective "closest" unitary matrix, in a Frobenius norm sense. If $\mathbf{Q}$ is a square matrix, and $\mathbf{Q} = \mathbf{U}\Sigma\mathbf{V}^H$ is its SVD, the "closest" unitary matrix to $\mathbf{Q}$ is $\hat{\mathbf{Q}} = \mathbf{U}\mathbf{V}^H$ [GOLU83]. Now, it is easily ascertained that $\mathbf{Q}_U$ defined by (5.20) satisfies the following property: $\mathbf{Q}_U\mathbf{Q}_U^H = \{\mathbf{Q}_U^H\mathbf{Q}_U\}^*$. $\mathbf{Q}_V$ in (5.21) satisfies the same property: $\mathbf{Q}_V\mathbf{Q}_V^H = \{\mathbf{Q}_V^H\mathbf{Q}_V\}^*$. The following theorem is relevant.

Theorem 1. If $\hat{\mathbf{Q}}$ denotes the closest unitary matrix, in a Frobenius norm sense, to a matrix $\mathbf{Q}$ satisfying $\mathbf{Q}\mathbf{Q}^H = \{\mathbf{Q}^H\mathbf{Q}\}^*$, then $\hat{\mathbf{Q}}$ is symmetric, i. e., $\hat{\mathbf{Q}} = \hat{\mathbf{Q}}^T$.

Proof: Since $\mathbf{Q}\mathbf{Q}^H = \{\mathbf{Q}^H\mathbf{Q}\}^*$, it follows that each eigenvector of $\mathbf{Q}^H\mathbf{Q}$ is the conjugate of the respective eigenvector of $\mathbf{Q}\mathbf{Q}^H$. Now, the eigenvectors of $\mathbf{Q}\mathbf{Q}^H$ are the left singular vectors of $\mathbf{Q}$, while the eigenvectors of $\mathbf{Q}^H\mathbf{Q}$ are the right singular vectors of $\mathbf{Q}$. Thus, the SVD of $\mathbf{Q}$ may be expressed in the following form:

$$\mathbf{Q} = \mathbf{U}\Sigma\mathbf{V}^H = \mathbf{U}\Sigma\{\mathbf{U}^*\}^H = \mathbf{U}\Sigma\mathbf{U}^T$$

and the closest unitary matrix according to Procrustes theorem is $\hat{\mathbf{Q}} = \mathbf{U}\mathbf{U}^T$ which satisfies $\hat{\mathbf{Q}} = \hat{\mathbf{Q}}^T$. Q.E.D.

Let $\hat{\mathbf{Q}}_U$ and $\hat{\mathbf{Q}}_V$ denote the "closest" unitary matrices to $\mathbf{Q}_U$ and $\mathbf{Q}_V$, respectively. It follows from this theorem and from observations made previously that $\hat{\mathbf{Q}}_U = \hat{\mathbf{Q}}_U^T$ and $\hat{\mathbf{Q}}_V = \hat{\mathbf{Q}}_V^T$. In addition, the above theorem also indicates that to determine the "closest" unitary matrix to either $\mathbf{Q}_U$ or $\mathbf{Q}_V$, we need only compute the corresponding left singular vectors. A full SVD of either matrix is not required. This has implications with regard to the computational load. From this point onward, we will assume that Procrustes processing has been incorporated into the construction of the CIM, Ψ_{2D}.

After Procrustes processing, the CIM is given by $\Psi_{2D} = \{\Sigma_X^{2D}\}^{-1}\hat{\mathbf{Q}}_U\Sigma_X^{2D}\hat{\mathbf{Q}}_V^H$, where $\hat{\mathbf{Q}}_U$ is a symmetric, unitary matrix as is $\hat{\mathbf{Q}}_V$. The following theorem is relevant.

Theorem 2. Let $\mathbf{Q}_1$ and $\mathbf{Q}_2$ each be a complex-valued, unitary matrix, of the same dimension, with each exhibiting symmetry as well, i. e.,

$$\mathbf{Q}_1\mathbf{Q}_1^H = \mathbf{Q}_1^H\mathbf{Q}_1 = \mathbf{I} \text{ and } \mathbf{Q}_1 = \mathbf{Q}_1^T \quad ; \quad \mathbf{Q}_2\mathbf{Q}_2^H = \mathbf{Q}_2^H\mathbf{Q}_2 = \mathbf{I} \text{ and } \mathbf{Q}_2 = \mathbf{Q}_2^T$$

Also, let Σ be a nonsingular matrix. If λ_i is an eigenvalue of the matrix

$\Sigma^{-1}\, \mathbf{Q}_1\, \Sigma\, \mathbf{Q}_2^H$, then $\frac{1}{\lambda_i^*}$ is an eigenvalue of $\Sigma^{-1}\, \mathbf{Q}_1\, \Sigma\, \mathbf{Q}_2^H$ as well.

The proof of this theorem is provided in Appendix A. Recall that in the ideal noiseless case, each eigenvalue (EV) of Ψ_{2D} is of multiplicity two and lies on the unit circle. In the case of noisy data, Theorem 2 indicates that the only thing we can say is that if λ_i is an EV of $\hat{\Psi}_{2D}$, $1/\lambda_i^*$ is an EV as well. Note that the fact that $\mathbf{Q}_1$ and $\mathbf{Q}_2$ are both symmetric as well as unitary was important in proving this theorem. Similar statements cannot be made with regard to the DxD CIM obtained from PRO-ESPRIT without PFBAVG. Now, invoking this theorem, we make two pertinent observations. First, if λ_i is a root of the characteristic polynomial of $\hat{\Psi}_{2D}$, $|\hat{\Psi}_{2D} - \lambda \mathbf{I}|$, $1/\lambda_i^*$ is a root as well. Note that $|\hat{\Psi}_{2D} - \lambda \mathbf{I}|$ is a polynomial of even order, 2D, such that it has an odd number of coefficients. Let α be a complex scalar such that the coefficient of the D-th power of λ in the polynomial $\alpha |\hat{\Psi}_{2D} - \lambda \mathbf{I}|$ is real. It follows from the property of the roots that the coefficients of $\alpha |\hat{\Psi}_{2D} - \lambda \mathbf{I}|$ exhibit conjugate symmetry about the D-th or center coefficient. This property will be stated mathematically shortly. The proof of this conjugate centro-symmetry property is straightforward and, hence, omitted. A second consequence of Theorem 2 is that the EV's of $\hat{\Psi}_{2D}$ may be grouped into those which lie on the unit circle and those which occur in reciprocal magnitude pairs. Each of these two groups contains an even number of EV's. By a reciprocal magnitude pair, we mean that the polar angle of both is the same while the magnitude of one is the reciprocal of that of the other. This suggests a procedure wherein we compute the 2D EV's of $\hat{\Psi}_{2D}$, group them into D pairs, and then take the geometric mean of each pair as the estimate of Φ_{kk}. For the EV pairs which lie on the unit circle, however, this procedure involves some subjective pairing. This may lead to trouble if the sources are closely-spaced. As an alternative, we develop a procedure which reduces the problem to that of solving for the roots of a D-th order polynomial that does not involve subjective decisions. The appropriate procedure is developed below.

Let $c(\lambda)$ denote the characteristic polynomial of $\hat{\Psi}_{2D}$, normalized such that the center coefficient is real, i. e., $c(\lambda) = \alpha |\hat{\Psi}_{2D} - \lambda \mathbf{I}|$, a polynomial of order 2D. Further, let the coefficients of $c(\lambda)$ be denoted, $c(n)$, $n=0,\ldots,2D$. Note that α is defined such that $c(D)$ is a real number. In this notation, then,

$$\alpha |\hat{\Psi}_{2D} - \lambda \mathbf{I}| = c(0) + c(1)\lambda + c(2)\lambda^2 + \cdots + c(2D)\,\lambda^{2D} \qquad (5.22)$$

Let's examine the form of $c(\lambda)$ under ideal noiseless conditions. In this case, each Φ_{kk}, $k=1,\ldots,D$, is a double root of $c(\lambda)$ such that

$$c(\lambda) = \alpha\Big[(\lambda-\Phi_{11}) (\lambda-\Phi_{22}) \ldots . (\lambda-\Phi_{DD}) \Big]^2 = b^2(\lambda) \tag{5.23}$$

where $b(\lambda)$ is the D-th order polynomial with single roots at Φ_{kk}, k=1,...,D. The coefficients of $b(\lambda)$ are denoted b(n), n=0,...,D, such that

$$b(\lambda) = \sqrt{\alpha}(\lambda-\Phi_{11}) (\lambda-\Phi_{22}) \ldots . (\lambda-\Phi_{DD}) \tag{5.24}$$

$$= b(0) + b(1)\lambda + b(2)\lambda^2 + \cdots + b(D)\,\lambda^D$$

Simple algebra tells us the sequence c(n), n=0,...,2D, is the linear convolution of the sequence b(n), n=0,...,D, with itself, i. e., c(n)=b(n)*b(n). Ideally, the sequence b(n) can be recovered from the sequence c(n) via simple deconvolution in accordance with the following recursion

$$b(D) = \sqrt{c(2D)} \tag{5.25}$$

$$b(D-n) = \frac{1}{2b(D)}\left\{c(2D-n) - \sum_{i=0}^{n-1} b(D-i)b(D-n+i)\right\} \qquad n=1,\ldots,D.$$

Two issues arise with regard to the procedure above. First, there are two valid square roots of c(2D) differing only by a factor of $e^{j\pi}$. This sign ambiguity arises due to the fact that $c(\lambda) = b^2(\lambda)$. Fortunately, this ambiguity is of no consequence since the roots of $b(\lambda)$ are the same as the roots of $-b(\lambda)$. Thus, either square root suffices. The second issue is that the recursion formula in (5.25) only uses the last D+1 coefficients of $c(\lambda)$, i. e., c(n), n=D,D+1,...,2D. Nevertheless, this formula is exact in the ideal noiseless case. In the practical situation involving noisy data, though, it would seem that this recursion formula does not optimally use all available information. However, even in the case of noisy data, the normalized characteristic polynomial $\alpha\,|\,\hat{\Psi}_{2D} - \lambda\mathbf{I}|$ obtained after Procrustes processing is such that its coefficients exhibit conjugate centro-symmetry, i. e., $c(n) = c^*(2D-n)$, n=0,...,2D. Thus, all of the information is, in fact, contained in the D+1 coefficients, c(n), n=D,D+1...,2D. These coefficients may be computed in a computationally efficient recursive fashion as described below.

Let c'(n), n=0,1,...,2D, denote the coefficients of $|\,\hat{\Psi}_{2D}-\lambda\mathbf{I}\,|$, i. e., without normalization by α. That is, $|\,\hat{\Psi}_{2D} - \lambda\mathbf{I}\,| = c'(0) + c'(1)\lambda + c'(2)\lambda^2 + \cdots + c'(2D)\,\lambda^{2D}$. The D+1 values c'(n), n=D,D+1,...,2D, may be computed in a recursive fashion according to the well-known Leverrier-Souriau-Faddeeva-Frame formulas:

$$c'(2D) = 1;\ \mathbf{S}_1 = \mathbf{I}\ ;\ c'(2D-1) = -tr\{\mathbf{S}_1 \hat{\Psi}_{2D}\} \tag{5.26}$$

$$\mathbf{S}_2 = \mathbf{S}_1 \hat{\Psi}_{2D} + c'(2D-1)\mathbf{I}\ ;\ c'(2D-2) = -\frac{1}{2} tr\{\mathbf{S}_2 \hat{\Psi}_{2D}\}$$

$$\vdots$$

$$\mathbf{S}_D = \mathbf{S}_{D-1} \hat{\Psi}_{2D} + c'(D+1)\mathbf{I}\ ;\ c'(D) = -\frac{1}{D} tr\{\mathbf{S}_{D-1} \hat{\Psi}_{2D}\}$$

Ostensibly, the input to the deconvolution recursion in (5.25) is c(n), n=D,D+1,...,2D, not c'(n), n=D,D+1,...,2D, as computed by the above recursion. However, by definition, $c(n) = \alpha c'(n)$, n=0,1,...,2D. In the deconvolution recursion described by (5.25), a scaling of each of the coefficients c(n), n=0,..,D, by the amount α results in a corresponding scaling of each of the coefficients b(n), n=0,..,D, by the amount $\alpha^{1/2}$. As the roots of $b(\lambda)$ are the same as those of $\alpha^{1/2} b(\lambda)$, it is not necessary to determine the normalizing factor α. Thus, the deconvolution recursion in (5.25) may be executed with the sequence c'(n), n=D,D+1,...,2D, provided by the recursion in (5.26). The quantities Φ_{kk}, k=1,2,...,D, are then estimated as the singles roots of the D-th order polynomial $b(\lambda)$ thus formed.

5.3 Incorporation of Array Manifold Modification

The conclusion that each Φ_{kk}, k=1,...,D, is a GEV of the noiseless pencil $\{\mathbf{X}_{FB}^{2D}, \mathbf{Y}_{FB}^{2D}\}$ of multiplicity 2 was deduced from observing (5.3). This conclusion was based on the assumption that the Mx2D matrix $[\mathbf{A} : \mathbf{A}^* \Phi^*]$ was of full column rank equal to $2D < M$. The fact that 2D must be less than M gives rise to the reduction in the number of resolvable sources by a factor of two, the penalty paid for the incorporation of PFBAVG as discussed previously. Let us assume that D is indeed less than M/2 as required. For the algorithm to work correctly, we further require that each column of $\mathbf{A}^*$ be linearly independent of the columns of **A**. We here make the practical assumption that the columns of **A** itself, and hence, $\mathbf{A}^*$, are linearly independent. Scenarios exist, however, in which the former condition may not hold. We illustrate the problem with an example.

Consider the elements comprising both the X and Y arrays to be isotropic. Further, consider the plane containing the X and Y arrays to be defined as the x-y plane in a 3D coordinate system; the z axis is perpendicular to the plane of the array. The i-th element of the X array is located at (x_i, y_i), i=1,...,M, such that

the corresponding element of the Y array is located at $(x_i+\vec{i}\cdot\vec{d}\ ,\ y_i+\vec{j}\cdot\vec{d})$, i=1,...,M. Finally, let the angular positions of the sources $(\theta_k\ ,\ \phi_k)$, k=1,...,D, be defined with respect to the spherical coordinate system. (θ_k is the angle measured with respect to the x-axis in the x-y plane and ϕ_k is the angle measured down from the z-axis.) Under these conditions, the i,k element of A, denoted A_{ik}, may be expressed as

$$A_{ik} = e^{j\frac{2\pi}{\lambda}\{x_i\cos\theta_k \sin\phi_k + y_i\sin\theta_k \sin\phi_k\}} \tag{5.27}$$

The i,k element of A^*, A^*_{ik}, is thus

$$A^*_{ik} = e^{-j\frac{2\pi}{\lambda}\{x_i\cos\theta_k \sin\phi_k + y_i\sin\theta_k \sin\phi_k\}} = e^{j\frac{2\pi}{\lambda}\{x_i\cos(\theta_k+180^\circ) \sin\phi_k + y_i\sin(\theta_k+180^\circ)\sin\phi_k\}} \tag{5.28}$$

where we have invoked simple trigonometric identities. (5.28) implies that the DOA vector for a source located at $(\theta_k + 180^\circ\ ,\ \phi_k)$ is the conjugate of the DOA vector for a source located at $(\theta_k\ ,\ \phi_k)$. Consider the case of D=2 sources with source 1 located at $(\theta_1\ ,\ \phi_1)$ and source 2 located at $(\theta_2\ ,\ \phi_2) = (\theta_1 + 180^\circ\ ,\ \phi_1)$. Under these conditions, $[\mathbf{A} : \mathbf{A}^*\Phi^*]$ has the following form:

$$\left[\mathbf{A} : \mathbf{A}^*\Phi^*\right] = \left[\mathbf{a}_1\ ,\ \mathbf{a}_1^* : \Phi_{11}\mathbf{a}_1^*\ ,\ \Phi_{22}\mathbf{a}_1\right] \tag{5.29}$$

It is obvious that this matrix is only of rank 2, not 4 as required in the use of PFBAVG. Hence, the incorporation of PFBAVG in this case will have a pejorative effect on the performance of **PRO–ESPRIT**. A similar breakdown occurs in the case of a source located directly at boresite, i. e., $\phi_1 = 0^\circ$, since the corresponding DOA vector, $\mathbf{a}_1$, is purely real. However, there is a simple means for averting this type of breakdown phenomenon.

A simple procedure for eliminating such is to pre-multiply both the X and Y data matrices, **X** and **Y**, by the same MxM complex-valued matrix. That is, execute **PRO–ESPRIT** with PFBAVG using the modified data matrices **VX** and **VY**, where **V** is an MxM matrix composed of strictly complex elements. The net effect of this is to modify the array manifold. The applicability of PFBAVG modified **PRO–ESPRIT** in the case of so-called v-modified data matrices is seen from the following sequence of observations. The v-modified FB data pencil has the following structure:

$$\mathbf{X}^v_{FB} = \left[\mathbf{VX} : \mathbf{V}^*\mathbf{Y}^*\right]\ ;\ \mathbf{Y}^v_{FB} = \left[\mathbf{VY} : \mathbf{V}^*\mathbf{X}^*\right] \tag{5.30}$$

In the noiseless case, $\mathbf{X} = \mathbf{AS}$ and $\mathbf{Y} = \mathbf{A}\Phi\mathbf{S}$. With these noiseless forms of **X** and **Y** substituted into (5.30), the pencil difference $\mathbf{Y}^v_{FB} - \lambda\mathbf{X}^v_{FB}$ is easily manipulated into the following form

$$\mathbf{Y}_{FB}^{v} - \lambda \mathbf{X}_{FB}^{v} = \left[\mathbf{VA} : \mathbf{V}^{*}\mathbf{A}^{*}\Phi^{*}\right]\begin{bmatrix}\Phi-\lambda\mathbf{I} & \mathbf{O} \\ \mathbf{O} & \Phi-\lambda\mathbf{I}\end{bmatrix}\begin{bmatrix}\mathbf{S} & \mathbf{0} \\ \mathbf{O} & \mathbf{S}^{*}\end{bmatrix} \tag{5.31}$$

For PFBAVG modified **PRO–ESPRIT** to work correctly, we now require the columns of $\mathbf{VA}$ to be linearly independent of the columns of $\mathbf{V}^{*}\mathbf{A}^{*}$. We note that if $\mathbf{V}$ is a purely real matrix, $[\mathbf{VA} : \mathbf{V}^{*}\mathbf{A}^{*}\Phi^{*}] = \mathbf{V}[\mathbf{A} : \mathbf{A}^{*}\Phi^{*}]$ such that v-modification has no effect on the possibility of the aforementioned breakdown phenomenon. Consider again the previous example involving D=2 sources with one located at (θ_1 , ϕ_1) and the other located at $(\theta_1 + 180^{\circ} , \phi_1)$. Under these conditions, $[\mathbf{VA} : \mathbf{V}^{*}\mathbf{A}^{*}\Phi^{*}]$ is of the following form

$$\left[\mathbf{VA} : \mathbf{V}^{*}\mathbf{A}^{*}\Phi^{*}\right] = \left[\mathbf{Va}_1 , \mathbf{Va}_1^{*} : \Phi_{11}\mathbf{V}^{*}\mathbf{a}_1^{*} , \Phi_{22}\mathbf{V}^{*}\mathbf{a}_1\right] \tag{5.32}$$

which is observed to be of rank 4 as required, assuming that $\mathbf{V}$ is not purely real. Similar comments can be made with regard to the case of a source located directly at boresite. The question arises, however, as to how to select $\mathbf{V}$. This problem will be addressed shortly. We first present the appropriate modifications to PFBAVG modified **PRO–ESPRIT** when the array manifold is transformed by the matrix $\mathbf{V}$.

The initial step of PFBAVG modified **PRO–ESPRIT** is the same regardless of whether array manifold modification is employed or not: the coarse "cleaning" of the Z correlation matrix described by (5.19). This step provides estimates of $\mathbf{C}_{XX}$, $\mathbf{C}_{YY}$, and $\mathbf{C}_{XY}$. With $\mathbf{X}$ and $\mathbf{Y}$ replaced by $\mathbf{VX}$ and $\mathbf{VY}$ in both (5.16) and (5.18), we find that the v-modified FB X correlation matrix, denoted $\mathbf{C}_{FB}^{XX\,v}$, and the v-modified FB X-Y correlation matrix, denoted $\mathbf{C}_{FB}^{XY\,v}$, are estimated from $\hat{\mathbf{C}}_{XX}$, $\hat{\mathbf{C}}_{YY}$, and $\hat{\mathbf{C}}_{XY}$ according to

$$\hat{\mathbf{C}}_{FB}^{XX\,v} = \frac{1}{2}\left\{\mathbf{V}\hat{\mathbf{C}}_{XX}\mathbf{V}^{H} + \mathbf{V}^{*}\hat{\mathbf{C}}_{YY}^{*}\mathbf{V}^{T}\right\} \tag{5.33}$$

$$\hat{\mathbf{C}}_{FB}^{XY\,v} = \frac{1}{2}\left\{\mathbf{V}\hat{\mathbf{C}}_{XY}\mathbf{V}^{H} + \mathbf{V}^{*}\hat{\mathbf{C}}_{XY}^{T}\mathbf{V}^{T}\right\} \tag{5.34}$$

When the array manifold is transformed by the matrix $\mathbf{V}$, the only change to the procedure developed previously is that $\hat{\mathbf{C}}_{FB}^{XX\,v}$ takes on the role of $\hat{\mathbf{C}}_{FB}^{XX}$ and $\hat{\mathbf{C}}_{FB}^{XY\,v}$ takes on the role of $\hat{\mathbf{C}}_{FB}^{XY}$.

With regard to the selection of $\mathbf{V}$, we chose to work with the simplest form possible: an MxM diagonal matrix with each element of the diagonal lying on the unit circle as described below.

$$\mathbf{V} = \text{diag}\{\, e^{j\nu_1}\,,\, e^{j\nu_2}\,,\, \cdots\,,\, e^{j\nu_M}\,\} \tag{5.35}$$

As long as each of the phase angles ν_i, i=1,...,M, is distinct, the array manifold will be sufficiently altered so as to avert the possibility of breakdown under the previously cited worst case conditions. One possibility is to choose the phase angles such that the diagonal elements of **V** are uniformly-spaced around the unit circle, encompassing the entire perimeter. Another possibility is to obtain each ν_i, i=1,...,M, from a random number generator emulating a random variable uniformly distributed over the interval $(0,\ 2\pi)$. Simulations have proven that both of these options provide **V** matrices which work quite well in worst case scenarios. The additional computational burden is negligible; **V** is constructed a-priori. An alternative is to select the phase angles in a data dependent fashion so as to improve the condition number associated with the 2D signal eigenvalues of $\hat{\mathbf{C}}_{FB}^{XX\,\mathbf{V}}$ relative to that of $\hat{\mathbf{C}}_{FB}^{XX}$. A suitable procedure for accomplishing such is described below.

With **V** diagonal and unitary as described by (5.35), it follows that the diagonal elements of $\hat{\mathbf{C}}_{FB}^{XX\,\mathbf{V}}$ are the same as those of $\hat{\mathbf{C}}_{FB}^{XX}$. This stipulates that the trace of $\hat{\mathbf{C}}_{FB}^{XX\,\mathbf{V}}$ is equal to the trace of $\hat{\mathbf{C}}_{FB}^{XX}$. This, in turn, implies that the sum of the EV's of $\hat{\mathbf{C}}_{FB}^{XX\,\mathbf{V}}$ is equal to the sum of the EV's of $\hat{\mathbf{C}}_{FB}^{XX}$. A third criterion for the selection of the phase angles ν_i, i=1,2,...,M, is the minimization of the Frobenius norm of $\hat{\mathbf{C}}_{FB}^{XX\,\mathbf{V}}$, $\|\hat{\mathbf{C}}_{FB}^{XX\,\mathbf{V}}\|_F$. This criterion is best motivated by considering the asymptotic case.

In the asymptotic case, $\hat{\mathbf{C}}_{FB}^{XX}$ is of rank 2D; $\hat{\mathbf{C}}_{FB}^{XX\,\mathbf{V}}$ is thus of rank 2D as well. The Frobenius norm of $\hat{\mathbf{C}}_{FB}^{XX\,\mathbf{V}}$ is then the square root of the sum of the squares of its 2D nonzero EV's. As a consequence of the above observations, the sum of the 2D nonzero EV's remains constant as we vary the phase angles in an attempt to decrease the value of $\|\hat{\mathbf{C}}_{FB}^{XX\,\mathbf{V}}\|_F$. This motivates consideration of the following constrained optimization problem.

$$\underset{\nu_1,\nu_2,\ldots,\nu_M}{\text{Minimize}} \quad \|\mathbf{C}_{FB}^{XX\,\mathbf{V}}\|_F^2 = \sum_{i=1}^{2D} \lambda_i^{\mathbf{V}\,2} \tag{5.36}$$

$$\text{subject to:} \quad \sum_{1=1}^{2D} \lambda_i^{\mathbf{V}} = c = \text{constant}$$

where $\lambda_i^{\mathbf{V}}$, i=1,2,...,2D, are the 2D nonzero EV's of $\hat{\mathbf{C}}_{FB}^{XX\,\mathbf{V}}$. The stipulation of the constraint is, in actuality, not necessary as it is already incorporated in the formation of $\hat{\mathbf{C}}_{FB}^{XX\,\mathbf{V}}$. It is included for purposes of illustration. Overlooking, for the moment, the dependence of $\lambda_i^{\mathbf{V}}$ on ν_i, i=1,2,...,M, the minimum of $\sum_{i=1}^{2D} \lambda_i^{\mathbf{V}\,2}$

subject to $\sum_{i=1}^{2D}\lambda_i^{\mathbf{V}} = \text{constant}$ is $\lambda_1^{\mathbf{V}} = \lambda_2^{\mathbf{V}} = \cdots = \lambda_{2D}^{\mathbf{V}} = \frac{c}{2D}$. Of course, this optimum condition is not attainable, in general, due to the functional dependence on v_i, $i=1,2,...,M$. However, this nevertheless illustrates the general effect of choosing the phase angles to minimize $\|\hat{\mathbf{C}}_{FB}^{XX^{\mathbf{V}}}\|_F$: it serves to decrease some of the largest of the 2D signal EV's while increasing some of the smallest. The net effect is to enhance the separation between the signal subspace and the (M-2D)-dimensional nullspace, the eigenspace associated with the eigenvalue zero.

The solution to the optimization in (5.36) with $\hat{\mathbf{C}}_{FB}^{XX^{\mathbf{V}}}$ and $\mathbf{V}$ defined by (5.33) and (5.35), respectively, is not a trivial undertaking. For the sake of computational simplicity, a suboptimal scheme is proposed which achieves the same desired effect. To this end, let $c_{i,j}^{\mathbf{V}}$ denote the i,j element of $\hat{\mathbf{C}}_{FB}^{XX^{\mathbf{V}}}$. Recall

$$\|\hat{\mathbf{C}}_{FB}^{XX^{\mathbf{V}}}\|_F^2 = \sum_{i=1}^{M}\left\{\sum_{j=1}^{M}|c_{i,j}^{\mathbf{V}}|^2\right\} \tag{5.37}$$

For the sake of simplicity, consider the minimization of $\sum_{j=1}^{M}|c_{i,j}^{\mathbf{V}}|^2$, the 2-norm of the i-th row, with respect to the phase angles v_k, $k=1,2,...,M$. Keep in mind that $c_{i,i}^{\mathbf{V}}$ is fixed. Let $x_{i,j}$ and $\mu_{i,j}$ denote the magnitude and phase of the i,j element of $\hat{\mathbf{C}}_{XX}$, respectively. Likewise, $y_{i,j}$ and $\nu_{i,j}$ denote the magnitude and phase of the i,j element of $\hat{\mathbf{C}}_{YY}$. In accordance with (5.4), $c_{i,j}^{\mathbf{V}}$ may be expressed as

$$c_{i,j}^{\mathbf{V}} = \frac{1}{2}x_{i,j}e^{j\mu_{i,j}}e^{j(v_i-v_j)} + \frac{1}{2}y_{i,j}e^{-j\nu_{i,j}}e^{j(v_j-v_i)} \tag{5.38}$$

Thus,

$$\sum_{j=1}^{M}|c_{i,j}^{\mathbf{V}}|^2 = \sum_{j=1}^{M}\left\{\frac{x_{i,j}^2}{4} + \frac{y_{i,j}^2}{4} + \frac{1}{2}x_{i,j}y_{i,j}\cos\left[2(v_i-v_j)+\mu_{i,j}+\nu_{i,j}\right]\right\} \tag{5.39}$$

By definition, $x_{i,j} \geq 0$ and $y_{i,j} \geq 0$ such that $\sum_{j=1}^{M}|c_{i,j}^{\mathbf{V}}|^2$ is minimized if

$$v_i - v_j = -\frac{1}{2}(\mu_{i,j}+\nu_{i,j}) + \frac{\pi}{2}k_{i,j} \qquad j=1,...,M;\ j\neq i \tag{5.40}$$

where $k_{i,j}$ is any odd integer. Thus, the minimization of the 2-norm of the i-th row of $\hat{\mathbf{C}}_{FB}^{XX^{\mathbf{V}}}$, subject to $c_{i,i}^{\mathbf{V}}$ fixed, uniquely determines the values of v_j, $j=1,...,M$, $j\neq i$, relative to v_i. Now, the square of the Frobenius norm is equal to the sum of the 2-norms of each of the rows. A suboptimal procedure is to build up an overdetermined system of equations in accordance with (5.11). Since $\hat{\mathbf{C}}_{FB}^{XX^{\mathbf{V}}}$ is Hermitian, we need only consider the $\frac{1}{2}M(M-1)$ equations associated with those

elements above (or below) the main diagonal. It can be shown (see Appendix B) that the least square error solution to this overdetermined system of equations yields the following simple expression for determining the phase angles:

$$v_i = \frac{1}{M}\sum_{\substack{j=1 \\ j\neq i}}^{M}\left\{ -\frac{(\mu_{i,j}+\nu_{i,j})}{2} + \frac{\pi}{2}k_{i,j}\right\} \qquad i=1,..,M \tag{5.41}$$

That is, v_i is simply the negative of the average of the average of corresponding angles associated with the elements of the i-th rows of $\hat{C}_{xx}$ and $\hat{C}_{yy}$, respectively, plus some integer multiple of $\frac{\pi}{2}$. The computation involved in evaluating (5.41) adds negligible contribution to the overall load. Simulations are presented in Section 5.6 which show that determination of the phase angles according to (5.41) yields the best performance out of the three methods proposed.

5.4 Estimation of Number of Sources Via Invariance Exploitation

One can estimate the number of sources, D, via a number of techniques including AIC and MDL [WAX85]. Exploitation of the invariance in the case of an array composed of two translationally invariant subarrays allows for the formulation of an alternative ad-hoc procedure for estimating the number of sources unique to PFBAVG modified **PRO–ESPRIT**. In short, the new procedure is based on determining that partition of the EV's and EVEC's of $\hat{\mathbf{C}}_{FB}^{xx\,v}$ for which the formation of $\mathbf{Q}_v$ according to (5.21) is "closest" to being unitary. The reason a test on the unitary nature of $\mathbf{Q}_v$ is chosen rather than a test on the unitary nature of $\mathbf{Q}_u$ formed according to (5.20) is due to the following observation. In the case of uncorrelated sources, it is easily shown that $\mathbf{C}_{yy} = \mathbf{C}_{xx}^{*}$ such that

$$\mathbf{C}_{FB}^{xx\,v} = \frac{1}{2}\left\{\mathbf{V}\mathbf{C}_{xx}\mathbf{V}^{H} + \mathbf{V}^{*}\mathbf{C}_{xx}^{*}\mathbf{V}^{T}\right\} = \mathrm{Re}\{\,\mathbf{V}\mathbf{C}_{xx}\mathbf{V}^{H}\} \tag{5.42}$$

Thus, in the case of uncorrelated sources the EVEC's of $\mathbf{C}_{FB}^{xx\,v}$ are real-valued such that $\mathbf{Q}_U = \mathbf{U}_X^{2\hat{D}H}\,\mathbf{U}_X^{2\hat{D}*} = \mathbf{U}_X^{2\hat{D}T}\,\mathbf{U}_X^{2\hat{D}} = \mathbf{I}$ regardless of the value of $\hat{D}$, i. e., for any partition of the EV's and EVEC's. Recall that each source makes a rank two contribution to $\mathbf{C}_{FB}^{xx\,v}$. As a consequence, both the designated signal subspace and the designated noise subspace for each partition should contain an even number of entries.

Let $\hat{D}$ denote the estimate of the number of sources. In light of the above observation, we restrict our attention to a test on the unitary nature of $\mathbf{Q}_v(\hat{D})$,

formed in accordance with (5.21), over the range of permissible values of $\hat{D}$. The new procedure for determining $\hat{D}$ is as follows. First, compute an EVD of $\hat{\mathbf{C}}_{FB}^{NN\,v}$ and order the EV's in descending order. Let $\mathbf{U}_X^{2\hat{D}}$ be composed of the $2\hat{D}$ EVEC's associated with the $2\hat{D}$ largest EV's, $\hat{D}= 1,2, \ldots, \frac{M}{2}-1$. Correspondingly, $\Sigma_X^{2\hat{D}}$ is the $2\hat{D}$ x $2\hat{D}$ diagonal matrix composed of the square roots of the corresponding $2\hat{D}$ largest EV's, $\hat{D}= 1,2, \ldots, \frac{M}{2}-1$. $\hat{D}$ is the solution to

$$\underset{\hat{D} \in \{1,2,\cdots,\frac{M}{2}-1\}}{\text{Minimize}} \quad f(\hat{D}) = w(\hat{D}) \,||\, \mathbf{Q}_v(\hat{D}) - \hat{\mathbf{Q}}_v(\hat{D})||_F^2 \tag{5.43}$$

$$\text{where:} \quad \mathbf{Q}_v(\hat{D}) = \Sigma_X^{2\hat{D}\,-1}\, \mathbf{U}_X^{2\hat{D}H}\, \frac{1}{2}\{\hat{\mathbf{C}}_{XY} + \hat{\mathbf{C}}_{XY}^T\}\, \mathbf{U}_X^{2\hat{D}*}\, \Sigma_X^{2\hat{D}\,-1}$$

$$\text{and} \quad \hat{\mathbf{Q}}_v(\hat{D}) \text{ is the closest unitary matrix to } \mathbf{Q}_v(\hat{D})$$

The reasons for the inclusion of the weighting function $w(\hat{D})$ will be discussed shortly. In accordance with Procrustes' Theorem, if the SVD of $\mathbf{Q}_v(\hat{D})$ is $\mathbf{Q}_v(\hat{D}) = \mathbf{U}\Sigma\mathbf{V}^H$,the "closest" unitary matrix is $\hat{\mathbf{Q}}_v(\hat{D}) = \mathbf{U}\mathbf{V}^H$. Hence,

$$||\, \mathbf{Q}_v(\hat{D}) - \hat{\mathbf{Q}}_v(\hat{D})||_F^2 = \sum_{i=1}^{2\hat{D}} \Big(1 - \sigma_i(\hat{D})\Big)^2 \tag{5.44}$$

where $\sigma_i(\hat{D})$, i=1,2,...,$2\hat{D}$, are the $2\hat{D}$ singular values of $\mathbf{Q}_v(\hat{D})$. Thus, the procedure for determining $\hat{D}$ in (5.43) may be alternatively expressed as

$$\underset{\hat{D} \in \{1,2,\cdots,\frac{M}{2}-1\}}{\text{Minimize}} \quad f(\hat{D}) = w(\hat{D}) \sum_{i=1}^{2\hat{D}} \Big(1 - \sigma_i(\hat{D})\Big)^2 \tag{5.45}$$

where $\sigma_i(\hat{D})$, i=1,2,...,$2\hat{D}$, are the $2\hat{D}$ singular values of

$$\mathbf{Q}_v(\hat{D}) = \Sigma_X^{2\hat{D}\,-1}\, \mathbf{U}_X^{2\hat{D}H}\, \frac{1}{2}\{\hat{\mathbf{C}}_{XY} + \hat{\mathbf{C}}_{XY}^T\}\, \mathbf{U}_X^{2\hat{D}*}\, \Sigma_X^{2\hat{D}\,-1}$$

One can simply use this procedure in and of itself to estimate the number of sources. Alternatively, one can use this procedure in conjunction with either AIC or MDL as a means of verification.

Note that $\mathbf{Q}_v(\hat{D}) - \hat{\mathbf{Q}}_v(\hat{D})$ in the objective function in (5.43) is a $2\hat{D}$x$2\hat{D}$ matrix. Thus, $||\, \mathbf{Q}_v(\hat{D}) - \hat{\mathbf{Q}}_v(\hat{D})||_F^2$ is rather small for small values of $\hat{D}$ regardless of the difference between $\hat{D}$ and the actual number of sources, D. This observation motivates the inclusion of the weighting function $w(\hat{D})$ in (5.43) and (5.45). The recommended weighting function is based on the number of nonzero entries comprising $\mathbf{Q}_v(\hat{D}) - \hat{\mathbf{Q}}_v(\hat{D})$ in the **noiseless** case. Three cases need to be considered: (i) $\hat{D}< D$, (ii) $\hat{D}=D$, and (ii) $\hat{D}> D$. $\mathbf{Q}_v(\hat{D}) - \hat{\mathbf{Q}}_v(\hat{D})$ is a $2\hat{D}$x$2\hat{D}$

matrix and thus has $4\hat{D}^2$ elements. If $\hat{D} < D$, all $4\hat{D}^2$ elements of $\mathbf{Q}_v(\hat{D}) - \hat{\mathbf{Q}}_v(\hat{D})$ are nonzero, in general. If $\hat{D} = D$, $\mathbf{Q}_v(\hat{D})$ is unitary under noiseless conditions such that $\mathbf{Q}_v(\hat{D}) - \hat{\mathbf{Q}}_v(\hat{D}) = \mathbf{O}$. Thus, for $\hat{D} = D$ there are no nonzero entries. Finally, it turns out that if $\hat{D} > D$, only $4(\hat{D} - D)^2$ of the $4\hat{D}^2$ elements of $\mathbf{Q}_v(\hat{D}) - \hat{\mathbf{Q}}_v(\hat{D})$ are nonzero. As it provides insight into the proposed method for estimating the number of sources, we quickly develop the last result.

The proof of the last result is based on properties of the right singular vectors of $\mathbf{X}_{FB}^v = \left[\mathbf{VX} : \mathbf{V}^*\mathbf{Y}^*\right]$ in the **noiseless** case. To this end, let $\mathbf{V}_X^{2\hat{D}}$ be the Nx2$\hat{D}$ matrix composed of the 2$\hat{D}$ right singular vectors of $\mathbf{X}_{FB}^v$ associated with the 2$\hat{D}$ largest singular values. In the noiseless case, $\mathbf{X}_{FB}^v$ is of rank 2D, where D is the actual number of sources. Thus, for $\hat{D} = D$, we know that $\mathbf{V}_X^{2D}$ satisfies the relationship in (5.13) which we repeat here.

$$\Gamma \mathbf{V}_X^{2D^*} = \mathbf{V}_X^{2D} \mathbf{Q}_v(D) \tag{5.46}$$

where Γ was defined in (4.8) and where $\mathbf{Q}_v(D)$ is the 2Dx2D unitary matrix

$$\mathbf{Q}_v(D) = \mathbf{V}_X^{2D^H} \Gamma \mathbf{V}_X^{2D^*} \tag{5.47}$$

Note that in the noiseless case, the expression above is exactly equal to the expression for $\mathbf{Q}_v(\hat{D})$ in (5.43)/(5.45) when $\hat{D}$=D. In the case of $\hat{D} > D$, 2($\hat{D}$-D) right singular vectors associated with the nullspace of $\mathbf{X}_{FB}^v$ are erroneously appended to $\mathbf{V}_X^{2D}$ such that $\mathbf{V}_X^{2\hat{D}}$ may be partitioned as

$$\mathbf{V}_X^{2\hat{D}} = \left[\mathbf{V}_X^{2D} : \mathbf{V}_N^{2E}\right] \tag{5.48}$$

where E=($\hat{D}$-D) and $\mathbf{V}_N^{2E}$ denotes the Nx2E matrix whose columns are the erroneously assigned 2E right singular vectors in the nullspace of $\mathbf{X}_{FB}^v$, i. e., associated with the singular value zero.

Now, we are interested in analyzing the structure of $\mathbf{Q}_v(\hat{D})$ formed according to the prescription
in (5.43)/(5.45) for $\hat{D}$=D+1,D+2,...,$\frac{M}{2}$−1. The classical relationship between the right and left singular vectors of a matrix tells us that we may alternatively analyze $\mathbf{Q}_v(\hat{D})$ formed according to (5.47) with $\mathbf{V}_X^{2D}$ replaced by $\mathbf{V}_X^{2\hat{D}}$. The two are equal under noiseless conditions. Thus, for $\hat{D}$=D+1,D+2,...,$\frac{M}{2}$−1,

$$\mathbf{Q}_v(\hat{D}) = \begin{bmatrix} \mathbf{V}_X^{2D^H}\Gamma\mathbf{V}_X^{2D^*} & \mathbf{V}_X^{2D^H}\Gamma\mathbf{V}_N^{2E^*} \\ \mathbf{V}_N^{2E^H}\Gamma\mathbf{V}_X^{2D^*} & \mathbf{V}_N^{2E^H}\Gamma\mathbf{V}_N^{2E^*} \end{bmatrix} = \begin{bmatrix} \mathbf{Q}_v(D) & \mathbf{O} \\ \mathbf{O} & \mathbf{V}_N^{2E^H}\Gamma\mathbf{V}_N^{2E^*} \end{bmatrix} \tag{5.49}$$

The result $\mathbf{V}_X^{2D^H}\Gamma\mathbf{V}_N^{2E^*} = \mathbf{O}$ follows from the orthogonality between the columns of

$\mathbf{V}_X^{2D}$ and those of $\mathbf{V}_N^{2E}$ and the relationship in (5.46):

$$\mathbf{V}_X^{2D^H}\Gamma\mathbf{V}_N^{2E^*} = \left(\mathbf{V}_X^{2D^*}\mathbf{Q}_v^*(D)\right)^H\mathbf{V}_N^{2E^*} = \mathbf{Q}_v^T(D^*)\,\mathbf{V}_X^{2D^T}\mathbf{V}_N^{2E^*} = \mathbf{O} \tag{5.50}$$

Now, it can be easily shown that the "closest" unitary matrix to a matrix of the form $\begin{bmatrix}\mathbf{Q}_1 & \mathbf{O}\\ \mathbf{O} & \mathbf{Q}_2\end{bmatrix}$, where $\mathbf{Q}_1$ and $\mathbf{Q}_2$ are both square, is $\begin{bmatrix}\hat{\mathbf{Q}}_1 & \mathbf{O}\\ \mathbf{O} & \hat{\mathbf{Q}}_2\end{bmatrix}$, where $\hat{\mathbf{Q}}_1$ and $\hat{\mathbf{Q}}_2$ are the respective "closest" unitary matrices to $\mathbf{Q}_1$ and $\mathbf{Q}_2$. Thus, under noiseless conditions we have the final result

$$\mathbf{Q}_v(\hat{D}) - \hat{\mathbf{Q}}_v(\hat{D}) = \begin{bmatrix}\mathbf{O} & \mathbf{O}\\ \mathbf{O} & \mathbf{Q}_N - \hat{\mathbf{Q}}_N\end{bmatrix} \tag{5.51}$$

where $\mathbf{Q}_N = \mathbf{V}_N^{2E^H}\Gamma\mathbf{V}_N^{2E^*}$ and $\hat{\mathbf{Q}}_N$ is the "closest" unitary matrix approximating $\mathbf{Q}_N$. It thus follows that for $\hat{D} > D$, the only nonzero entries of $\mathbf{Q}_v(\hat{D}) - \hat{\mathbf{Q}}_v(\hat{D})$ are the elements of the 2Ex2E matrix $\mathbf{Q}_N - \hat{\mathbf{Q}}_N$. Since $E = \hat{D} - D$, the number of nonzero elements is $4(\hat{D}-D)^2$ as stipulated previously.

Returning to the development of the proposed weighting scheme, consider D, the actual number of sources, to be a random variable with $\Pr\{D = i\} = \frac{1}{\frac{M}{2}-1}$, $i = 1,2,\ldots,\frac{M}{2}-1$. This is a reasonable assumption in the absence of a-priori knowledge. Let $F_z^{\hat{D}}$ denote the number of nonzero elements comprising $\mathbf{Q}_v(\hat{D}) - \hat{\mathbf{Q}}_v(\hat{D})$. Under the above condition, $F_z^{\hat{D}}$ is a random variable. For a fixed $\hat{D}$, the expected value of $F_z^{\hat{D}}$ is

$$E\{F_z^{\hat{D}}\} = \frac{1}{\frac{M}{2}-1}\left\{\sum_{D=1}^{\hat{D}} 4(\hat{D}-D)^2 + \sum_{D=\hat{D}+1}^{\frac{M}{2}-1} 4\hat{D}^2\right\} \tag{5.52}$$

$$= \frac{1}{\frac{M}{2}-1}\left\{(2M-6)\hat{D}^2 - \frac{8}{3}\hat{D}^3 + \frac{2}{3}\hat{D}\right\}$$

The weighting function $w(D)$ is chosen to satisfy the following desirable condition:

$$w(\hat{D})\,E\{F_z^{\hat{D}}\} = \text{constant} \qquad \hat{D} = 1,2,\ldots,\tfrac{M}{2}-1 \tag{5.53}$$

A suitable weighting function is thus the reciprocal of (5.52)

$$w(\hat{D}) = \frac{(2M-6)\hat{D}^2 - \frac{8}{3}\hat{D}^3 + \frac{2}{3}\hat{D}}{\frac{M}{2}-1} \qquad \hat{D}=1,2,\ldots,\frac{M}{2}-1 \tag{5.54}$$

The proposed method for estimating the number of sources is then given by (5.45) with $w(\hat{D})$ given by (5.54). Simulations are presented in Section 5.6 which demonstrate the excellent performance of this scheme.

5.5 Methods for Angle Pairing

The problem considered here is that of matching estimates resulting from the application of **PRO–ESPRIT** to an **ESPRIT** array that can orient doublets along more than one independent axis. We have already shown, for example, that in the case of a corrugated box array, one can obtain four, pairwise independent axis. Again, let vector $\hat{r}^d$ denote the displacement axis between the sensors in a doublet, and $\hat{c}_p = u_p\hat{i} + v_p\hat{j}$ be the projection of the p-th wave on the x-y plane. $\hat{i}$ and $\hat{j}$ are the unit vectors along the x and y axes respectively. The relation between the corresponding azimuth, elevation angles to u_p, v_p is given by (2.1). D represents the total number of radiating sources and it is assumed that at this stage this is a known quantity. Estimating each $\hat{c}_p$ p=1,..,D, is equivalent to estimating each pair (u_p,v_p), p=1,..,D. So apparently it would suffice to have two independent linear equations relating each pair (u_p,v_p). However, this is not enough. To see why, suppose the two doublet orientation axes are $\hat{r}_1^d=\hat{i}$ and $\hat{r}_2^d=\hat{j}$. Then processing along $\hat{r}_1^d$ provides D numbers that are estimates for $u_1,..,u_D$. Let these estimates be the set $\mathcal{D}=\{u^e_{i_1},..,u^e_{i_D}\}$. On the other hand, processing with respect to $\hat{r}_2^d$ provides another D numbers that are estimates for $v_1,..,v_D$. Let these estimates be the elements of the set $\mathcal{E}=\{v^e_{j_1},..,v^e_{j_D}\}$. Note that subscripts i_p and j_p, p=1,..,D are used to index the p-th element of the corresponding set. No other information is available. The problem arises when we try to match each entry from $\mathcal{D}$ to the appropriate entry found in $\mathcal{E}$. What we need is additional information or properties regarding the elements of $\mathcal{D}$ and $\mathcal{E}$. For this, one can either use a **MUSIC** based technique or an **ESPRIT** technique. First we consider the latter method.

The idea here is simple. Apply **PRO–ESPRIT** to three or more, pairwise independent, doublet axes $\hat{r}_1^d$, $\hat{r}_2^d$ and $\hat{r}_3^d$.. To illustrate with respect to the previous example, let the 3-rd axis of doublet orientation be $\hat{r}_3^d = \hat{i}+\hat{j}$. Processing with respect to this axis, gives estimates for $u_1+v_1,..,u_D+v_D$. These estimates are the elements of set $\mathcal{F}=\{(u+v)^e_{k_1},..,(u+v)^e_{k_D}\}$. We first assume that the data were

noiseless so that we have perfect estimates for all u, v and (u+v). Then the following argument is valid. For any $u_{i_p} \in \mathcal{D}$ there exists a $v_{j_q} \in \mathcal{E}$ and $(u+v)_{k_r} \in \mathcal{F}$ such that $u_{i_p}+v_{j_q}=(u+v)_{k_r}$. Thus, under such circumstances, one would take the first element of $\mathcal{D}$, and then start a search over $\mathcal{E}$ to find that element such that the sum of both would be identically equal to one element of $\mathcal{F}$. This is one matched pair. This process continues, taking into account the remaining elements of $\mathcal{D}$, $\mathcal{E}$ and $\mathcal{F}$, until they are all exhausted.

In the presence of noise, the task of correctly pairing the elements of $\mathcal{D}$ and $\mathcal{E}$ becomes more complicated. The reason is that we cannot recover each pair independently as we did in the no noise case. Instead, consider the following minimization problem

$$\min_{\substack{i_1,..,i_D \\ j_1,..,j_D \\ k_1,..,k_D}} \sum_{p=1}^{D} \left| u^e_{i_p}+v^e_{j_p} - (u+v)^e_{k_p} \right| \tag{5.56}$$

So the attempt here is to search over all combinations of the indices i_p, j_p and k_p until that combination is found that reduces the overall distance between the sum of the estimates of u_i ,v_i, i=1,..,D, and the estimate of their sum $(u+v)_i$. Once the optimal index combinations are found, the D pairs can be matched accordingly.

In general, the search must be carried over all combinations of the three index sequences, however several combinations can be eliminated due to the fact that the corresponding elevation angles fall outside the permissible range $(0^\circ \leq \phi \leq 90^\circ)$. An advantage offered by this method, is that the extra information relating u_i and v_i, i=1,..,D that is obtained can also be used to further enhance the quality of the estimates. In particular, since when processing relative to a specific orientation axis $\hat{\mathbf{r}}^d$ we obtain estimates of linear combinations of the u_i and v_i, i=1,..,D, for three or more such combinations we can use the method of least squares to improve the estimates. Regarding the number of numerical operations that are required to perform the search, it is proportional to $(D!)^2$. This number can be large, so for this reason plus the fact that this method requires an additional eigenvalue decomposition, it may be desired to use some other procedure to pair the u and v estimates. One such alternative is the following technique that is conceptually based on **MUSIC**.

Consider again the no noise case. Suppose the pairs (u_i^*, v_i^*), i=1,..,D are properly matched. Each of the D pairs uniquely defines the corresponding array manifold vector $\mathbf{a}_i$, i=1,..,D. Also, each $\mathbf{a}_i$ is orthogonal to the (M-D) dimensional nullspace of $\mathbf{R}_{xx}$. M is the number of doublets. Let $\mathbf{U}_x^D$ be a matrix

containing the orthonormalized eigenvectors of $\mathbf{R}_{xx}$ corresponding to its nonzero eigenvalues. Then

$$\mathbf{P}_x = \mathbf{I} - \mathbf{U}_x^D \mathbf{U}_x^{DH}$$

is a projection operator on the nullspace of $\mathbf{R}_{xx}$. The following expression must then be true.

$$\sum_{i=1}^{D} \left| \mathbf{a}_i^H \mathbf{P}_x \mathbf{a}_i \right| = 0$$

With noisy data, equality to zero will never be achieved. However, one would expect that the left hand side of the last equation achieves its minimum when the elements of $\mathscr{D}$ are correctly paired with the elements of $\mathscr{E}$. Formulating this, we want to

$$\min_{\substack{i_1,..,i_D \\ j_1,..,j_D}} \sum_{p=1}^{D} \left| \mathbf{a}_p^H(u_{i_p}, v_{j_p}) \mathbf{P}_x \mathbf{a}_p(u_{i_p}, v_{j_p}) \right| \tag{5.57}$$

Note that with noisy data the projection operator is formed using the eigenvectors of the clean covariance matrix $\hat{\mathbf{C}}_{xx}$. Also, $\mathbf{a}_p(u_{i_p}, v_{j_p})$ is expressed like this in order to indicate that the p-th array manifold vector is constructed using the p-th elements of $\mathscr{D}$ and $\mathscr{E}$ respectively. Although so far we have exclusively made use of the forward covariance matrix $\hat{\mathbf{C}}_{xx}$, we could easily have used the F-B correlation matrix, $\hat{\mathbf{C}}_{xx}^{FB}$, with almost no change in the final result. With respect to the computational task, it is noted that in contrast to the previous scheme, no additional eigenvalue decompositions, other than the ones required for the estimation part of the algorithm, have to be computed. However, the construction of the projection operator and the subsequent evaluation of all the terms on the right hand side of (5.57) demand non-trivial computational effort.

A comparison between the performance of the the two methods is done in the next section. We briefly state at this point that the two procedures perform equally well, with no major advantage of one over the other. The simulations we carried out showed that the probability of incorrect pairing diminishes very rapidly with an increase in either the number of snapshots or the signal to noise ratio of each received signal. This is very encouraging, because with two dimensional arrays, obtaining good individual u or v estimates but failing to pair them correctly is still catastrophic.

5.6 Computer Simulations

Computer simulations were conducted to demonstrate the computation reduction and performance improvement achieved when PFBAVG is employed in conjunction with **PRO–ESPRIT**. The array employed in the first set of simulations is the 2M = 28 element square corrugated box array depicted in Figure 1.1(a) [ZOLT89a]. The coordinate system is defined such that the array is situated in the x-y plane. Each set of three adjacent elements around the perimeter of the array forms a right isosceles triangle with the length of each leg equal to a half-wavelength. In the SI **ESPRIT** configuration depicted in Fig. 1.1(a), the array is decomposed into two translationally invariant 14 element subarrays with the displacement or doublet axis aligned with the x-axis. This configuration allows one to estimate the direction cosine of each source relative to the x-axis, $u_k = \cos(\alpha_k)$, k=1,2,...,D. In the SI **ESPRIT** configuration depicted in Fig. 1.1(b), the array is decomposed into two translationally invariant 14 element subarrays with the displacement axis aligned with the y-axis. This configuration allows one to estimate the direction cosine of each source relative to the y-axis, $v_k = \cos(\beta_k)$, k=1,2,...,D. In either configuration, the individual arrays comprising the translationally invariant pair have no sensors in common.

Note that the angles u_i, i=1,2,...,D, and the angles v_i, i=1,2,...,D, may be estimated via PFBAVG modified **PRO–ESPRIT** simultaneously in a parallel fashion. It should be noted that the corrugated box array was chosen for simulation purposes for two reasons. First, in either of the two configurations depicted in Figure 1.1, the individual arrays comprising the respective translationally invariant pair are observed to be nonlinear. Second, with respect to either u estimation or v estimation, the overall array exhibits only a single invariance. The corrugated box array thus represents an illustrative example where multiple invariance **ESPRIT** [ROY88b,ROU89b,OTT89,SWI89] is not applicable. The point is that if an array exhibits multiple translational invariances, one should employ MI **ESPRIT** as opposed to PFBAVG modified **PRO–ESPRIT**.

The first scenario simulated consisted of three sources. Two highly correlated, equal strength sources were located at $(\theta_1 , \phi_1) = (45^\circ , 5^\circ)$, corresponding to $(u_1 , v_1) = (.0616 , .0616)$, and $(\theta_2 , \phi_2) = (225^\circ , 5^\circ)$, corresponding to $(u_2 , v_2) = (-.0616 , -.0616)$. The degree of correlation was 95% and the SNR of each these two sources was 13.4 dB. If one examines the u=v planar slice of the 2D quiescent array pattern associated with the overall 28 element array pointed to boresite, i. e., the z-axis, the 3 dB beamwidth is computed to be 14.3°. The angular separation of the two sources in the u=v

plane is 10° or seven-tenths of a beamwidth. A third uncorrelated source with SNR = 15.8 dB was located at $(\theta_3 , \phi_3) = (32° , 20°)$, corresponding to $(u_3 , v_3) = (.29 , .1812)$. The noise was modeled to be independent from element to element and of equal power. Thus, formation of the Z correlation matrix and the coarse "cleaning" described by (5.22) was not required.

It is noted that the difference between θ_1 and θ_2 is 180° while $\phi_1 = \phi_2$. Thus, without array manifold modification as prescribed in Section 5.4, PFBAVG modified **PRO–ESPRIT** breaks down. This will be illustrated by examining the EV's of the PFBAVG'd correlation matrix with and without array manifold modification at a later point. To avert breakdown, v-modification according to (5.33) and (5.34) was employed. The phase angles, v_i, i=1,2,...,14, were selected according to the prescription in (5.41).

The results of 200 independent trials are plotted and tabulated in Figure 5.1. The number of snapshots was N=25 in each trial run. In Figures 5.1(a) and 5.1(b), estimates of $\Phi_{kk} = e^{j\pi u_k}$, k=1,2,3 obtained from the original and PFBAVG modified versions of **PRO–ESPRIT**, respectively, are plotted. The corresponding estimates of $\Phi_{kk} = e^{j\pi v_k}$, k=1,2,3 obtained from the same 200 independent trials are plotted in Figures 5.1(c) and 5.1(d), respectively. Sample means (SMEANS) and sample variances (SVARS's) were computed for both estimation schemes. An immediate observation is that the estimates of Φ_{kk}, k=1,2,3, obtained with PFBAVG modified **PRO–ESPRIT** are more closely clustered near the unit circle, indicated by the dotted line, than the corresponding estimates obtained with the original version of **PRO–ESPRIT**. As argued previously, this may be attributed to the fact that PFBAVG modified **PRO–ESPRIT** explicitly exploits the unity magnitude of the elements of the diagonal invariance operator, i. e., Φ_{kk}, k=1,...,D, while the original version of **PRO–ESPRIT** does not. The corresponding average number of floating point operations (flops) per run, as calculated by the PRO-MATLAB software used to conduct the simulations, is indicated in each of the Figures 5.1(a) thru 5.1(d) as well. In the case of u estimation, a single execution of **PRO–ESPRIT** corresponding to a single trial required approximately 552,164 flops. In contrast, each corresponding execution of PFBAVG modified **PRO–ESPRIT** required 382,478 flops. A similar substantial reduction in computation was realized in the case of v estimation as well. At the same time, the quality of the estimates obtained from PFBAVG modified **PRO–ESPRIT** is observed to be significantly better than the quality of the estimates obtained from **PRO–ESPRIT**. This conclusion is substantiated by comparing corresponding SVAR's indicated on the appropriate plots. In each case, the reduction in variance achieved with

PFBAVG is by a factor between 1.5 and 1.8. As a final note, the price paid for these gains should be pointed out. For this specific array scenario, **PRO–ESPRIT** can handle up to 13 sources, while the maximum number of sources PFBAVG modified **PRO–ESPRIT** can handle is 6.

Figure 5.2 illustrates the effect of array manifold modification on the distribution of the EV's. The arithmetic mean of each EV of the 14x14 PFBAVG'd correlation matrix, $\hat{C}_{FB}^{XX\,V}$, in the case of u estimation was computed over 200 independent trials with the array and source parameters described above. As noted previously, $\theta_2 - \theta_2 = 180^\circ$ and $\phi_1 = \phi_2$ giving rise to a deflation of the signal subspace as discussed in Section 5.3. This deflation of the signal subspace is illustrated by the graph of the average eigenvalue distribution in the case of no array manifold modification. Recall that with PFBAVG each source takes up two degrees of freedom. With no v-modification, it appears that there are only four signal eigenvalues corresponding to two sources. It should be noted that if one nevertheless executes PFBAVG modified **PRO–ESPRIT** under the correct assumption of six signal eigenvalues, i. e., three sources, the situation is not corrected and the algorithm still breaks down. The situation is corrected, however, in a computationally simplistic manner by simple v-modification of $\hat{C}_{FB}^{XX}$ and $\hat{C}_{FB}^{XY}$ according to (5.33) and (5.34), respectively. Two methods of determining the phase angles, v_i, i=1,2,...,M, were investigated. The method used in the simulations discussed above and presented in Figure 5.2 was that based on the minimization of the Frobenius norm of $\hat{C}_{FB}^{XX\,V}$. The corresponding prescription for the phase angles is given by (5.41) and involves negligible computation. The graph labeled as "optimal V" illustrates the corresponding effects on the average eigenvalue distribution. This curve gives the appearance of six signal eigenvalues, corresponding to three sources. Relative to the situation with no v-modification, two of the six largest EV's have decreased in magnitude while the other four have increased in magnitude. As discussed in Section 5.4, the sum of all 14 EV's was the same in both cases. For purposes of comparison, selection of the phase angles according to $v_i = \frac{2\pi i}{M}$, i=0,1,...,M-1, was examined as well. In this case, the elements of the diagonal matrix V are uniformly-spaced around the unit circle. Observing the graph labeled "Uniform V", we find that it lies between the "No V" and "Optimal V" curves. Correspondingly, we find that the signal subspace deflation problem is remedied, but the SVAR's of the estimates achieved with "Uniform V" modification are slightly higher than the the SVAR's of the estimates achieved with "Optimal V" modification under the same conditions. This claim is substantiated by simulations not presented here due to space constraints.

Figure 5.3 illustrates the performance of the weighted Procrustes difference scheme described by (5.43) for estimating the number of sources. Empirical probabilities were computed from the results of 200 independent trials. For purposes of comparison, the performance of the Procrustes difference scheme described by (5.48) with $w(\hat{v}) = 1$, $\hat{D}=1,2,...,6$, i.e., without weighting, is plotted as well. For Figure 5.3(a), the array and source parameters were exactly equal to those indicated in the previous simulations except that the number of snapshots varied from N=7 to N=200 in nonuniform increments. For the case of N=25 snapshots and weighting according to (5.54), which yielded the estimator performance displayed in Figures 5.1 and 5.2, the empirical probability of correct detection was .975, i. e., the procedure correctly determined that there were D=3 sources 195 times out of 200. Recall that two of the sources were 95% correlated and separated by seven-tenths of the 3 dB beamwidth. In addition, the third uncorrelated source was several dB above the other two sources, and was angularly located approximately one 3 dB beamwidth away from the second source. With weighting, an empirical probability of 1, i. e., no errors out of 200 runs, was achieved with N=35 snapshots, and for all values of N greater than 35. For the values of N tested, an empirical probability of 1 **without** weighting, i. e., with uniform weighting, was not achieved until N=50 snapshots. Prior to N=50, it is observed that the empirical probability of correct detection obtained with weighting according to (5.54) is significantly higher than that obtained with uniform weighting. Similar comments hold with regard to the performance of the method as a function of SNR as plotted in Figure 5.3(b). In generating Figure 5.3(b), the array and source parameters were again exactly equal to those associated with the previous simulations except that the SNR of each source was varied in nonuniform increments. The value k=1 corresponds to the SNR values used in the simulations presented in Figures 5.1 and 5.2. With weighting according to (5.56), an empirical probability of 1 was achieved with k=2 in which case the SNR of source 1 and 2 is 16.4 dB. Without weighting, the same condition was not achieved until k=2.5.

Figure 5.4 presents the results of a simple simulation example illustrating the improvement in performance achieved by spacing the doublets over a large aperture in order to achieve a greater resolution capability with a limited number of elements. For this set of simulation results, the array was linear composed of M=14 equi-spaced doublets. In the first set of simulations presented in Figure 5.4(a), the spacing between the two elements comprising each doublet was a half-wavelength, while the inter-doublet spacing was a half-wavelength. In this case, the overall array was simply a uniformly-spaced linear array of 28 elements with inter-element spacing of a half-wavelength. The corresponding effective aperture

is thus 14λ giving rise to a 3 dB beamwidth of approximately 4°. In the second set of simulations presented in Figure 5.4(b), the inter-doublet spacing was increased by a factor of 3, while the spacing between the two elements comprising each doublet was held fixed at a half-wavelength. This configuration gives rise to an effective aperture of $14\left(\frac{3\lambda}{2}\right) + 14\left(\frac{\lambda}{2}\right) = 28\lambda$, twice that occurring with an inter-doublet spacing of a half-wavelength. Correspondingly, the 3 dB beamwidth is 2°. This translates into an increase in the resolution capability by a factor of 2, roughly speaking. The price paid for this factor of 2 increase in resolution capability will be addressed shortly. We first present the simulation results.

The source scenario consisted of two highly correlated, equal strength sources located at $\theta_1 = 2^\circ$, corresponding to $u_1 = .0349$, and $\theta_2 = -2^\circ$, corresponding to $u_2 = -.0349$. In accordance with convention for linear arrays, $u = \sin(\theta)$, where θ is the angle of a source relative to broadside. The degree of correlation was 95% and the SNR of each was 13.4 dB. The results of 200 independent trials are plotted and tabulated in Figure 5.4. In each trial run, the number of snapshots was $N = 25$ and estimates of the two source angles were computed via PFBAVG modified **PRO–ESPRIT**. It is noted that each of the two SVAR'S achieved with an inter-doublet spacing of $\frac{3\lambda}{2}$, listed in Figure 5.4(b), is smaller than the corresponding SVAR achieved with an inter-doublet spacing of $\frac{\lambda}{2}$, listed in Figure 5.4(a), by a factor of either 2.5 or 2.75. This may be attributed to the factor of two increase in effective aperture length achieved with an inter-doublet spacing of $\frac{3\lambda}{2}$ relative to that achieved with an inter-doublet spacing of $\frac{\lambda}{2}$. The average number of flops is very nearly equal for the two cases since each array has the same number of elements, 28.

What is the price paid for the factor of 2 increase in resolution capability achieved with an inter-doublet spacing of $\frac{3\lambda}{2}$? Since the spacing between the two elements comprising each doublet is $\frac{\lambda}{2}$, there is a one-to-one mapping between u and the displacement scalar $\Phi = e^{j\frac{2\pi}{\lambda}\frac{\lambda}{2}u} = e^{j\pi u}$ over the interval $-1 < u < 1$, i. e., from endfire to endfire. However, the mapping between u and the array manifold vector $\mathbf{a}(u)$ associated with either of the two translationally invariant subarrays is **not** one-to-one over the interval $-1 < u < 1$. $\mathbf{a}(u)$ is the array manifold vector associated with a uniformly-spaced linear array of 14 elements

with an inter-element spacing of $\frac{3\lambda}{2}$. Any two sources separated by either $\Delta u=\frac{2}{3}$ or $\Delta u=\frac{4}{3}$ give rise to the same $\mathbf{a}(u)$ and, as a consequence, make a rank one contribution to either of the two data matrices, **X** and **Y**. As an example, consider two sources with one located at u_1 and the other at $u_2 = u_1 + \frac{2}{3}$. The noiseless X and Y data matrices may be expressed as

$$\mathbf{X} = \sum_{i=1}^{2} \mathbf{a}(u_i)\mathbf{s}_i^T = \mathbf{a}(u_1)\{\mathbf{s}_1 + \mathbf{s}_2\}^T \tag{5.58}$$

$$\mathbf{Y} = \sum_{i=1}^{2} e^{j\pi u_i}\mathbf{a}(u_i)\mathbf{s}_i^T = e^{j\pi u_1}\{1 + e^{j\pi\frac{2}{3}}\}\mathbf{a}(u_1)\{\mathbf{s}_1 + \mathbf{s}_2\}^T \tag{5.59}$$

It should be noted, though, that as long as no two sources are separated by either $\Delta u=\frac{2}{3}$ or $\Delta u=\frac{4}{3}$, it is ideally possible to determine the direction of each and every source in the interval $-1 < u < 1$ via SI **ESPRIT without ambiguity!!** In contrast, this statement does not hold for a uniformly-spaced linear array with an inter-element spacing of $\frac{3\lambda}{2}$. In this case, without a-priori knowledge, one would not be able to determine via SI **ESPRIT** or MI **ESPRIT** in which of the three intervals, $-1 < u < -\frac{1}{3}$, $-\frac{1}{3} < u < \frac{1}{3}$, $\frac{1}{3} < u < 1$, a particular source lies regardless of the angular separations between sources.

In order to avoid the array manifold ambiguity problem occurring in the case of equi-spaced doublets spaced greater than a half-wavelength, one should space the doublets aperiodically over an aperture commensurate with resolution requirements as depicted in Figure 1.2(b). A linear array of aperiodically spaced doublets exhibits only a single invariance, thus negating the use of multiple invariance **ESPRIT** [ROY88b,ROY89b]. In this case, the PFBAVG modified **PRO–ESPRIT** developed within serves as a computationally efficient manifestation of SI **ESPRIT**.

In the next set of simulations we examine the performance of the techniques outlined in Section 5.5 that can be used to pair the u and v estimates. The scenario we simulated was the following. In total there were three sources coming from the following directions. $(\theta_1,\phi_1)=(25°,15°)$, $(\theta_2,\phi_2)=(55°,5°)$ and $(\theta_3,\phi_3)=(42°,30°)$. In terms of (u,v), these angles translate into $(u_1,v_1)=(.235,.1094)$, $(u_2,v_2)=(.05,.0714)$ and $(u_3,v_3)=(.3716,.3346)$ respectively. The array was the corrugated box array described before, and the method that was used to estimate u_i and v_i, i=1,2,3 was the version of **PRO–ESPRIT** with

no pseudo FB averaging incorporated. When the **ESPRIT**-based method was used, the axis of the doublets was oriented first along the x-axis, then along the y-axis, and finally along the line y=-x, to give estimates of u, v and u-v respectively. For the MUSIC based method the only orientation axes used were the x-axis and y-axis. In the two simulations we carried out we considered the empirical probability of correct pairing, first as a function of the number of snapshots, and then as a function of the signal powers. Before discussing the results, it is appropriate to explain what we mean by probability of correct pairing. We assumed that our algorithm paired correctly the D pairs (u_i, v_i) i=1,..,D, if the combined absolute deviation of the corresponding azimuth and elevation angles from their true value was the least amongst all other possible pairings. If the least angular deviation was given by a different combination, and the deviation did not exceed some threshold, then the assumed pairing was assumed in error. If the threshold was exceeded, the results of that particular run were completely disregarded, and this was as an indication that no possible combination made sense. In Figure 5.5(a) we show what happens if the SNR of each source was held fixed at 13 dB, while the number of snapshots varied starting at N=5. The three sources were uncorrelated, and the empirical probabilities were obtained from 200 independent runs. Observe that even with 5 snapshots, both methods managed to pair the u and v estimates quite successfully. With 25 snapshots, no error occurred. It can also be seen that the MUSIC-based method worked slightly better that the **ESPRIT**-based method, for almost all number of snapshots. For both cases, in 3% of the total number of runs the threshold was exceeded, basically because of bad estimates. In this particular example, for the **ESPRIT**-based method we had to check a total of 36 different combinations, while for the MUSIC-based method this number was only 6. Figure 5.5(b) shows how the empirical probability of correct pairing varies as a function of the SNR. The three sources were again uncorrelated, and the number of snapshots was held fixed at N=10. The results here are not surprising either. Even when the signal and noise have the same power, the probability of correct pairing is almost 90%. The better performance of the MUSIC-based method is observed here as well. Using this, probability one is reached when the SNR is close to 17 dB, while the **ESPRIT**-based technique does not reach this point until the SNR is almost 30. The most probable explanation for this is that if there is an outlier in the noise, this will result in bad estimates for u, v and u-v. Hence, the u-v estimates in such a case contain no information at all, and the outcome of the matching process is more or less a random event.

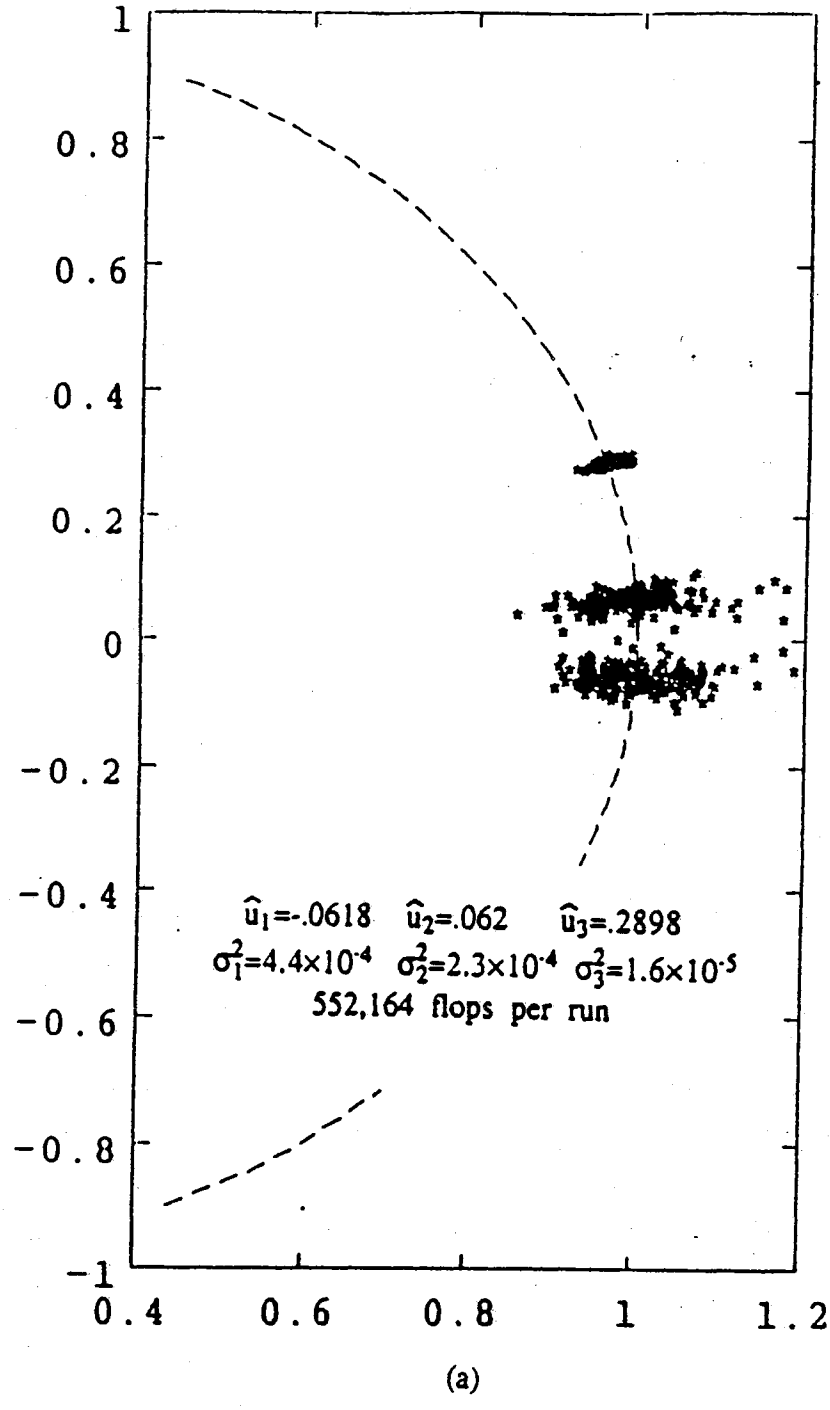

Figure 5.1 **Comparison of the estimation of the u and v parameters via the original version of PRO–ESPRIT and the new one based on pseudo F-B Averaging. 5.2(a) and 5.2(b) compare the u estimates, while Figures 5.2(c) and 5.2(d) compare the v estimates.**

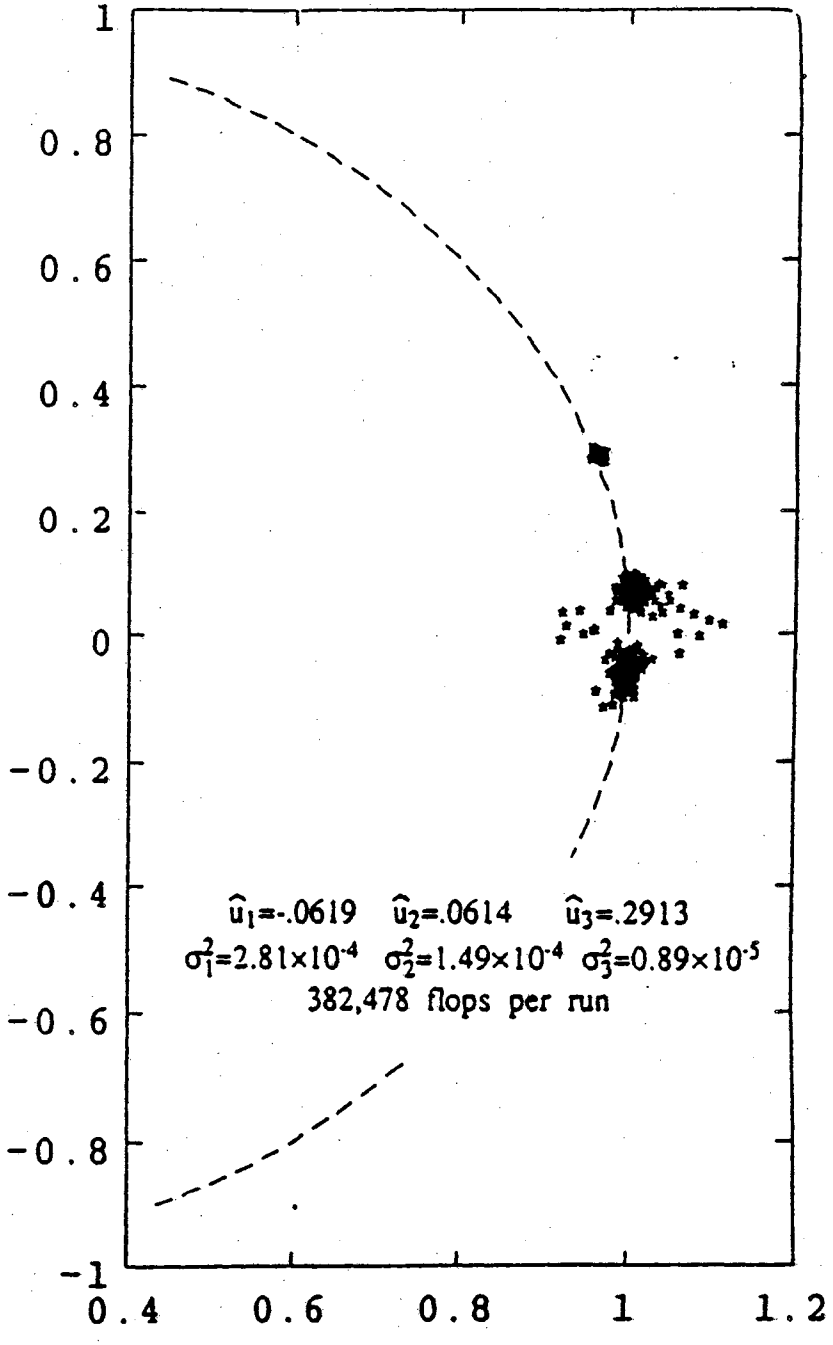

(b)

Figure 5.1 (continued)

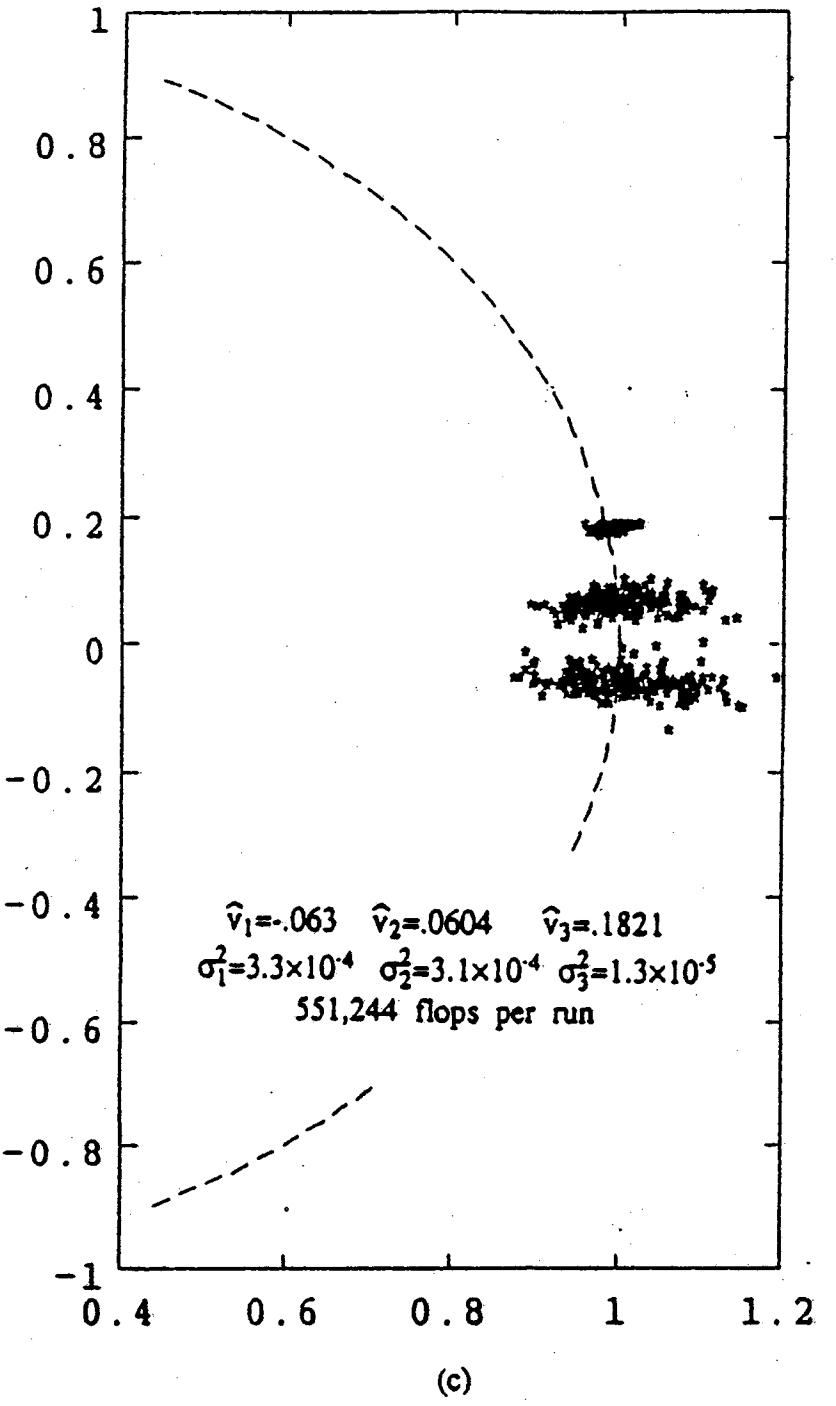

Figure 5.1 (continued)

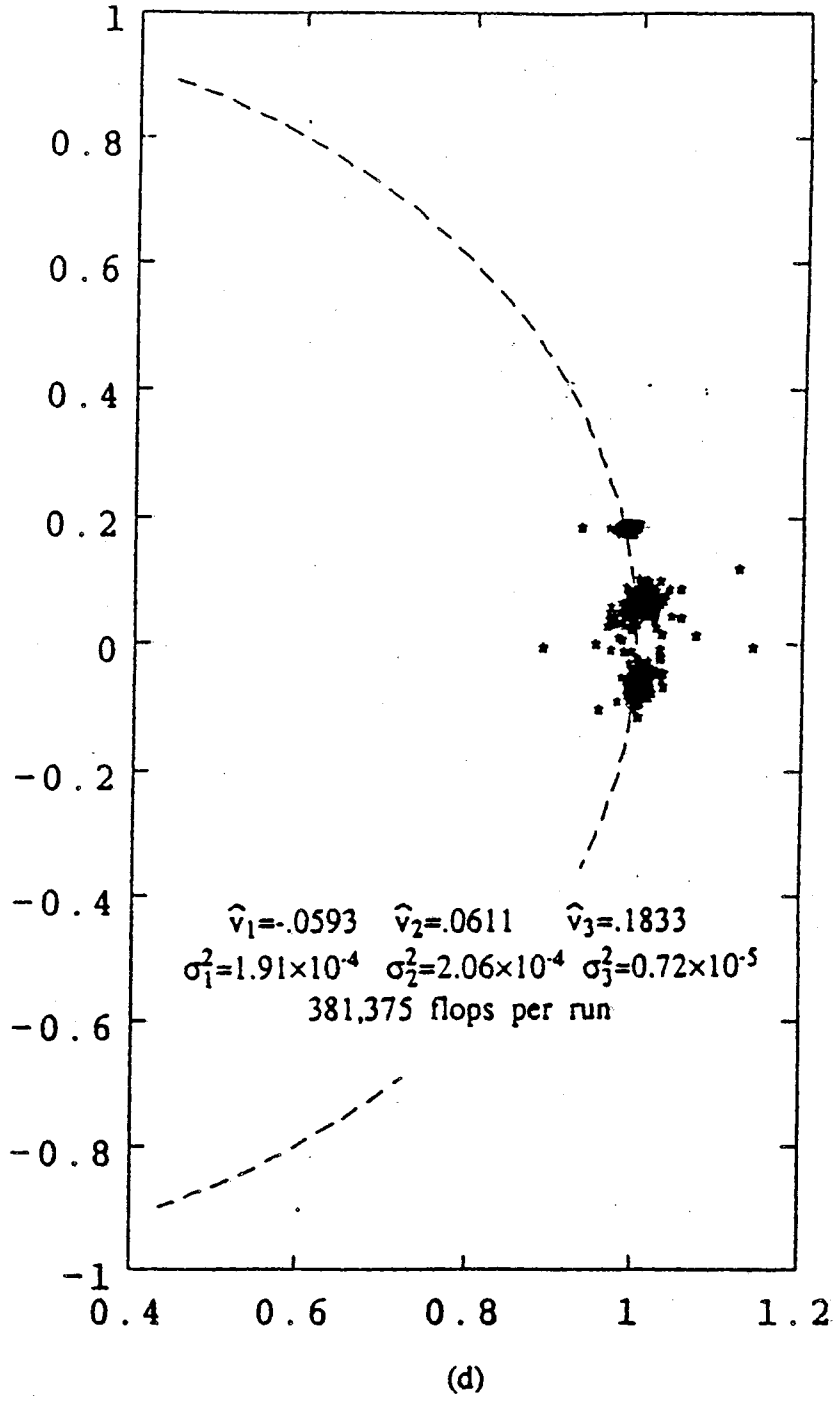

(d)

Figure 5.1 (continued)

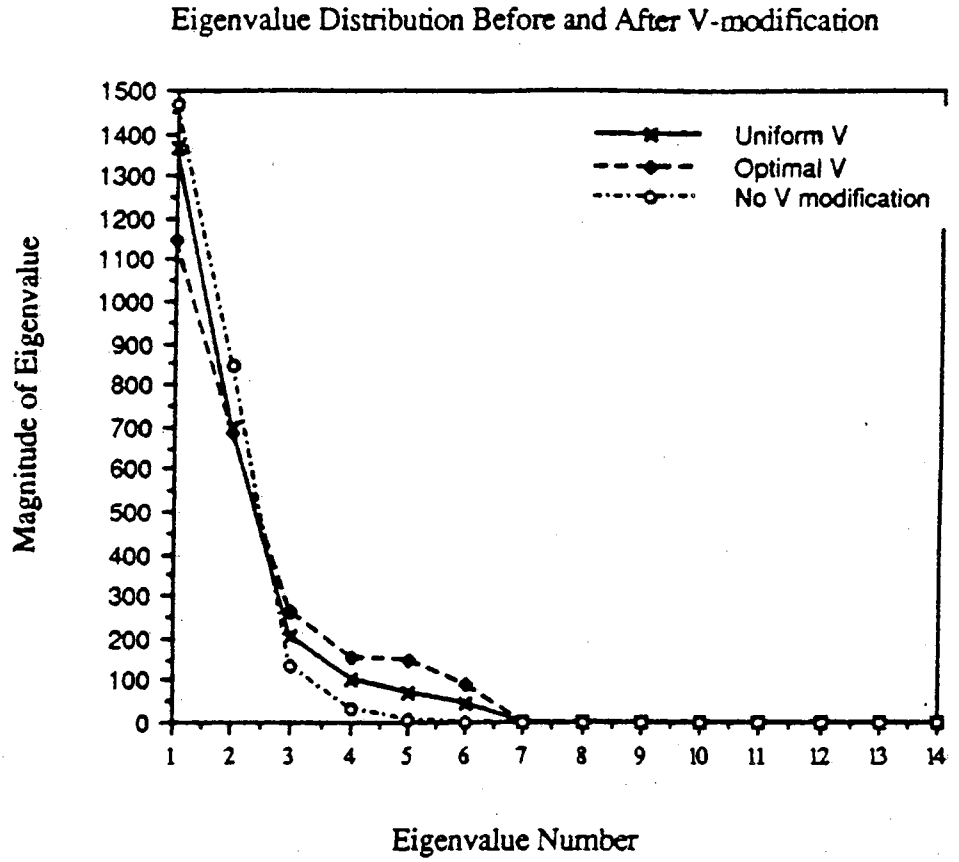

Figure 5.2 Average eigenvalue distribution before and after array manifold modification. The eigenvalues are averaged over 200 independent trials. The sources are located at (θ_1,ϕ_1)=(45°,5°), (θ_2,ϕ_2)=(225°,5°) and (θ_3,ϕ_3)=(32°,20°). The SNR of the first two sources is 13.4 dB and are 95% correlated. The third source is uncorrelated with the first two and has an SNR of 15.8 dB. 25 snapshots were used.

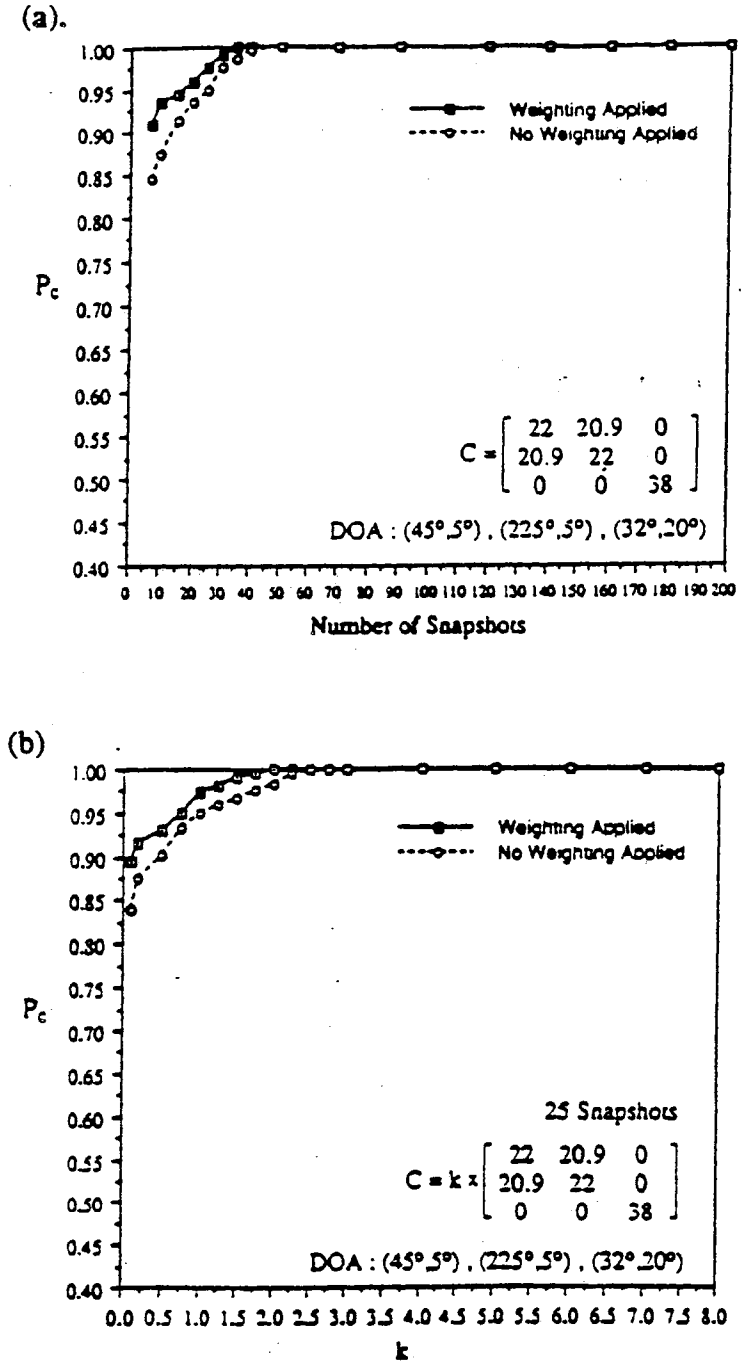

Figure 5.3 Empirical probability of detecting the correct number of sources (a) as a function of the number of snapshots and (b) as a function of the SNR, with the weighted Procrustes difference scheme. The array and source parameters are described in Figure 5.2. For each set of parameters, the corresponding probability was computed from the results of 200 independent runs.

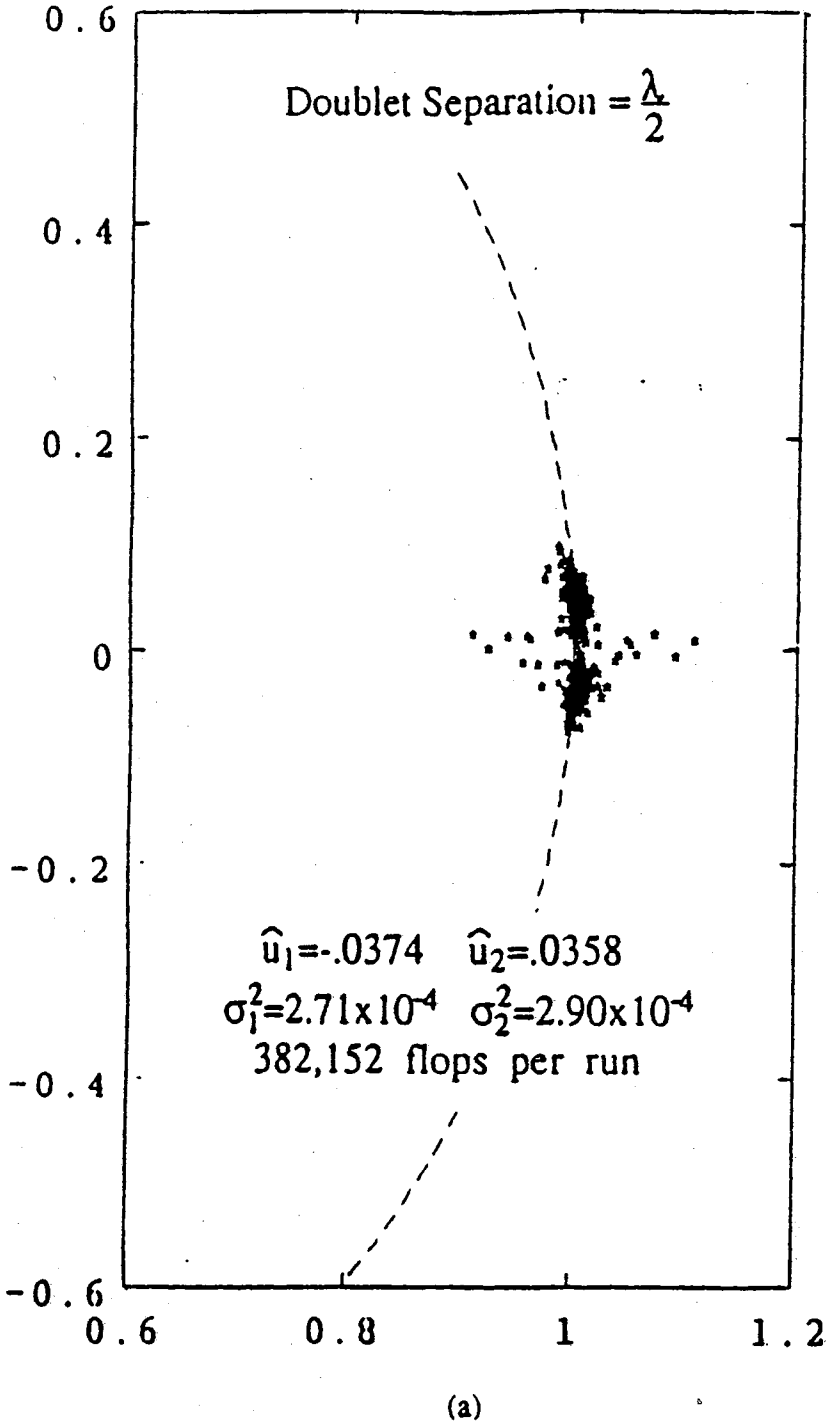

Figure 5.4 A comparison of the performance of pseudo F-B **PRO–ESPRIT** when it is applied to a linear array of 28 sensors. The estimated quantities are u_1 and u_2 for $\theta_1=-2°$ and $\theta_2=2°$. In both cases the sensors in a doublet are separated by $\lambda/2$. In 5.6(a) the inter-doublet separation is $\lambda/2$ and in 5.6(b) it is $3\lambda/2$.

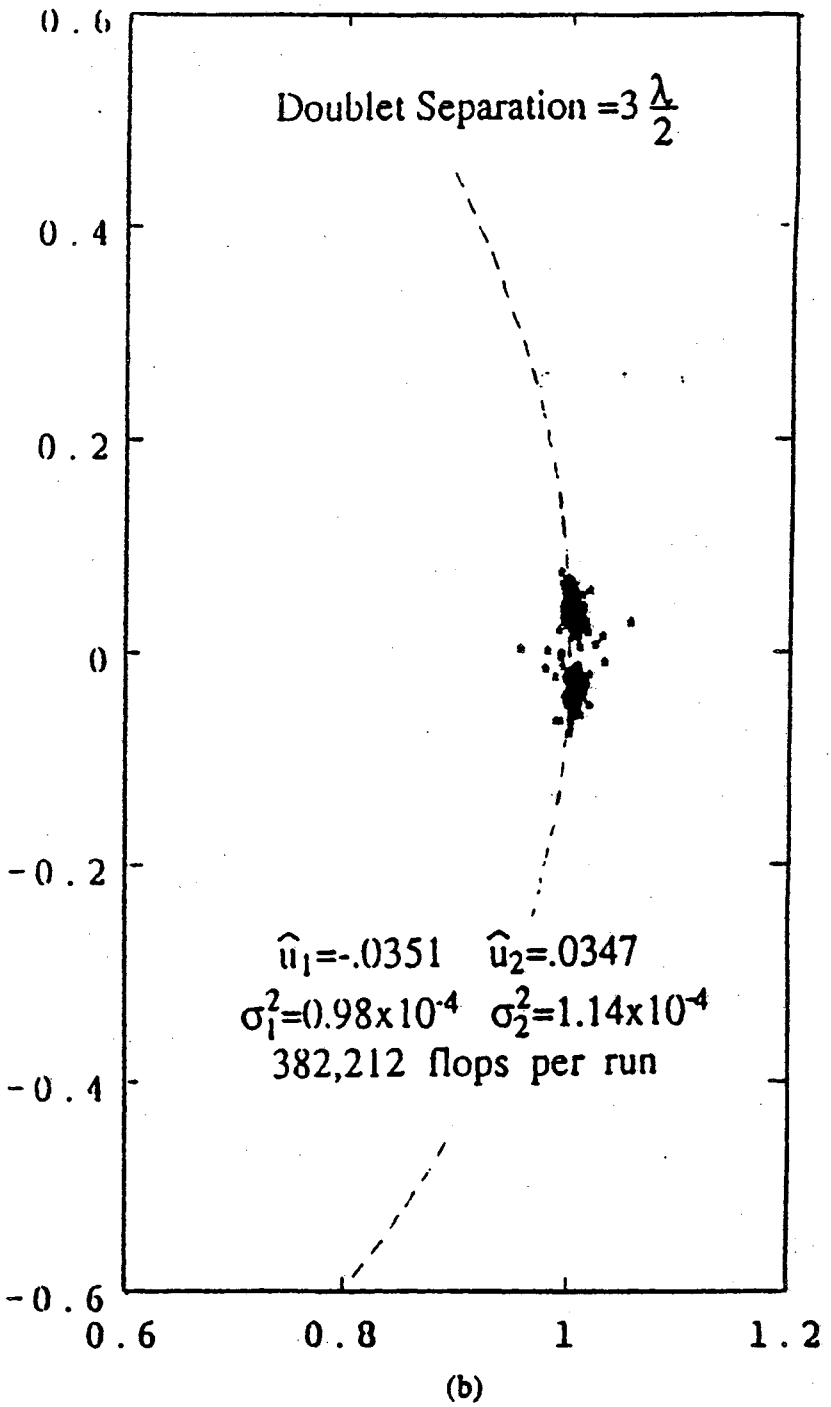

Figure 5.4 (continued)

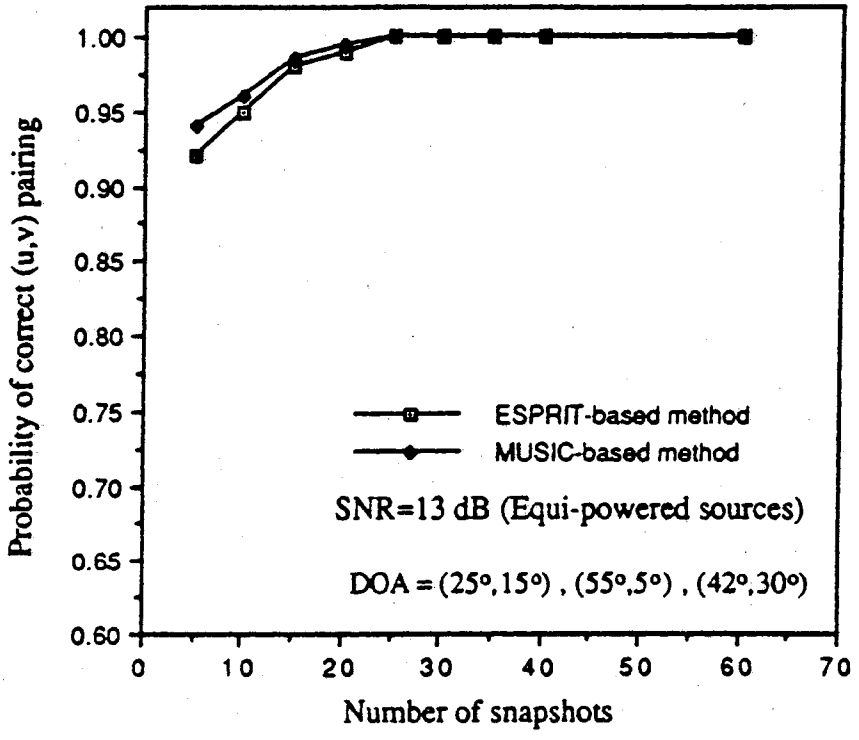

(a)

Figure 5.5 The probability of correct pairing of the u and v estimates obtained from **PRO–ESPRIT**. In 5.7(a) the SNR is held fixed and the number of snapshots changes. In 5.7(b) the number of snapshots is fixed and the SNR varies.

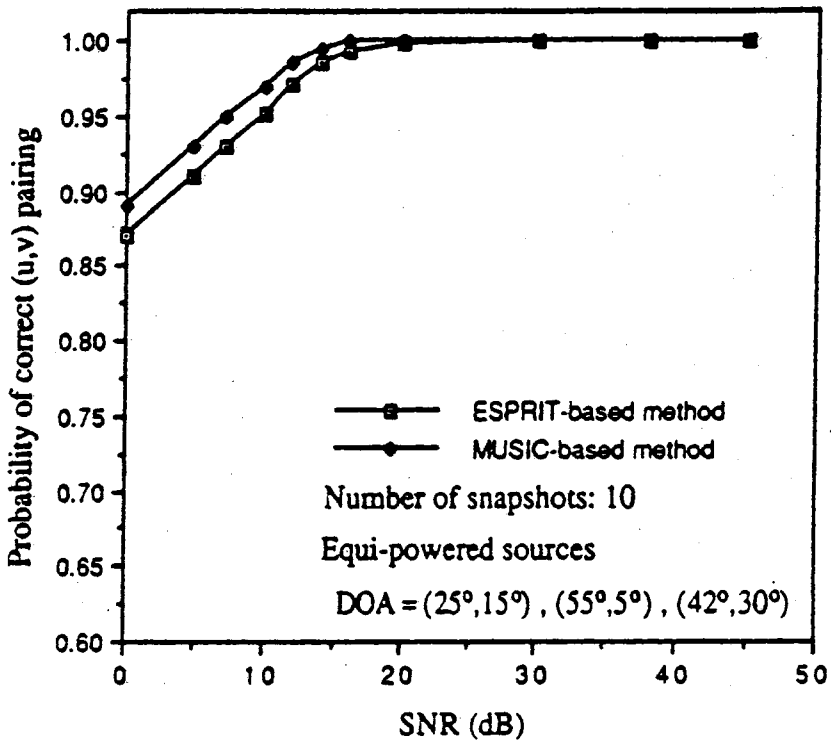

(b)

Figure 5.5 (continued)

CHAPTER 6
APPLICATION OF PRO-ESPRIT IN BEAMSPACE

6.1 Introduction

We have concluded in the previous chapters that the major computational task in the application of PRO-ESPRIT is the initial EVD of the MxM correlation matrices $\mathbf{R}_{xx}$ and $\mathbf{R}_{yy}$, where M is the number of sensors comprising each array. Today, there are in operation arrays that consist of hundreds even thousands of sensors. Correspondingly, the respective dimensions of $\mathbf{R}_{xx}$ and $\mathbf{R}_{yy}$ can be extremely large. The eigenvalue decomposition of matrices of such large dimensions is not a practical requirement, despite the availability of highly sophisticated and robust software and hardware. Our experience has indicated that even when dealing with matrices of moderate dimensions, results provided by EVD and SVD routines are of dubious accuracy when the given matrices are not very well conditioned. Assuming that we can overcome the accuracy problem, the requirement of real time operation makes PRO-ESPRIT prohibitive when M is large. Depending on the array structure, that is, if it is a ULA or a 2-D ESPRIT array, one can employ Forward-Backward averaging or pseudo Forward-Backward averaging of the data, respectively, to avoid one, of the two required, EVD's. This, however, can hardly be considered the best solution to the problem at hand. A better solution is to apply PRO-ESPRIT in beamspace. Contrary to the element space where the data is taken to be the raw snapshot vectors, in beamspace these snapshot vectors are first acted upon by a beamformer matrix yielding a beamspace snapshot vector of lower dimensionality. Operation in beamspace has advantages as well as disadvantages. The primary benefit is the reduction in computation. This is due to the reduced dimensionality of the beamspace snapshot vectors yielding correlation matrices of lower dimensionality. In addition, with proper selection of the elements of the beamformer matrix, it is possible to steer the beam in a specified direction, i.e., suppress all signals that fall outside a desired range of DOA's and amplify signals falling within this range.

The ultimate goal is to detect and localize sources that originate from any point in the angular region θ=−90° θ=90°. Since we concentrate completely on

ULA's, instead of denoting directions using the variable θ, it is preferable to use the variable u where $u=\sin\theta$. Thus, as θ varies in the interval -90° to 90°, u varies from -1 to 1. The approach here is to divide the interval u=-1 to 1 into a number of bands, and then cover each band with a set of beams, symmetrically positioned around its center. If we do this, then the data corresponding to each band may be processed simultaneously in parallel, for the purpose of estimating the DOA's. This approach poses several interesting questions. For example is it necessary for the bands to overlap, and if so, by how much? If there is no overlap among bands, what is the effect of a source in close proximity to the boundary of two consecutive bands? These and other questions will be addressed and discussed as we proceed. The discussion and analysis here will mainly focus on a set of beams centered around the point u=0. The analysis for beam sets steered to other pointing angles follows directly from this. The reader is reminded that we are only considering ULA's. The procedures developed here may be extended to arbitrary, 2-D arrays on a rectangular grid. The reason for concentrating on the linear arrays is the Vandermonde structure of the array manifold vector. This structure may be judiciously exploited to yield computationally efficient implementations. We begin by considering a certain class of weight vectors for forming the desired beams.

6.2 Choice and Construction of the Beamforming Matrix

Consider an ESPRIT array system made up of two translationally invariant arrays X and Y. Following the procedure outlined in Chapter 3, we form the "raw" data matrices **X** and **Y**. Summarizing the results developed in Chapter 3, **X** and **Y** may be decomposed in the noiseless case as

$$\mathbf{X} = \mathbf{AS} \quad , \quad \mathbf{Y} = \mathbf{A\Phi S} \tag{6.1}$$

where the dimension of **A** is MxD. Recall that M is the number of sensors in each array, D is the number of sources and **S** is DxN, N being the number of snapshots. Next, consider the effect of pre-multiplying both **X** and **Y** by the same beamformer matrix $\mathbf{W}^H$; the dimensions of **W** is MxB. B is then the number of beams formed, i.e. B is the length of the beamspace snapshot vectors. Substituting into (6.1), the corresponding beamspace data matrices $\mathbf{X}_b$ and $\mathbf{Y}_b$ are:

$$\mathbf{X}_b = \mathbf{W}^H\mathbf{X} = \mathbf{W}^H\mathbf{AS} \tag{6.2a}$$

$$\mathbf{Y}_b = \mathbf{W}^H\mathbf{Y} = \mathbf{W}^H\mathbf{A\Phi S} \tag{6.2b}$$

From (6.2a) and (6.2b) it follows that the matrix pencil $\{\mathbf{Y}_b - \lambda\mathbf{X}_b\}$ is an

ESPRIT matrix pencil whose Generalized Eigenvalues are Φ_{ii}, i=1,..,D. Hence, PRO-ESPRIT may be applied to obtain estimates of Φ_{ii} i=1,..,D. For proper operation of PRO-ESPRIT, however, we require that the beam number, B, be at least one greater than the number of sources. In general, the number of sources is not known a-priori, and the user must ensure that the expected number of sources does not exceed B. In the practical case of noisy data, **W** also influences the form of the resulting X and Y beamspace noise correlation matrices, $\mathbf{R}_{xx}^{nnb}$ and $\mathbf{R}_{yy}^{nnb}$. In terms of the element space noise correlation matrices $\mathbf{R}_{xx}^{nn}$ and $\mathbf{R}_{yy}^{nn}$, $\mathbf{R}_{xx}^{nnb}$ and $\mathbf{R}_{yy}^{nnb}$ may be expressed as

$$\mathbf{R}_{xx}^{nnb} = \mathbf{W}^H \mathbf{R}_{xx}^{nn} \mathbf{W} \quad , \quad \mathbf{R}_{yy}^{nnb} = \mathbf{W}^H \mathbf{R}_{yy}^{nn} \mathbf{W} \tag{6.3}$$

It should be noted that even if the element space noise is spatially white, the noise in beamspace is correlated, in general. Uncorrelated noise in beamspace may be achieved, however, by employing a beamforming matrix composed of mutually orthogonal columns. In contrast to element space operation in the case of white noise, proper beamspace operation requires an EVD of $\mathbf{R}_{bb}^{xx} - \sigma^2 \mathbf{R}_{xx}^{nnb}$ and $\mathbf{R}_{bb}^{yy} - \sigma^2 \mathbf{R}_{yy}^{nnb}$ respectively, where σ^2 is the noise power. σ^2 must be estimated prior to performing the above decompositions. A quick and efficient method for doing such will be presented in section 6.4.

We now elaborate on the choice of the beamforming matrix **W**. The structure of **W** is dictated by many parameters. The most important parameters are the pointing angles of the beams. An important factor to consider is the structure of the beamspace array manifold vector. From (6.2) we see that it is not required that the beamspace array manifold vectors $\mathbf{W}^H\mathbf{A}$ exhibit Vandermonde structure. However, the Vandermonde structure is a prerequisite for the applicability of F-B averaging in beamspace. Recall that F-B averaging serves to substantially reduce the computational burden. We thus concentrate on a class of matrix beamformers which yield a beamspace manifold vector possessing the Vandermonde structure.

To construct a beamforming matrix which preserves the Vandermonde structure in beamspace, consider the following prescription. Choose any (M-B+1)x1 vector **h** and generate **W** as

$$\mathbf{W} = \begin{bmatrix} \mathbf{h} & 0 & 0 & . & . & 0 \\ 0 & \mathbf{h} & 0 & . & . & 0 \\ 0 & 0 & \mathbf{h} & . & . & 0 \\ 0 & 0 & 0 & . & . & 0 \\ . & . & . & . & . & 0 \\ . & . & . & . & . & 0 \\ 0 & 0 & 0 & 0 & 0 & \mathbf{h} \end{bmatrix} \tag{6.4}$$

Let $\mathbf{a}_i(u)$ denote the i-th column of $\mathbf{A}$ and $\mathbf{w}_i$ be the i-th column of $\mathbf{W}$. If $\mathbf{a}_i(u)$ is a Vandermonde vector with parameter $\Phi_{ii} = \exp(j2\frac{\pi}{\lambda}u_i)$,

$$\mathbf{W}^H\mathbf{a}_i(u) = \mathbf{h}^H\mathbf{a}_i(u)\begin{bmatrix} 1 \\ \Phi_{ii} \\ \Phi_{ii}^2 \\ . \\ . \\ \Phi_{ii}^{(M-1)} \end{bmatrix} \tag{6.5}$$

The final vector in (6.5) is clearly a scalar multiple of a Vandermonde vector with exactly the **same** parameter Φ_{ii} but of dimension B, rather than M, the dimension of the original vector. Of course, B<M. Let us now consider the structure of $\mathbf{X}_b$. In view of the result in (6.5), it follows that $\mathbf{X}_b$ may be expressed as

$$\mathbf{X}_b = \mathbf{A}_B\Psi\mathbf{S} \tag{6.6}$$

The subscript B is used to indicate the row dimension of **A**. $\Psi = \text{diag}\{\mathbf{h}^H\mathbf{a}(u_1),...,\mathbf{h}^H\mathbf{a}(u_D)\}$ and may be viewed as an "amplification" matrix, since each of its diagonal elements scales the corresponding row of the source signal matrix **S**. Ψ is a function of the direction of arrival of the D incident signals, as well as the beamforming vector **h**. Therefore, through judicious selection of **h**, we may "amplify" signals coming from a certain region of the interval u=−1 1, and, at the same time, attenuate signals from outside the above region.

Although the beamforming matrix structure in (6.4) yields a beamspace manifold vector with the desired Vandermonde structure, its use is not recommended since it reduces the resolution capability to that of a ULA of B sensors separated by a half wavelength. That is, the resolution cabability is reduced by a factor of M/B. This is clearly not desirable. However, the result in

(6.5) is important in analyzing the structure of the beamspace manifold vector generated by a DFT (Discrete Fourier Transform) matrix beamformer. We proceed motivated by the work of Zoltowski and Lee [ZOLT89d,ZOLT89e].

Consider the use of a beamforming matrix composed of B mutually orthogonal classical beamforming vectors, denoted by $\mathbf{s}_M(u_o)$ with equi-spaced pointing angles. If M is even, $\mathbf{s}_M(u_o)$ has the form

$$\mathbf{s}_M(u_o) = \left[e^{-j\pi\frac{(M-1)}{2}(u-u_o)} \quad e^{-j\pi\frac{(M-3)}{2}(u-u_o)} \quad \cdots \quad e^{j\pi\frac{(M-1)}{2}(u-u_o)} \right]^T \tag{6.7}$$

while if M is odd

$$\mathbf{s}_M(u_o) = \left[e^{-j\pi\frac{M}{2}(u-u_o)} \quad e^{-j\pi\frac{M-2}{2}(u-u_o)} \quad \cdots \quad e^{j\pi\frac{M}{2}(u-u_o)} \right]^T \tag{6.8}$$

where u_o is the pointing angle of the beam generated by $\mathbf{s}_M(u_o)$ Without loss of generality, assume that the number of beams, B, is an odd number. Similar results hold for the case of M even. In this case, **S** is constructed as

$$\mathbf{S}(u_o) = [\, \mathbf{s}_M(u_o - \tfrac{B-1}{2}\Delta u_B) \,\vdots\, \cdots \,\vdots\, \mathbf{s}_M(u_o - \Delta u_B) \,\vdots\, \mathbf{s}_M(u_o) \,\vdots$$

$$\mathbf{s}_M(u_o + \Delta u_B) \,\vdots\, \cdots \,\vdots\, \mathbf{s}_M(u_o + \tfrac{B-1}{2}\Delta u_B) \,] \tag{6.9}$$

where $\Delta u_B = 2/M$, the spacing between the pointing angles of adjacent beams. With this separation, the columns of $\mathbf{S}(u_o)$ are mutually orthogonal, such that $\mathbf{S}(u_o)^H\mathbf{S}(u_o) = M\mathbf{I}$. Thus, this beamforming matrix yields uncorrelated noise in beamspace. However, $\mathbf{S}(u_o)$ does not exhibit the structure described by (6.4). Thus, the beamspace manifold vector does not exhibit the Vandermonde structure. However, note that $\mathbf{S}(u_o)$ may be expressed in terms of a matrix product as

$$\mathbf{S}(u_o) = \mathbf{P}(u_o)\mathbf{E}(u_o) \tag{6.10}$$

where $\mathbf{P}(u_o)$ is an MxB banded Toeblitz matrix of the form

$$\mathbf{P}(u_o) = \begin{bmatrix} p_o & 0 & . & . & 0 \\ 0 & p_o & . & . & 0 \\ 0 & 0 & . & . & 0 \\ . & . & . & . & . \\ . & . & . & . & . \\ 0 & 0 & 0 & 0 & p_o \end{bmatrix} \tag{6.11}$$

and $\mathbf{E}(u_o)$ is a BxB matrix. To substantiate the validity of this decomposition, we extend the results of Zoltowski and Lee in [ZOLT89e]. To this extend, consider the M-th order polynomial associated with each of the B columns of $\mathbf{S}(u_o)$. That is, let $s_j(z)$ be the polynomial in z whose coefficients are the components of the j-th column of $\mathbf{S}(u_o)$, j=1,..B. It can be shown that each of these B polynomials have M-B roots in common. Consider u_o=0, i.e, broadside operation. In this case, the common roots of the B polynomials are located at $z=\exp\{j\pi\frac{2}{M}k\}$, $k=\frac{(B+1)}{2}, \frac{(B+3)}{2}, .., M-\frac{(B+1)}{2}$. If u_o is not zero, the location of the corresponding common roots may be simply obtained by multiplying all above roots by $e^{j2\frac{\pi}{M}u_o}$. Let p(z) be the polynomial whose roots are the common roots of $s_j(z)$ j=1,..,B. Finally, let $e_j(z)$ j=1,..,B denote the polynomials which satisfy $s_j(z) = p(z)e_j(z)$ j=1,..,B. The polynomials $e_j(z)$ j=1,..,B are each of order B. For a given $s_j(z)$ and corresponding $e_j(z)$, j=1,..,B, let us stack the coefficients of these polynomials in the Mx1 vector $\mathbf{s}_j$ and the Bx1 vector $\mathbf{e}_j$ j=1,..,B. The coefficients of p(z) are placed in vector **p**. Note that that the coefficients of the product of two polynomials can be obtained from the convolution of their respective coefficients. If we express the convolution operation $\mathbf{s}_j = \mathbf{p}_o * \mathbf{e}_j$, j=1,..B, in terms of matrix multiplication, we obtain (6.10). Note that whereas $\mathbf{S}(u_o)$ does not have the property required by (6.4), $\mathbf{P}(u_o)$ does. Define $\mathbf{X}_s = \mathbf{S}^H(u_o)\mathbf{X}$ and $\mathbf{X}_p = \mathbf{P}^H(u_o)\mathbf{X}$. $\mathbf{Y}_s$ and $\mathbf{Y}_p$ are defined similarly. Note

$$\mathbf{X}_p = (\mathbf{E}^H(u_o))^{-1}\mathbf{X}_s = (\mathbf{E}^H(u_o))^{-1}\mathbf{S}^H(u_o)\mathbf{X} \tag{6.12}$$

Thus, start again from the raw data matrices **X** and **Y**, pre-multiply them by $\mathbf{S}^H(u_o)$ followed by a further pre-multiplication by $(\mathbf{E}^H(u_o))^{-1}$. Apparently, this procedure would require the formation and storage of both $\mathbf{S}(u_o)$ and $(\mathbf{E}^H(u_o))^{-1}$. We shall demonstrate, however, that pre-multiplication by $\mathbf{S}^H(u_o)$ can be more efficiently accomplished via the use of DFT or FFT routines.

We confine ourselves again to the case of u_o=0. Similar results follow for the more general case. Consider a beam pointed to $u = \frac{2}{M}l$, $l=-\frac{(B-1)}{2}, .., \frac{B-1}{2}$ and

let $\mathbf{s}_l = \mathbf{s}_M(l\frac{2}{M})$ be the weight vector associated with this beam. If $\mathbf{x}(n)$ denotes the n-th raw snapshot vector from the X array data, then (6.7) dictates

$$\mathbf{s}_l^H \mathbf{x}(n) = \sum_{p=0}^{M-1} x(p) e^{-j\pi(M-2p-1)\frac{l}{M}}$$

or equivalently

$$\mathbf{s}_l^H \mathbf{x}(n) = e^{-j\frac{\pi}{M}l(M-1)} \sum_{p=0}^{M-1} x(p) e^{j2\frac{\pi}{M}pl}$$

By direct comparison of the above equation with the expression for the Discrete Fourier Transform (DFT) of $\mathbf{x}(n)$

$$X(k) = \sum_{n=0}^{M-1} x(n) e^{-j2\frac{\pi}{M}kn}$$

we conclude that the following equality holds.

$$\mathbf{s}_l^H \mathbf{x}(n) = e^{-j\frac{\pi}{M}l(M-1)} X(-l) \quad l = -\frac{(B-1)}{2}, .., \frac{(B-1)}{2} \tag{6.13}$$

Hence, the Bx1 beamspace snapshot vector $\mathbf{S}^H\mathbf{x}(n)$ can be obtained by selecting the appropriate coefficients of the Discrete Fourier Transform of $\mathbf{x}(n)$. From (6.14) it also follows that only B of the M DFT values must be computed. As practical matter, the availability of dedicated Fast Fourier Transform software and hardware suggests that if the number of sensors, M, is a power of two, the beamspace domain snapshot vectors may be formed in a very computationally efficient manner.

6.3 Large Arrays and Ill-Conditioning Problems

In this section we point out and illustrate by example a possible limitation of the beamforming method based on the the decomposition of **S** into **PE**. First, it must be pointed out that **S** by itself has a very sound condition number, equal to one regardless of the value of M. This follows from the fact that $\mathbf{S}^H\mathbf{S}$ is a multiple of the identity matrix. However, ill-conditioning can manifest itself in both **P** and **E**. The circumstances under which this can happen are illustrated by the following example. The case under consideration involves the formation of three beams, with the center beam directed right at boresight, u=0. For this case the following closed form expression for the 3x3 matrix **E** can be found in [ZOLT89e].

$$\mathbf{E} = \begin{bmatrix} -e^{-j\frac{\pi}{M}} & 1 & -e^{j\frac{\pi}{M}} \\ 2\cos(\frac{\pi}{M}) & -2\cos(2\frac{\pi}{M}) & 2\cos(\frac{\pi}{M}) \\ -e^{j\frac{\pi}{M}} & 1 & -e^{-j\frac{\pi}{M}} \end{bmatrix} \tag{6.14}$$

One can easily show that as a result of the conjugate symmetry in both its columns and rows, the eigenvectors and eigenvalues of **E** have the following properties. For any M, **E** has one imaginary and two real eigenvalues. The imaginary eigenvalue λ_1 and the two real eigenvalues λ_2 , λ_3 are given by the following expressions.

$$\lambda_1 = 2j\sin(\frac{\pi}{M})$$

$$\lambda_{2,3} = -\cos(2\frac{\pi}{M})-\cos(\frac{\pi}{M})\pm\left[\left(\cos(2\frac{\pi}{M})-\cos(\frac{\pi}{M})\right)^2 + 4\cos(\frac{\pi}{M})\right]^{0.5}$$

We are primarily interested in the case of M large. Under this assumption, a Taylor series approximations yields

$$\lambda_1 \simeq j\frac{2\pi}{M} \ , \ \lambda_2 \simeq 2\frac{\pi^2}{M^2} \ , \ \lambda_3 \simeq -4+3\frac{\pi^2}{M^2}$$

If we consider the absolute values of $\lambda_1,\lambda_2,\lambda_3$, the one with the smallest magnitude, λ_2, approaches the value of zero at a rate proportional to M^2, while the one with the largest magnitude, λ_3, approaches the value of four at a rate again proportional to M^2. λ_1 also converges to zero at a slower rate, however, proportional to M. This implies that, if the number of elements, M, is exceedingly high, **E** will be ill-conditioned, nearly of rank one. An alternative way to see this is that as M grows, each column of **E** converges element-wise to a scalar multiple of the vector $[1\ -2\ 1]^T$. In this case, the result of any operation involving **E**, especially inversion such as the one in (6.12), may yield erroneous results.

The reason why **P** is troublesome is rather peculiar. Ostensibly, **P** should well conditioned since it is a banded Toeblitz matrix, such that any two columns are linearly independent. However, let us again assume that M is large, and that the number of beams formed is small compared to M. As explained above, **P**(0) is constructed by first generating an (M-B)-th order polynomial whose roots are the M-B common roots of the B beams, stacking its M-B+1 coefficients in a vector and using this vector construct **P**. The trouble here is caused by the large ratio of the magnitude of the middle coefficient and the coefficients of the highest

degree or constant terms. As an example, in the case of B=3 beams and M=128 elements, this ratio is in the order of 10^{17}. Under these conditions, the initial and final rows of $\mathbf{P}(0)$ are almost negligible in magnitude compared to the middle rows, causing once more an ill-conditioning problem.

Similar results follow for the case of any other number of beams. This analysis serves to point out that when it comes to implementing this algorithm, the mathematical precision of the processor used is of vital importance. To give some numbers, in the simulations we carried out on the computer with PRO-MATLAB, a software using double precision, we found that with 15 beams, the algorithm experienced no conditioning problems until the number of elements approached 80.

6.4 PRO-ESPRIT With F-B Averaging and White Noise

In this section we prescribe the algorithm to be followed to apply PRO-ESPRIT in beamspace with the previously described procedure for forming the beamspace data matrices. We also intend to incorporate F-B averaging because of the advantages offered by this mode of processing. Compared to the F-B averaging scheme described in Chapter 4, two basic adjustments are required. This is due to the correlation introduced among the noise components as a result of the multiplication by $(\mathbf{E}(u_o)^H)^{-1}$. In Chapter 4, the F-B noise correlation matrix was a scalar multiple of the identity matrix. This represented a great advantage, both in the noise cleaning process as well as in the sources detection process. However, unless the beamforming matrix has some special structure such as columns that are orthonormal, both noise cleaning as well as source detection become more complicated tasks, even with spatially white noise.

The analysis that follows is greatly simplified if we assume that the beamspace snaphot vectors are generated via pre-multiplication of the "raw" snapshot vectors by $(\mathbf{P}(u_o)^H)^{-1}$. It is emphasized that in practice, the beamspace snapshot vectors are obtained via the procedure outlined in Section 6.2. Let us define $\mathbf{P}_k^i(u_o)$ be the matrix derived from columns i to k of $\mathbf{P}(u_o)$ as this matrix is defined in (6.11). Following the steps outlined earlier, we first operate on $\mathbf{X}$ containing the raw data snapshot vectors to obtain the beamspace snapshot matrix $\mathbf{X}_b$. From $\mathbf{X}_b$, we can obtain two matrices $\mathbf{X}_F^b$ and $\mathbf{Y}_F^b$ having the ESPRIT structure if we construct them according to step 1 of the PRO-ESPRIT summary for the ULA scenario, found in Chapter 4. The symbol L is again used to denote the subarray length. This step is repeated here, using the newly introduced notation.

$$\mathbf{X}_F^b = \left[\mathbf{P}_L^{1\,H}(u_o)\mathbf{X} \mid \ldots \mid \mathbf{P}_{B-1}^{B-1\,H}(u_o)\mathbf{X}\right] \tag{6.15}$$

and

$$\mathbf{Y}_F^b = \left[\mathbf{P}_{L+1}^{2\,H}(u_o)\mathbf{X} \mid \ldots \mid \mathbf{P}_B^{B-L+1\,H}(u_o)\mathbf{X}\right] \tag{6.16}$$

From $\mathbf{X}_F^b$ and $\mathbf{Y}_F^b$ we construct $\mathbf{X}_{FB}^b$ and $\mathbf{Y}_{FB}^b$ as follows.

$$\mathbf{X}_{FB}^b = \left[\mathbf{X}_F^b \mid \tilde{\mathbf{I}}\mathbf{Y}_F^{b\,*}\right] \quad , \quad \mathbf{Y}_{FB}^b = \left[\mathbf{Y}_F^b \mid \tilde{\mathbf{I}}\mathbf{X}_F^{B\,*}\right] \tag{6.17}$$

where $\tilde{\mathbf{I}}$ is the reverse permutation matrix defined in (4.2). The common steps of the beamspace algorithm with the element space algorithm stem from the following two facts. Firstly, we can express $\mathbf{Y}_{FB}^b$ as

$$\mathbf{Y}_{FB}^b = \tilde{\mathbf{I}}\mathbf{X}_{FB}^{b\,*}\tilde{\mathbf{J}} \tag{6.18}$$

where $\tilde{\mathbf{J}}$ is a block reverse permutation matrix defined by

$$\tilde{\mathbf{J}} = \begin{bmatrix} \mathbf{0}_{N'} & \mathbf{I}_{N'} \\ \mathbf{I}_{N'} & \mathbf{0}_{N'} \end{bmatrix} \quad N'=N(B-L)$$

Thus, through relations similar to the ones in (4.10), the components of the Singular Value Decomposition or the Eigenvalue Decomposition of $\mathbf{Y}_{FB}^b$ can be extracted from the corresponding decompositions of $\mathbf{X}_{FB}^b$. Secondly, since by construction the manifold vectors $\mathbf{A}_L$ of $\mathbf{X}_F^b$ and $\mathbf{Y}_F^b$ satisfy $\mathbf{A}_L=\tilde{\mathbf{I}}\mathbf{A}_L^*\Phi^{L-1}$, PRO-ESPRIT can be applied to solve for the eigendata Φ_{ii} i=1,..,D. This is the justification why $\mathbf{P}(u_o)$ was required to have a banded Toeblitz structure.

For the most part, the discussion made and conclusions reached in Chapter 4 apply equally well here, with the exception of the techniques that are used to obtain clean estimates of the true auto and cross correlation matrices as well as estimating both the noise power and the number of sources. As it has already been mentioned, the reason for making changes is that the beamspace noise covariance matrices are no longer scalar multiples of the identity matrix. By definition, the noise correlation matrix of any subset of the element space snapshot vectors is $\sigma^2\mathbf{I}$. After going through the necessary manipulations, the F-B auto and cross correlation matrices $\mathbf{Q}_{xx}^{FB}$ $\mathbf{Q}_{yy}^{FB}$ and $\mathbf{Q}_{xy}^{FB}$ are,

$$\mathbf{Q}_{xx}^{FB} = \sigma^2 \sum_{i=1}^{B-L} (\mathbf{P}_{L+i-1}^{i}(u_o))^H (\mathbf{P}_{L+i-1}^{i}(u_o)) + \sigma^2\tilde{\mathbf{I}}\left[\sum_{i=2}^{B-L+1} (\mathbf{P}_{L+i-1}^{i}(u_o))^T (\mathbf{P}_{L+i-1}^{i}(u_o))^*\right]\tilde{\mathbf{I}} \tag{6.19a}$$

$$\mathbf{Q}_{yy}^{FB} = \sigma^2 \sum_{i=2}^{B-L+1} (\mathbf{P}_{L+i-1}^{i}(u_o))^H (\mathbf{P}_{L+i-1}^{i}(u_o)) + \sigma^2 \tilde{\mathbf{I}} \left[\sum_{i=1}^{B-L} (\mathbf{P}_{L+i-1}^{i}(u_o))^T (\mathbf{P}_{L+i-1}^{i}(u_o))^* \right] \tilde{\mathbf{I}} \quad (6.19b)$$

$$\mathbf{Q}_{xy}^{FB} = \sigma^2 \sum_{i=1}^{B-L} (\mathbf{P}_{L+i-1}^{i}(u_o))^H (\mathbf{P}_{L+i}^{i+1}(u_o)) + \sigma^2 \tilde{\mathbf{I}} \left[\sum_{i=2}^{B-L+1} (\mathbf{P}_{L+i-1}^{i}(u_o))^T (\mathbf{P}_{L+i-2}^{i-1}(u_o))^* \right] \tilde{\mathbf{I}} \quad (6.20)$$

Consider first the structure of $\mathbf{Q}_{xx}^{FB}$. We show this matrix satisfies the following property.

$$\mathbf{Q}_{xx}^{FB} = \mathbf{Q}_{yy}^{FB} = \tilde{\mathbf{I}} \mathbf{Q}_{xx}^{FB^*} \tilde{\mathbf{I}} \quad (6.21)$$

(6.21) dictates that the Eigenvalue Decomposition of $\{\mathbf{R}_{xxb}^{FB} - \sigma^2 \mathbf{Q}_{xx}^{FB}\}$ is related to the Eigenvalue Decomposition of $\{\mathbf{R}_{yyb}^{FB} - \sigma^2 \mathbf{Q}_{yy}^{FB}\}$. That is, we can get the reduction in computation discussed previously, even after "cleaning" the data correlation matrices. The proof of (6.21), commences with the following relationships.

$$(\mathbf{P}_L^1(u_o))^H (\mathbf{P}_L^1(u_o)) = (\mathbf{P}_{L+i-1}^{i}(u_o))^H (\mathbf{P}_{L+i-1}^{i}(u_o)) \quad i=2,..,B-L+1 \quad (6.22)$$

(6.22) is a direct result of the special structure of $\mathbf{P}(u_o)$; the proof of (6.21) involves simple but tedious algebraic manipulations and is omitted here. As a consequence of (6.22), (6.19a) and (6.19b) simplify as

$$\mathbf{Q}_{xx}^{FB} = \sigma^2 (B-L)(\mathbf{P}_L^1(u_o))^H (\mathbf{P}_L^1(u_o)) + \sigma^2 (B-L) \tilde{\mathbf{I}} (\mathbf{P}_L^1(u_o))^T (\mathbf{P}_L^1(u_o))^* \tilde{\mathbf{I}} \quad (6.23a)$$

$$\mathbf{Q}_{yy}^{FB} = \sigma^2 (B-L)(\mathbf{P}_L^1(u_o))^H (\mathbf{P}_L^1(u_o)) + \sigma^2 (B-L) \tilde{\mathbf{I}} (\mathbf{P}_L^1(u_o))^T (\mathbf{P}_L^1(u_o))^* \tilde{\mathbf{I}} \quad (6.23b)$$

A second property stemming from the special structure of $\mathbf{P}(u_o)$ is described as

$$(\mathbf{P}_L^1(u_o))^H (\mathbf{P}_L^1(u_o)) = \tilde{\mathbf{I}} (\mathbf{P}_L^1(u_o))^T (\mathbf{P}_L^1(u_o))^* \tilde{\mathbf{I}} \quad (6.24)$$

Exploitation of this property further simplifies the results for $\mathbf{Q}_{xx}^{FB}$ and $\mathbf{Q}_{yy}^{FB}$

$$\mathbf{Q}_{xx}^{FB} = \mathbf{Q}_{yy}^{FB} = 2\sigma^2 (B-L)(\mathbf{P}_L^1(u_o))^H (\mathbf{P}_L^1(u_o)) \quad (6.25)$$

(6.24) and (6.25) validate (6.21).

Knowledge of the beamspace noise correlation matrices is important for the following reason. With a noise correlation matrix, equal to a scalar multiple of the identity, such as the case dealt with in Chapter 4, and an adequate number of snapshots, the Eigenvalue Decomposition of $\mathbf{R}_{xx}^{FB}$ yields asymptotically unbiassed estimates of the signal subspace $\mathbf{U}_{xx}^{D}$, the noise power, and the number of sources. This will not be the case, however, in the presence of colored noise. Noise power estimation and cleaning must be done in two steps, i.e., first estimate the noise

power σ^2, and then subtract $\sigma^2\mathbf{Q}_{xx}^{FB}$ from both $\mathbf{R}_{xxb}^{FB}$ and $\mathbf{R}_{yyb}^{FB}$. In the absence of any a-priori information regarding the noise power level one may employ the procedure outlined in Section 3.4 to estimate the noise power. Recall that the procedure in 3.4 exploited the fact that the eigenvectors of the noiseless $\mathbf{R}_{xxb}^{FB}$ corresponding to the eigenvalue $\lambda=0$ are also the generalized eigenvectors of the matrix pair $\{\mathbf{R}_{xxb}^{FB},\mathbf{Q}_{xx}^{FB}\}$ corresponding to the generalized eigenvalue $2(B-L)\sigma^2$. Therefore, B-D of the B generalized eigenvalues of $\{\mathbf{R}_{xxb}^{FB},\mathbf{Q}_{xx}^{FB}\}$ asymptotically approach the value of $2(B-L)\sigma^2$ and, as a consequence, the average of the these "noise" eigenvalues should an accurate estimate of σ^2. This result also holds if we extract a subarray out of the overall array, and form the FB data correlation matrices with the elements of this subarray. However, one must insure that the subarray length is, larger than the expected number of sources, in order that at least one of the the computed GEV's, is a noise GEV. The appropriate noise correlation matrix should also be used. Instead of working with the FB correlation matrices, one can also estimate the noise power from the Eigenvalue Decomposition of the correlation matrix derived from either $\mathbf{X}_F^b$ or $\mathbf{Y}_F^b$. In such a case the noise correlation matrix would a be scalar multiple of the identity matrix.

At this point, we simply assume an estimate of σ^2 is available using one of the methods described above. This allows cleaning of both $\mathbf{R}_{xxb}^{FB}$ and $\mathbf{R}_{yyb}^{FB}$, yielding $\mathbf{C}_{xxb}^{FB}$ and $\mathbf{C}_{yyb}^{FB}$, respectively. The corresponding "clean" and "unclean" matrices are related as

$$\mathbf{C}_{xxb}^{FB}=\mathbf{R}_{xxb}^{FB}-\sigma^2\mathbf{Q}_{xx}^{FB}\quad,\quad \mathbf{C}_{xy}^{FB}=\mathbf{R}_{yyb}^{FB}-\sigma^2\mathbf{Q}_{xx}^{FB} \tag{6.26}$$

A question that arises is this: under what conditions is it possible to obtain a relationship between the eigenvalue decompositions of $\mathbf{C}_{xxb}^{FB}$ and $\mathbf{C}_{yyb}^{FB}$? More specifically, under what conditions the following property hold?

$$\mathbf{C}_{yyb}^{FB}=\tilde{\mathbf{I}}\mathbf{C}_{xxb}^{FB^*}\tilde{\mathbf{I}} \tag{6.27}$$

If (6.27) were to hold, it would then imply that the eigenvalues of $\mathbf{C}_{xxb}^{FB}$ and $\mathbf{C}_{yyb}^{FB}$ are identical, and for a particular eigenvalue the corresponding eigenvectors would be $\mathbf{e}$ and $\tilde{\mathbf{I}}\mathbf{e}^*$ respectively. To check for this, consider $\tilde{\mathbf{I}}\mathbf{C}_{xxb}^{FB^*}\tilde{\mathbf{I}}$. From (6.26)

$$\tilde{\mathbf{I}}\mathbf{C}_{xxb}^{FB^*}\tilde{\mathbf{I}}=\tilde{\mathbf{I}}\mathbf{R}_{xxb}^{FB^*}\tilde{\mathbf{I}}-\sigma^2\tilde{\mathbf{I}}\mathbf{Q}_{xx}^{FB^*}\tilde{\mathbf{I}} \tag{6.28}$$

$$=\mathbf{R}_{yyb}^{FB}-\sigma^2\mathbf{Q}_{xx}^{FB}\;=\;\mathbf{C}_{yyb}^{FB}$$

It is emphasized that if the relationship $\tilde{\mathbf{I}}\mathbf{Q}_{xx}^{FB^*}\tilde{\mathbf{I}}=\mathbf{Q}_{xb}^{FB}$, did not hold, (6.28) would not be true. This would further imply that the EVD of $\mathbf{C}_{yyb}^{FB}$ could not be extracted from that of $\mathbf{C}_{xxb}^{FB}$. Before we summarize all the steps of the algorithm, we comment on the beamspace noise cross correlation matrix $\mathbf{Q}_{xy}^{FB}$. Again as a

result of the special structure of $\mathbf{P}(u_o)$, one can easily show that the following property holds.

$$(\mathbf{P}_L^1(u_o))^H(\mathbf{P}_{L+1}^2(u_o)) = ,\ldots, = (\mathbf{P}_B^{B-L}(u_o))^H(\mathbf{P}_B^{B-L+1}(u_o)) \qquad (6.29)$$

The above expression reduces $\mathbf{Q}_{xy}^{FB}$ to

$$\mathbf{Q}_{xy}^{FB}=\sigma^2(B-L)(\mathbf{P}_L^1(u_o))^H(\mathbf{P}_{L+1}^2(u_o)) + \sigma^2(B-L)\tilde{\mathbf{I}}(\mathbf{P}_{L+1}^2(u_o))^T(\mathbf{P}_L^1(u_o))^*\tilde{\mathbf{I}} \quad (6.30)$$

So, a clean estimate of the cross covariance matrix $\mathbf{C}_{xyb}^{FB}$ can be obtained from the unclean cross correlation matrix $\mathbf{R}_{xyb}^{FB}$ via

$$\mathbf{C}_{xyb}^{FB} = \mathbf{R}_{xyb}^{FB} - \sigma^2\mathbf{Q}_{xy}^{FB} \qquad (6.31)$$

We now proceed to summarize PRO-ESPRIT as it would be applied in the beamspace domain. The B beams will be centered symmetrically about $u=u_o$.

Summary of beamspace PRO-ESPRIT (white noise)

(1) For each raw snapshot vector, $\mathbf{x}(n)$, use (6.13) to form $\mathbf{x}_s(n) = \mathbf{S}^H(u_o)\mathbf{x}(n)$

(2) Pre-multiply $\mathbf{x}_s(n)$ by $(\mathbf{E}^H(u_o))^{-1}$ to obtain the beamspace snapshot vector $\mathbf{x}_b(n)$

(3) With N snapshots, stack the N beamspace snapshot vectors as the columns of the NxB data matrix $\mathbf{X}_b$

(4) Use $\mathbf{X}_b$ to construct $\mathbf{X}_F^b$ and $\mathbf{Y}_F^b$ according to (6.15) and (6.16)

(5) Use (6.17) to construct $\mathbf{X}_{FB}^b$ and $\mathbf{Y}_{FB}^b$

(6) Form $\mathbf{R}_{xxb}^{FB}=\frac{1}{N}\mathbf{X}_{FB}^{bH}\mathbf{X}_{FB}^b$ and $\mathbf{R}_{yyb}^{FB}=\frac{1}{N}\mathbf{Y}_{FB}^{bH}\mathbf{Y}_{FB}^b$

(7) Estimate the noise power, σ^2, and perform rough cleaning of the noise from $\mathbf{R}_{xxb}^{FB}$ and $\mathbf{R}_{xyb}^{FB}$ to obtain $\mathbf{C}_{xxb}^{FB}$ and $\mathbf{C}_{xyb}^{FB}$

(8) Take an EVD of $\mathbf{C}_{xxb}^{FB}$: $\mathbf{C}_{xxb}^{FB}\mathbf{u}_i=\lambda_i\mathbf{u}_i$, $i=1,..,L$

(9) Form $\mathbf{U}_{xx}^D=[\mathbf{u}_1, \ldots, \mathbf{u}_D]$ and $\Sigma=\text{diag}\{\lambda_1^{1/2}, \ldots, \lambda_D^{1/2}\}$

(10) Form $\mathbf{Q}_u = \mathbf{U}_{xx}^{D1}\tilde{\mathbf{I}}\mathbf{U}_{xx}^{D*}$ and $\mathbf{Q}_v = \Sigma^{-1}\mathbf{U}_{xx}^{DH}\mathbf{C}_{xyb}^{FB}\tilde{\mathbf{I}}\mathbf{U}_{xx}^{D*}\Sigma^{-1}$

(11) Take SVD of $\mathbf{Q}_u=\mathbf{U}_l\Sigma_l\mathbf{V}_l^H$ and $\mathbf{Q}_v=\mathbf{U}_r\Sigma_r\mathbf{V}_r^H$

(12) $\tilde{\mathbf{Q}}_u = \mathbf{U}_l \mathbf{V}_l^H \quad , \tilde{\mathbf{Q}}_v = \mathbf{U}_r \mathbf{V}_r^H$

(13) Find the D Eigenvalues of $\Sigma^{-1}\mathbf{Q}_u \Sigma \mathbf{Q}_v^H$

6.5 Simulations and Discussion

In the first simulation we considered the following scenario. The array was a uniform linear array of M=64 sensors separated by half a wavelength. The number of beams was 13, with the middle beam pointed at u=0. The pointing angles of the beams were equi-spaced by $\Delta u = 2/64$. In terms of angles away from boreside, this beamforming configuration approximately covers the region $\theta = -11°$ to $\theta = -11°$. A signal originating from outside of this range will be suppressed by the beamformer. The 3 dB beamwidth for this array size is about 1.8°. In the first simulation we assume that there are three sources arriving from the following directions. $\theta_1 = -5°$, $\theta_2 = 0°$ and $\theta_3 = 0.9°$. Therefore, the second and third sources are separated by almost half a beamwidth. The source covariance matrix was the following.

$$\mathbf{R}_{ss} = \begin{bmatrix} 0.5 & 0.4 & 0.4 \\ 0.4 & 0.5 & 0.4 \\ 0.4 & 0.4 & 0.5 \end{bmatrix}$$

Thus all three sources are 80% correlated with each other. The signal to noise ratio for each source is $10\log(.5) \simeq -3$ dB. For this simulation we used 20 snapshots. The results of 120 independent runs are displayed in Figure 6.1. Observe that despite the low signal to noise ratio of the signals, the estimates are quite good, as also indicated by their sample mean and variance. The second and third sources are resolved quite well despite their close proximity. As the numbers indicate, the source which is at 0° has the smallest variance relative to the other two sources, while one would expect that the smallest variance would be exhibited by the source at −5° because its estimates are not affected by resolution problems. The reason for this is that the source at 0° coincides exactly with the beam steered at u=0, and therefore the gain associated with this source is large. The remaining two sources are situated in the interval between two consecutive beams. In the next simulation (Fig. 6.2) we kept all array and signal parameters unchanged, however we reduced the number of beams to 7, that is almost half the value of beams we had in the first simulation. So, if the different set of beams were to be non-overlapping, we would now require almost twice as many sets of beams than before in order to cover the interval u=-1 to u=1. The advantage is that the computation would decrease since the dimensions of the matrices we had

to work with was almost halved. The sample means and sample variances are comparable to the ones we observed earlier. Note that although the number of beams was decreased, the ones which remained did not change their position, so the same reason as before can be used to explain the small variance exhibited by the estimates of the source coming from θ=0°. Next, we try to illustrate what will happen if a signal falls outside the band. In particular, we shifted the three sources to the following locations. θ_1=−5°, θ_2=6° and θ_3=12.8°. The number of beams was 13, so the array is sensitive to signals whose direction of arrival is in the range of −11° to 11°. The direction of the third source is clearly outside this range. The number of snapshots was raised to 25, while the source covariance matrix was unchanged from before. The results of 120 independent runs are shown in Figure 6.3. In this Figure, the estimates for the signals at θ_1 and θ_2 were almost perfect, with small bias and little variance. As far as the estimates for θ_3 are concerned, they are the ones concentrated about the (x,y) point (1,0). This is a typical behavior of PRO-ESPRIT in beamspace. If a source falls close or outside the edge of the band, it is decoded as a source coming right from bireside. Of course, in this simulation we assumed that the number of sources was 3. In fact, if one was to look at the GEV's of $\{\mathbf{R}_{xxb}^{FB}, \mathbf{Q}_{xx}^{FB}\}$ he would unambiguously reach the conclusion that there were only two sources in the band we are interested in. However, in many cases, a source close to the edge of the band can cause ambiguities, especially if its power is significantly higher than the power of the remaining sources. In including this simulation we tried to raise the question of designing overlapping bands rather orthogonal ones, to avoid various mishappenings such as the one demonstrated via this simulation. If the bands are orthogonal, sources on the boundaries of two adjacent bands will be invisible to both of them and will go undetected. If on the other hand there is overlapping, a source invisible to one band because it is positioned at its edge, will be visible to the next. Typical percentages of overlapping that are suggested in literature are 33% to 50%. Of course, as the level of overlapping increases, the required number of bands also increases, and so does the total amount of computation to cover the region u=-1 to u=1. If each band can be processed in parallel, then the number of bands is not a crucial matter.

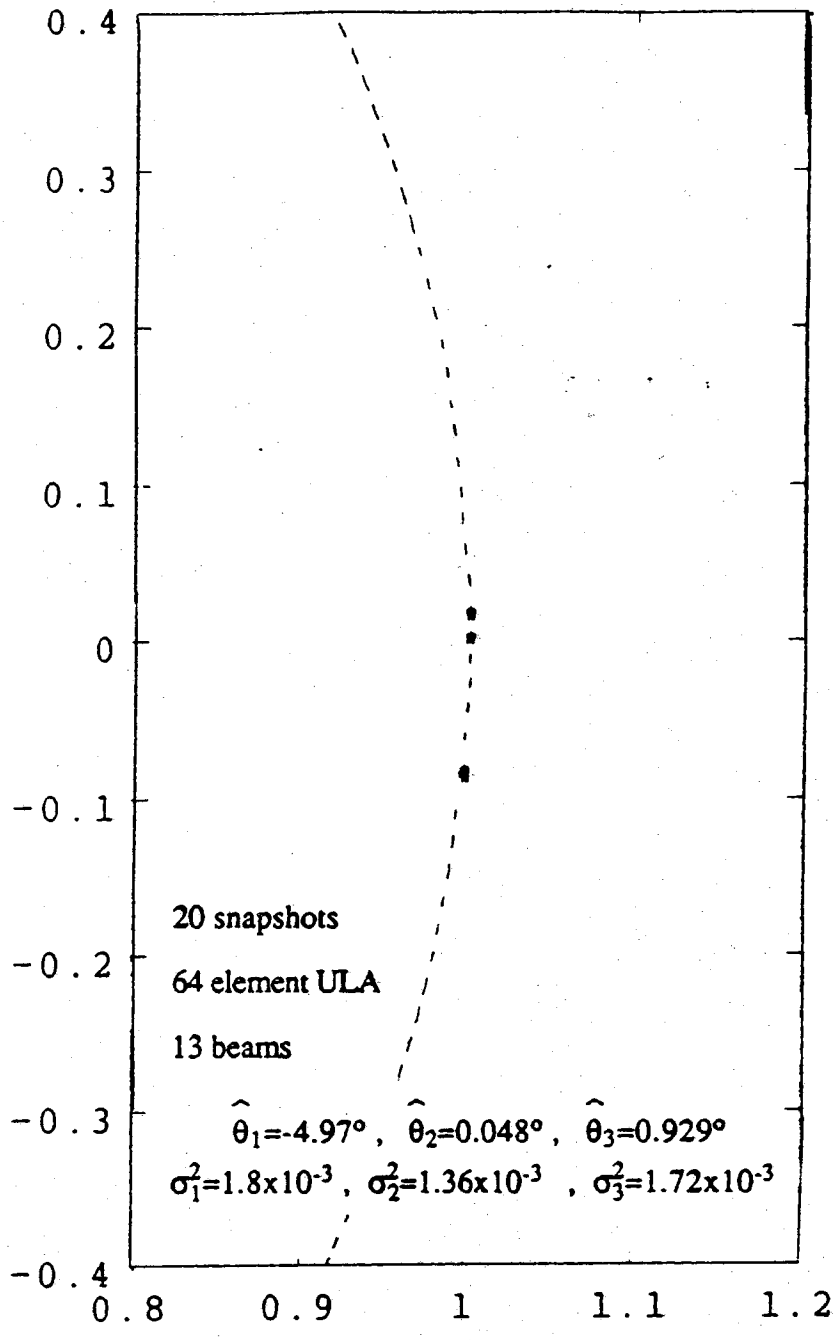

Figure 6.1 The performance of beamspace PRO-ESPRIT with a 64 element array and bands of 13 beams. The beams cover the range θ=−11° to θ=11°, or u=-.1875 to u=.1875. The source at θ=0° is at the peak of the beam centered at u=0.

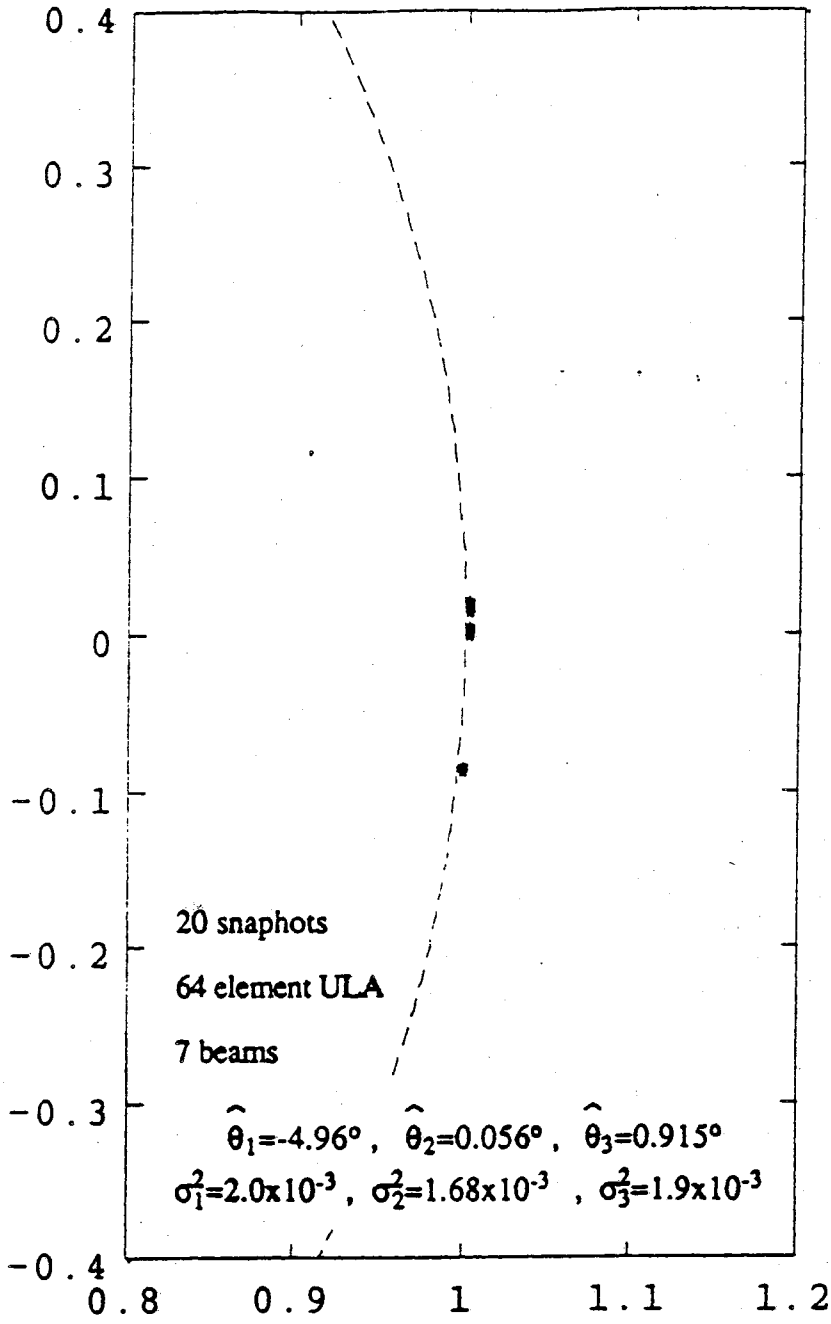

Figure 6.2 Effect caused by reducing the number of beams from 13 to 7. There is no significant change in the estimates.

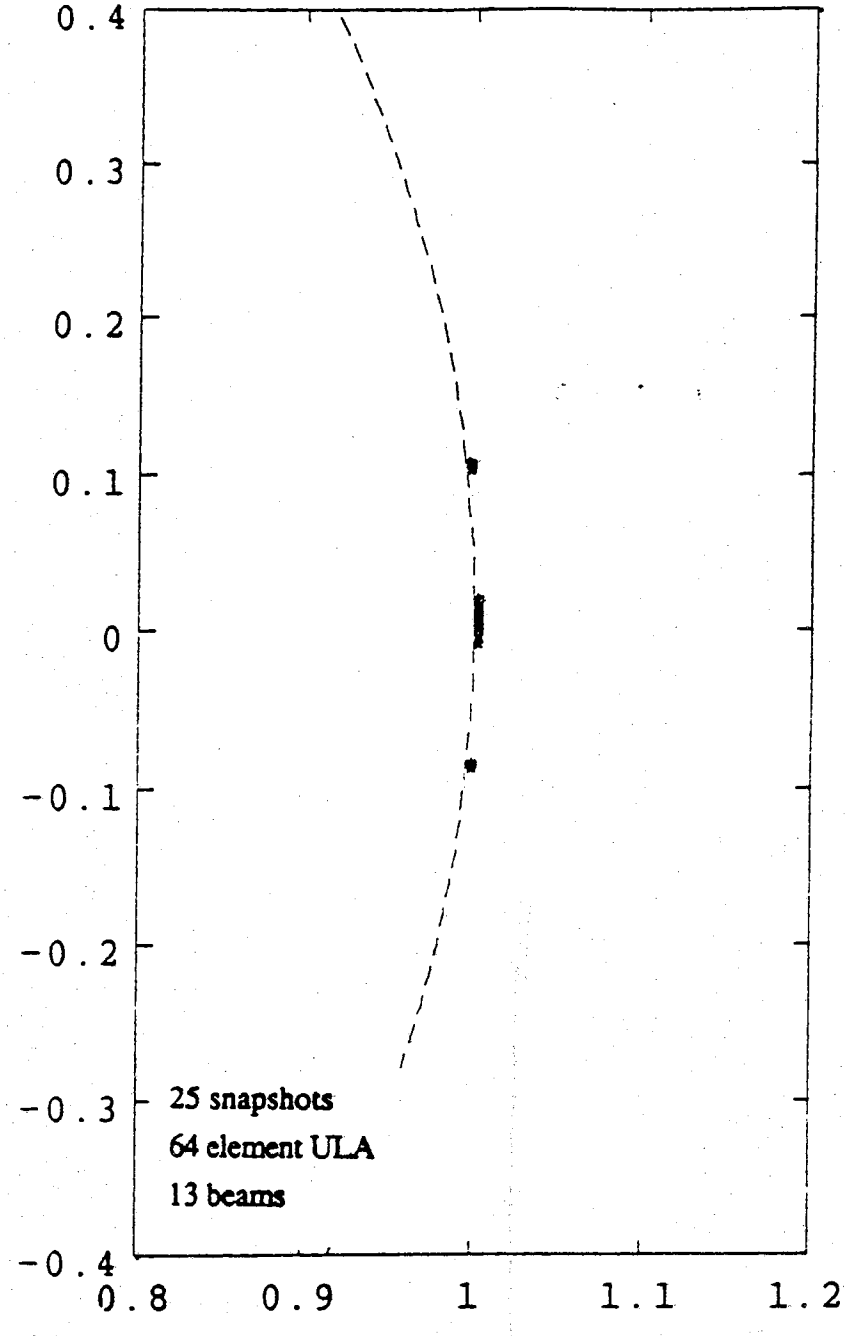

Figure 6.3 With 13 beams, the result of assigning one source a direction outside the visible interval θ=−11° to θ=11°. The sources at θ=−5° and θ=6° are estimated almost perfectly. The source at θ=12.8° appears as coming right from boreside.

CHAPTER 7
CONCLUSION

We have introduced a new array signal processing algorithm, PRO-ESPRIT, that can be used for the estimation of the azimuth and elevation of multiple radiating sources. Following the development of the general algorithm that is applicable to any array geometry exhibiting the ESPRIT structure, we concentrated on the specific application of PRO-ESPRIT first with linear, uniformly spaced arrays, and then with arbitrarily shaped, two dimensional arrays. We discussed in detail the exploitation of the redundancies built in either array configuration that result to a reduction of the required computational task by almost a factor of two. This, we feel, has been our major contribution, especially in view of the fact that in radar applications, the execution time is one of the most vital constraints the designer must take into account. For linear, uniformly spaced arrays the reduction of computation via the incorporation of Forward-Backward of the data has was achieved with almost no complication at all. In contrast, the application of pseudo Forward-Backward to the planar, two dimensional arrays had to be further examined to deal with cases of instability in the associated matrices. In both cases there was no apparent degradation in the performance of either algorithm. The v-modification of the pseudo-FB correlation matrices we introduced in the Section 5.5 is, perhaps, not the only way out of the mentioned ill-conditioning problem. For example, the design of arrays whose manifold matrix exhibits uniform stability as a function of the source directions is another alternative. In the development of the v-modification technique, we assumed a diagonal $\mathbf{V}$. It is also possible to increase the degrees of freedom in $\mathbf{V}$, and theoretically this should lead to even more, numerically stable, correlation matrices.

To accommodate large arrays, in Chapter 6 we demonstrated the application of PRO-ESPRIT in beamspace. The motivation, there, was the fact that with increasing array sizes, the application of any array signal processing algorithm in element space, is severely limited by the ability of the available software and hardware to handle matrices with large dimensions. We hope, that it became apparent from the discussion that the application of PRO-ESPRIT in beamspace

will result in substantial reduction of the computational load. Although we concentrated exclusively on one specific beamforming matrix that allowed both the use DFT fast computation of the beamspace snapshot vectors plus the option of using F-B averaging, the results for any other beamforming would not be very different than the ones obtained here. Also of interest is the application of PRO-ESPRIT in beamspace but also with a two dimensional array.

The actual application is quite straight forward, however, there is more to be done in this area to deal with problems such as the design of good beamformers and interference cancellation.

LIST OF REFERENCES

LIST OF REFERENCES

[ZOLT89a]
M. Zoltowski and D. Stavrinides, "Sensor Array Signal Processing via a Procrustes Rotations Based Eigenanalysis of the ESPRIT Data Pencil," *IEEE Trans. Acoust., Speech, and Signal Process.,* vol. ASSP-37, no. 6, pp. 832-861, June 1989.

[ZOLT89b]
M. Zoltowski and D. Stavrinides, "A variant of forward-backward averaging for single invariance ESPRIT with aperiodic/nonlinear arrays," submitted to *IEEE Trans. Acoust., Speech, and Signal Process.,*

[ZOLT89c]
M. Zoltowski and D. Stavrinides, "Multiple Source Localization Via Redundancy Exploitation With Geometrically Redundant Planar Sensor Arrays," *Proceedings of the Topical Meeting on Signal Recovery and Synthesis III,* Cape Cod, MA, June 1989.

[ZOLT89f]
M. Zoltowski and D. Stavrinides, "Computationally Efficient Estimation of the Azimuth and Elevation of Multiple Sources with Planar Sensor Arrays," *Proceedings of the 32-nd Midwest Symposium on Circuits and Systems,* University of Illinois, Champaign, pp. 582-585, August 1989.

[PAUL85]
A. Paulraj, R. Roy, and T. Kailath, "Estimation of Signal Parameters via Rotational Invariance Techniques - ESPRIT," *Proceedings of the Asilomar Conference on Circuits, Systems, and Computers,* pp. 83-89, Nov. 1985.

[PAUL86]
A. Paulraj, R. Roy, and T. Kailath, "A subspace rotation approach to signal parameter estimation," *IEEE Proceedings,* vol. 74, pp. 1044-1045, July 1986.

[ROY86]
R. Roy, A. Paulraj, and T. Kailath, "ESPRIT - A subspace rotation approach to estimation of parameters of cisoids in noise," *IEEE Trans. Acoustics, Speech, Signal Process.,* vol. 74, pp. 1044-1045, July 1986.

[ROY87a]
R. Roy, A. Paulraj, and T. Kailath, "Comparative performance of ESPRIT and MUSIC for direction-of-arrival estimation," *Proceedings of Int'l Conference on Acoustics, Speech, and Signal Processing,* vol. 4, pp. 2344-2347, April 1987.

[ROY87b]
R. Roy and T. Kailath, "ESPRIT and Total Least Squares", *Conference Record of the 21st Asilomar Conference on Signals, Systems, and Computers,* pp. 297-301, November 1987.

[ROY88a]
R. Roy and T. Kailath, "ESPRIT and Total Least Squares", presented at *Indo-U.S. Workshop on Systems and Signals Processing,* January 1988.

[ZOLT87a]
M. Zoltowski, "Solving the semi-definite generalized eigenvalue problem with application to ESPRIT," *Proceedings of IEEE Int'l Conference on Acoust., Speech, and Signal Process.,* vol. 4, pp. 2316-2319, April 1987.

[ZOLT87b]
M. Zoltowski, "Solving the Generalized Eigenvalue Problem with Singular Forms," *Proceedings of the IEEE,* vol. 75, no. 11, pp. 1546-1548, Nov. 1987.

[ZOLT87c]
M. Zoltowski, "Novel Techniques for the Estimation of Array Signal Parameters Based on Matrix Pencils, Subspace Rotations, and Total Least Squares," *Proceedings of IEEE Int'l Conference on Acoust., Speech, and Signal Process.,* vol. 4, pp. 2861-2864, April 1987.

[SPEI87]
J. Speiser, "Some observations concerning the ESPRIT direction finding method," presented at *Mathematical Theory of Networks and Systems Conference* (MTNS-87), Phoenix, Arizona, June 15-19, 1987.

[VAN87]
C. Van Loan, "A Unitary Method for the ESPRIT Direction-of-Arrival Estimation Algorithm," *Proc. of SPIE Int'l. Symposium on Optical & Optoelectronic Applied Science & Eng.,* August 1987.

[QUIB86]
H. Ouibrahim, D. D. Weiner, and T. K. Sarkar, "Matrix Pencil Approach to Angle of Arrival Estimation," *Conference Record of the 20th Asilomar Conference on Signals, Systems, and Computers,* pp. 203-206, Nov. 1986.

[QUIB87]
H. Ouibrahim, "A generalized approach to direction finding," Ph.D. dissertation, Syracuse University, 1987.

[QUIB88]
H. Ouibrahim, D. D. Weiner, and T. K. Sarkar, "A generalized approach to direction finding," *IEEE Trans. Acoustics, Speech, Signal Process.*, vol. 36, pp. 610-612, April 1988.

[HUA88a]
Y. Hua and T. K. Sarkar, "Matrix Pencil Method and its Performance," *Proceedings of IEEE Int'l Conference on Acoust., Speech, and Signal Process.*, pp. 2476-2479, April 1988.

[HUA88b]
Y. Hua and T. K. Sarkar, "On SVD for Estimating Generalized Eigenvalues of Singular Matrix Pencils in Noise," *Submitted for Publication*

[SHAN85]
T. J. Shan, M. Wax, and T. Kailath, "On spatial smoothing for direction-of-arrival estimation of coherent signals," *IEEE Trans. Acoustics, Speech, Signal Process.*, vol. 33, pp. 806-811, Aug. 1985.

[EVAN82]
J. E. Evans, J. R. Johnson, and D. F. Sun, "Application of advanced signal processing techniques to angle-of-arrival estimation in ATC navigation and surveillance systems," M. I. T. Lincoln Lab., Tech. Report No. 582, 23 June 1982.

[WILL88]
R. T. Williams, S. Prasad, A. K. Mahalanabis, and L. H. Sibul, "An improved spatial smoothing technique for bearing estimation in a multipath environment," *IEEE Trans. Acoustics, Speech, Signal Process.*, vol. 36, pp. 425-432, April 1988.

[REDD87]
V. U. Reddy, A. Paulraj, and T. Kailath, "Performance analysis of the optimum beamformer in the presence of uncorrelated sources and its behavior under spatial smoothing," *IEEE Trans. Acoustics, Speech, Signal Process.*, vol. 35, pp. 927-936, July 1987.

[SPEI84]
J. Speiser and C. Van Loan, "Signal processing computations using the generalized singular value decomposition," *Proc. of SPIE Int'l. Symposium on Optical & Optoelectronic Applied Science & Eng.*, Vol. 495, August 1984.

[GOLU83a]
G. Golub and C. Van Loan, *Matrix Computations*, Johns Hopkins University Press, Baltimore, MD, Sect. 12.4 on "Comparing Subspaces using the Singular Value Decomposition", pp. 425-431, 1983.

[BARN80]
E. R. Barnes, "Some matrix minimization problems," 1980 IEEE Decision and Control Conference Proceedings, pp. 244-246, 1980.

[GOLU83b]
G. Golub and C. Van Loan, *Matrix Computations*, Johns Hopkins University Press, Baltimore, MD, Sect. 12.3 on "Total Least Squares", pp. 420-425, 1983.

[GOLU80]
G. Golub and C. Van Loan, "An Analysis of the Total Least Squares problem," SIAM J. on Numerical Analysis, vol. 17, no. 6, pp. 883-893, Dec. 1980.

[SVAN85]
S. Van Huffel and J. Vandewalle, "The use of Total Linear Least Squares techniques for identification and parameter estimation," *IFAC Identification and System Parameter Estimation 1985,* vol. 2-c, pp. 1167-1172, 1985.

[ZOLT87e]
M. Zoltowski, "Signal Processing Applications of the Method of Total Least Squares," *Conference Record of the 21st Asilomar Conference on Signals, Systems, and Computers,* pp. 290-296, November 1987.

[WAX85]
M. Wax and T. Kailath, "Detection of signals by information theoretic criteria," IEEE Trans. Acoustics, Speech, and Signal Processing, vol. ASSP-33, no. 2, pp. 387-392, April 1985.

[LEC89]
J. P. LeCadre, "Parametric methods for spatial signal processing in the presence of unknown colored noise fields," *IEEE Trans. Acoust., Speech, Signal Process.,* vol. ASSP-37, no. 7, pp. 965-983, July 1989.

[KAV87]
M. Kaveh, H. Wang, and H. Hung, "On the threshold performance of a class of estimators of the number of narrow-band sources," *IEEE Trans. Acoust., Speech, Signal Process.,* vol. ASSP-35, no. 9, pp. 1350-1352, Sept. 1987.

[SCH86]
R. O. Schmidt, "Multiple emitter location and signal parameter estimation," *IEEE Trans. Antennas Propagat.,* vol. AP-34, no. 3, pp. 276-281, March 1986.

[KAV86]
M. Kaveh and J. Barabell, "The statistical performance of the MUSIC and the Minimum-Norm algorithms in resolving plane waves in noise," *IEEE Trans. Acoust., Speech, Signal Process.*, vol. ASSP-34, no. 2, pp. 331-341, April 1986.

[WANG86]
H. Wang and M. Kaveh, "On the performance of signal-subspace processing--Part I: narrowband systems," *IEEE Trans. Acoust., Speech, Signal Process.*, vol. ASSP-34, no. 5, pp. 1201-1209, Oct. 1986.

[BEDR86]
S. D. Bedrosian, "Nonuniform linear arrays: a graph-theoretic approach to minimum redundancy," *Proceedings of the IEEE*, vol. 74, no. 7, pp. 1040-1043, July 1986.

[PILL86]
S. U. Pillai, Y. Bar-Ness, and F. Haber, "A new approach to array geometry for improved spatial spectrum estimation," *Proceedings of the IEEE*, vol. 74, no. 10, pp. 1522-1524, Oct. 1986.

[BRES86]
Y. Bresler and A. Macovski, "On the number of signals resolvable by a uniform linear array," *IEEE Trans. Acoust., Speech, Signal Process.*, vol. ASSP-34, no. 6, pp. 1361-1375, Dec. 1986.

[COX88]
H. Cox, R. M. Ziskind, and M. M. Owen, "Effects of amplitude and phase errors on linear predictive array processors," *IEEE Trans. Acoust., Speech, Signal Process.*, vol. ASSP-36, no. 1, pp. 10-19, Jan. 1988.

[POH88]
S. C. Pohlig, "Hybrid adaptive feedback nulling in the presence of channel mismatch," *Proceedings of IEEE Int'l Conference on Acoust., Speech, and Signal Process.*, pp. 1588-1591, April 1988.

[MON80]
R. A. Monzingo and T. W. Miller, *Introduction to Adaptive Arrays*, Wiley, New York, 1980.

[ROY89a]
R. Roy and T. Kailath, "ESPRIT - Estimation of Signal Parameters via Rotational Invariance Techniques," *IEEE Trans. Acoust., Speech, Signal Process.*, vol. 37, pp. 984-995, July 1989.

[ROY88b]
R. Roy, B. Ottersten, A. L. Swindlehurst, and T. Kailath, "Multiple Invariance ESPRIT," *Conference Record of the 22nd Asilomar Conference on Signals, Systems, and Computers*, Nov. 1988, pp. 583-587.

[ROY89b]
R. Roy, M. Goldburg, B. Ottersten, A. L. Swindlehurst, M. Viberg, and T. Kailath, "ESPRIT and Uniform Linear Arrays," *SPIE Int'l. Symposium, Advanced Algorithms and Architectures for Signal Processing IV,* 8-10 August 1989, SPIE Vol. 1152, pp. 370-380.

[OTT89]
B. Ottersten, M. Viberg, and T. Kailath, "Asymptotic Analysis of the Total Least Squares ESPRIT Algorithm," *SPIE Int'l. Symposium, Advanced Algorithms and Architectures for Signal Processing IV,* 8-10 August 1989, SPIE Vol. 1152, pp. 146-157.

[SWI89]
A. L. Swindlehurst, R. Roy, and T. Kailath, "Suboptimal Subspace-Fitting Methods for Multidimensional Signal Parameter Estimation," *SPIE Int'l. Symposium, Advanced Algorithms and Architectures for Signal Processing IV,* 8-10 August 1989, SPIE Vol. 1152, pp. 197-208.

[OTT88]
B. Ottersten and M. Viberg, "Analysis of Subspace Fitting Methods for Sensor Array Processing," *Proceedings of 1989 IEEE Int'l Conference on Acoustics, Speech, and Signal Processing,* May 1988, pp. 2807-2810.

[ZOLT89d]
M. Zoltowski and T.Lee , "Maximum Likelihood Based Sensor Array Signal Processing in the Beamspace Domain for Low Angle Radar Tracking," *Submitted for Publication*

[ZOLT89e]
M. Zoltowski and T.Lee , "Bisector Angle Estimation in a Nonsymmetric Multipath Radar Scenario," *Submitted for Publication*

[CAP69]
J. Capon , "High-Resolution Frequency-Wavenumber Spectrum Analysis," *Proceedings of the IEEE,* vol. 57, pp. 1408-1418, Aug. 1969.

[MAR87]
S. L. Marple, *Digital Spectral Analysis*, Prentice-Hall, Englewood Cliffs, N.J., 1987

[KAY88]
S. M. Kay, *Modern Spectral Estimation,* Prentice-Hall, Englewood Cliffs, N.J., 1988, Chapter 11

APPENDICES

Appendix A

Proof of theorem 2: Let $\mathbf{Q}_1$ and $\mathbf{Q}_2$ each be a complex-valued, unitary matrix, of the same dimension, with each exhibiting symmetry as well, i. e.,

$$\mathbf{Q}_1\mathbf{Q}_1^H = \mathbf{Q}_1^H\mathbf{Q}_1 = \mathbf{I} \text{ and } \mathbf{Q}_1 = \mathbf{Q}_1^T \quad ; \quad \mathbf{Q}_2\mathbf{Q}_2^H = \mathbf{Q}_2^H\mathbf{Q}_2 = \mathbf{I} \text{ and } \mathbf{Q}_2 = \mathbf{Q}_2^T$$

Also, let Σ be a nonsingular matrix. If λ_i is an eigenvalue of the matrix $\Sigma^{-1}\,\mathbf{Q}_1\,\Sigma\,\mathbf{Q}_2^H$, then $\frac{1}{\lambda_i^*}$ is an eigenvalue of $\Sigma^{-1}\,\mathbf{Q}_1\,\Sigma\,\mathbf{Q}_2^H$ as well.

Proof: Since λ_i is an eigenvalue of $\Sigma^{-1}\,\mathbf{Q}_1\,\Sigma\,\mathbf{Q}_2^H$, it is also a generalized eigenvalue of the pencil $\{\mathbf{Q}_1\,\Sigma\,\mathbf{Q}_2^H\,,\,\Sigma\}$. Hence, λ_i satisfies:

$$\left|\,\mathbf{Q}_1\,\Sigma\,\mathbf{Q}_2^H - \lambda_i\,\Sigma\,\right| = 0 \tag{A.1}$$

Factoring out $\mathbf{Q}_1$ on the left of the expression in the determinant, and $\mathbf{Q}_2$ on the right, and subsequently dividing both sides of the equation by $|\mathbf{Q}_1|\,|\mathbf{Q}_2|$, yields:

$$\left|\,\Sigma - \lambda_i\,\mathbf{Q}_1^H\Sigma\,\mathbf{Q}_2\,\right| = 0 \tag{A.2}$$

where we have invoked the fact that $\mathbf{Q}_1$ and $\mathbf{Q}_2$ are unitary matrices. In turn, factoring out $-\lambda_i\Sigma$ on the left of the expression inside this determinant and dividing by $|-\lambda_i\Sigma|$ yields:

$$\left|\,\Sigma^{-1}\,\mathbf{Q}_1^H\Sigma\,\mathbf{Q}_2 - \frac{1}{\lambda_i}\mathbf{I}\,\right| = 0 \tag{A.3}$$

Now, if $|\mathbf{A}| = 0$, then $|\mathbf{A}^*| = 0$. Thus, taking the conjugate of the expression in the determinant yields:

$$\left|\,\Sigma^{-1}\,\mathbf{Q}_1^T\Sigma\,\mathbf{Q}_2^* - \frac{1}{\lambda_i^*}\mathbf{I}\,\right| = 0 = \left|\,\Sigma^{-1}\,\mathbf{Q}_1\Sigma\,\mathbf{Q}_2^H - \frac{1}{\lambda_i^*}\mathbf{I}\,\right| \tag{A.4}$$

where the expression on the RHS follows from the fact that $\mathbf{Q}_1 = \mathbf{Q}_1^T$ and $\mathbf{Q}_2^* = \mathbf{Q}_2^H$.

This indicates that $\frac{1}{\lambda_i^*}$ is an eigenvalue of $\Sigma^{-1}\,\mathbf{Q}_1\,\Sigma\,\mathbf{Q}_2^H$ as well. Q.E.D.

Appendix B

Proof of Equation (5.44): We start by repeating the problem to be solved. Let $\mu_{i,j}$ and $\nu_{i,j}$ be the pre-determined phases of entry (i,j) of $\hat{C}_{xx}$ and $\hat{C}_{yy}$ respectively. We want to estimate parameters $v_1,..,v_M$ such that the following equation holds for all indices i in the range 1,..,M and for all j>i.

$$v_i - v_j = -\frac{1}{2}(\mu_{i,j}+\nu_{i,j})+\frac{\pi}{2}k_{i,j} \tag{B.1}$$

$k_{i,j}$ is an arbitrary but also odd integer. For convenience, assume $k_{i,j}=-k_{j,i}$. This is basically a definition, since (B.1) is defined only for j>i. Because of the restriction of i and j, the total number of equations is $\frac{1}{2}M(M-1)$. In general, the set of equations we have to work with will constitute an overdetermined system of linear equations. Instead, the problem can be re-expressed as a least squares minimization problem, i.e.,

$$\min_{v\in\mathbb{R}^M} \| \mathbf{A}v-\mathbf{c} \|_F \tag{B.2}$$

$\mathbf{v}=[v_1..v_M]^T$ is an Mx1 vector containing the variables we want to solve for, $\mathbf{c}$ is an $\frac{1}{2}M(M-1)$x1 vector containing the terms on the right hand side of (B.1), and $\mathbf{A}$ is an $\frac{1}{2}M(M-1)$ x M sparse matrix. If we try to solve the problem directly using the left pseudo inverse of $\mathbf{A}$, we will soon run into numerical trouble because $\mathbf{A}$ does not have full rank. Specifically, its rank is M-1 instead of M. Hence, there should exist a vector $\mathbf{v}^\circ$ that is in the null space of $\mathbf{A}$, i.e., $\mathbf{A}\mathbf{v}^\circ=\mathbf{0}$. Let $\mathbf{v}^*$ be the minimizing solution. Then, for any scalar α, $\mathbf{v}^*+\alpha\mathbf{v}^\circ$ would also be a minimizing solution. In view of this observation, we would like to to limit the search over $\mathbf{v}$ to those vectors that lie in the (M-1) dimensional space spanned by the rows of $\mathbf{A}$. This can be accomplished if we first obtain an Mx(M-1) matrix $\mathbf{D}$ whose columns span the same space as the space spanned by the rows of $\mathbf{A}$ and then define

$$\mathbf{z}=\begin{bmatrix} z_1 & z_2 & \cdots & z_{M-1} \end{bmatrix}^T$$

Now force $\mathbf{v}=\mathbf{D}\mathbf{z}$. We are now guaranteed that $\mathbf{v}$ does not belong to the null space of $\mathbf{A}$. This further implies that minimization can be carried out with respect to the auxiliary variables $z_1,..,z_{M-1}$. The problem is therefore reformulated as follows.

$$\min_{\mathbf{z}\in\mathbb{R}^{(M-1)}} \| \mathbf{ADz}-\mathbf{c} \|_F \tag{B.3}$$

We are now guaranteed of a unique solution, and it is given by

$$\mathbf{z}^* = \left[(\mathbf{AD})^T(\mathbf{AD})\right]^{-1}\mathbf{ADc} \quad , \quad \mathbf{v}^*=\mathbf{Dz}^* \tag{B.4}$$

Taking advantage of the inherent sparsity in **A** we can obtain the following closed form solution for each element of the optimal vector $\mathbf{v}^*$.

$$v_p^*=\frac{1}{M}\left[\sum_{j=1}^{M-p}\gamma_{p,j+p} - \sum_{j=1}^{p-1}\gamma_{j,p}\right] \quad p=1,..,M \tag{B.5}$$

where

$$\gamma_{i,j}=-\tfrac{1}{2}(\mu_{i,j}+\nu_{i,j})+\frac{\pi}{2}k_{i,j}$$

It is now a matter of some tricks before (B.5) can be put into its desired form given by (5.44). Observe that since both Forward data correlation matrices $\hat{\mathbf{C}}_{xx}$ and $\hat{\mathbf{C}}_{yy}$ are Hermitian, $\mu_{i,j}=-\mu_{j,i}$. Similarly for $\nu_{i,j}$. The above two facts in conjunction with the previous constrain imposed on $k_{i,j}$, allow us to write

$$\gamma_{j,i} = -\gamma_{j,i} \tag{B.6}$$

Substituting (B.6) into (B.5), the result is

$$v_p^*=\frac{1}{M}\left[\sum_{j=1}^{M-p}\gamma_{p,j+p} - \sum_{j=1}^{p-1}\gamma_{p,j}\right] \quad p=1,..,M \tag{B.7}$$

The last thing that remains to be done is to put both parts of the summation under the same index. If we go through this step, (B.5) reduces to

$$v_p^* = \frac{1}{M}\sum_{\substack{j=1\\ j\neq p}}^{M}\gamma_{p,j} \; p=1,..,M$$

$$=\frac{1}{M}\sum_{\substack{j=1\\ j\neq p}}^{M}\left\{-\frac{1}{2}(\mu_{p,j}+\nu_{p,j})+\frac{\pi}{2}k_{p,j}\right\} \quad p=1,..,M \tag{B.8}$$

This is the expression we were after, and it is identical to (5.44).